PULSE GENERATION IN 1.55 μm REGION USING A METAL CARBIDE ABSORBER

MUHAMMAD AFIQ ASHRAF BIN BADSHA SAHIB

INSTITUTE FOR ADVANCED STUDIES
UNIVERSITY MALAYA
KUALA LUMPUR

2023

PULSE GENERATION IN 1.55 μm REGION USING A METAL CARBIDE ABSORBER

MUHAMMAD AFIQ ASHRAF BIN BADSHA SAHIB

THESIS SUBMITTED IN FULFILMENT OF THE REQUIREMENTS FOR THE DEGREE OF MASTER OF PHILOSOPHY

INSTITUTE FOR ADVANCED STUDIES
UNIVERSITY MALAYA
KUALA LUMPUR

2023

UNIVERSITY OF MALAYA

ORIGINAL LITERARY WORK DECLARATION

Name of Candidate: MUHAMMAD AFIQ ASHRAF BIN BADSHA SAHIB

Matric No: S2106871/1

Name of Degree: MASTER OF PHILOSOPHY

Title of Project Paper/Research Report/Dissertation/Thesis ("this Work"):

PULSE GENERATION IN 1.55 μm REGION USING A METAL CARBIDE ABSORBER

Field of Study: PHOTONICS

I do solemnly and sincerely declare that:

(1) I am the sole author/writer of this Work;
(2) This Work is original;
(3) Any use of any work in which copyright exists was done by way of fair dealing and for permitted purposes and any excerpt or extract from, or reference to or reproduction of any copyright work has been disclosed expressly and sufficiently and the title of the Work and its authorship have been acknowledged in this Work;
(4) I do not have any actual knowledge nor do I ought reasonably to know that the making of this work constitutes an infringement of any copyright work;
(5) I hereby assign all and every rights in the copyright to this Work to the University of Malaya ("UM"), who henceforth shall be owner of the copyright in this Work and that any reproduction or use in any form or by any means whatsoever is prohibited without the written consent of UM having been first had and obtained;
(6) I am fully aware that if in the course of making this Work I have infringed any copyright whether intentionally or otherwise, I may be subject to legal action or any other action as may be determined by UM.

Candidate's Signature Date: 15 JANUARY 2023

Subscribed and solemnly declared before,

Witness's Signature Date:

Name:

Designation:

PULSE GENRATION IN 1.55 µm REGION USING A METAL CARBIDE ABSORBER

ABSTRACT

Attributed to their unique properties of compact structure, good flexibility, and low cost, pulsed fiber lasers are excellent light sources for various applications, such as optical communications, biology or medical sciences, micromachining etc. Passive Q-switching and mode-locking techniques are two common methods for generating pulsed lasers, with the key component of a saturable absorber (SA). Titanium silicon carbide (Ti_3SiC_2) MAX phase and titanium carbide ($Ti_3C_2T_x$) MXene are typical transition-metal carbide materials with excellent nonlinear and temperature resilience characteristics, which are emerging as promising saturable absorption materials for pulsed fiber lasers. In this dissertation, Ti_3SiC_2 and $Ti_3C_2T_x$ have been used to develop thin film based SAs using a drop casting technique while using a PVA as a host polymer. The fabricated Ti_3SiC_2 and $Ti_3C_2T_x$ thin films have a modulation depth of 51 %, 4.8 %, respectively and thus suitable for Q-switching and mode-locking applications. By integrating the prepared Ti_3SiC_2/PVA thin film into an EDFL cavity, stable Q-switched pulses operating at 1561.8 nm were obtained and the maximum energy of 100.7 nJ was achieved at a repetition rate of 43.5 kHz. The minimum pulse width of the output pulses was 5.6 µs at a pump power of 71.5 mW. The Ti_3SiC_2 PVA thin film also capable of achieving picosecond pulse when integrated with the extended EDFL ring cavity with a length of 106 m. The proposed mode locked EDFL operated at repetition frequency of 1.88 MHz with a pulse width of 3.03 ps, maximum pulse energy of 6.0 nJ and maximum peak power of 2.0 kW. This study also successfully demonstrated the use of a $Ti_3C_2T_x$ MXene SA for Q-switching application. The results show that the SA successfully produces Q-switched laser pulses with a pulse width of 3.11 µs and repetition rate of 65.59 kHz at the input pump power of

66.3 mW. At the same pump power, the pulse energy is 125 nJ and the maximum output power is 8.17 mW. It is also found that the $Ti_3C_2T_x$ PVA SA successfully produces mode-locked pulses within a pump power from 40.2 mW to 87.2 mW. It operates at 1561.2 nm with a repetition rate of 1.89 MHz and pulse width of 154 ns. At 87.2 mW pump power, the average output power, pulse energy and peak power is 11.85 mW, 6.24 nJ, and 40.7 mW, respectively. These results validated the simplicity and feasibility of both SAs for producing a stable Q-switched and mode-locked pulse train.

Keywords: MAX Phase, MXene, Passive Saturable Absorber, Q-switching and Mode-locking

PENGULUARAN DENYUT DALAM LINGKUNGAN 1.55 µm MENGGUNAKAN PENYERAP LOGAM KARBIDA

ABSTRAK

Disebabkan oleh sifat unik struktur padat, fleksibiliti yang baik, dan kos rendah, laser gentian berdenyut merupakan sumber cahaya yang sangat baik untuk pelbagai aplikasi, seperti komunikasi optik, biologi atau sains perubatan, pemesinan mikro dan lain-lain. Teknik pensuisan Q pasif dan selakan-mod adalah dua kaedah biasa untuk menghasilkan laser berdenyut, dengan komponen utama penyerap boleh tepu (SA). Titanium silikon karbida (Ti_3SiC_2) *MAX Phase* dan Titanium Karbida ($Ti_3C_2T_x$) *MXene* ialah bahan karbida logam peralihan biasa dengan ciri ketahanan tak linear dan suhu yang sangat baik, yang muncul sebagai bahan penyerap boleh tepu yang menjanjikan untuk laser gentian berdenyut. Dalam disertasi ini, Ti_3SiC_2 dan $Ti_3C_2T_x$ telah digunakan untuk membangunkan SA berasaskan filem nipis menggunakan teknik tuangan titisan semasa menggunakan PVA sebagai polimer perumah. Saput nipis Ti_3SiC_2 dan $Ti_3C_2T_x$ yang direka mempunyai kedalaman modulasi masing-masing 51 %, 4.8 % dan dengan itu sesuai untuk aplikasi pensuisan-Q dan selakan-mod. Dengan menyepadukan saput nipis Ti_3SiC_2/PVA yang disediakan ke dalam rongga EDFL, denyutan suis-Q yang stabil yang beroperasi pada 1561.8 nm diperolehi dan tenaga maksimum 100.7 nJ dicapai pada kadar pengulangan 43.5 kHz. Lebar denyut minimum bagi keluaran denyut ialah 5.6 µs pada kuasa pam 71.5 mW. Saput nipis Ti_3SiC_2 PVA juga mampu mencapai denyut *picoseconds* apabila disepadukan dengan kaviti cincin EDFL yang dilanjutkan dengan panjang 106 m. Mod yang dicadangkan selakan-mod EDFL beroperasi pada kekerapan ulangan 1.88 MHz dengan lebar denyut 3.03 ps, tenaga nadi maksimum 6.0 nJ dan kuasa puncak maksimum 2.0 kW. Kajian ini juga berjaya menunjukkan penggunaan $Ti_3C_2T_x$ *MXene* SA untuk aplikasi pensuisan-Q. Keputusan menunjukkan bahawa SA berjaya menghasilkan denyutan laser suis-Q dengan lebar denyut 3.11 µs dan kadar pengulangan

65.59 kHz pada kuasa pam input 66.3 mW. Pada kuasa pam yang sama, tenaga denyut ialah 125 nJ dan kuasa keluaran maksimum ialah 8.17 mW. Ia juga didapati bahawa $Ti_3C_2T_x$ PVA SA berjaya menghasilkan denyutan selakan-mod dalam kuasa pam daripada 40.2 mW hingga 87.2 mW. Ia beroperasi pada 1561.2 nm dengan kadar pengulangan 1.89 MHz dan lebar denyut 154 ns. Pada kuasa pam 87.2 mW, kuasa keluaran purata, tenaga denyut dan kuasa maksimum ialah masing-masing 11.85 mW, 6.24 nJ dan 40.7 mW. Keputusan ini mengesahkan kesederhanaan dan kebolehlaksanaan kedua-dua SA untuk menghasilkan pawai denyut suis-Q dan selakan-mod yang stabil.

Kata kunci: *MAX Phase, MXene*, Penyerap boleh tepu pasif, pensuisan-Q and Selakan-mod

ACKNOWLEDGEMENTS

In the name of Allah, the Most Gracious, the Most Merciful.

All praise be to Allah, for because of His Graciousness and Mercy, this thesis would not come into existence. I am extremely grateful for the assistance and guidance of my supervisor Prof. Ir. Dr. Sulaiman Wadi Harun in my journey to obtain a master's degree. He has given me all the freedom and all the help that I need to carry-out my research study, while non-obtrusively ensuring that I stay on track of study and stay in focus. He not only provided me with guidance and assistance, but also provided friendship and solace when I needed it, and it made it like my family always be my side. Without his guidance and help, this thesis would not have been possible, and I shall eternally be grateful to him for their continuous support.

I take pride in acknowledging my colleagues and friends: Dr. Ahmad Haziq Aiman Rosol, Dr. Nur Farhanah Zulkipli, Athirah and Abdulkadir for their fruitful ideas and help when I need them most. For because of their friendship and help, the lab is look like a home and the experiments are pleasure.

My deepest appreciations from bottom of my heart go to my family for all support and love. The study would not have been completed without their unwavering thoughts and unselfish love as well as support always given to me.

To everyone and everything, thank you.

TABLE OF CONTENTS

LIST OF FIGURES

LIST OF TABLES

LIST OF SYMBOLS AND ABBREVIATIONS

0D	:	Zero-dimensional
2D	:	Two-dimensional
ASE	:	Amplified spontaneous emission
Bi2Te3	:	Bismuth telluride
BP	:	Black phosphorus
CNT	:	Carbon nanotubes
CW	:	Continuous-wave
DI	:	Deionized
EDF	:	Erbium-doped fiber
EDFA	:	Erbium doped fiber amplifier
EDFL	:	Erbium-doped fiber laser
EDS	:	Energy-dispersive X-ray spectroscopy
Er	:	Erbium
FESEM	:	Field Emission Scanning Electron Microscope
FWHM	:	Full width at half maximum
GO	:	Graphene oxide
GVD	:	Group velocity dispersion
HBr	:	Hydrogen bromide
Ho	:	Holmium
LASER	:	Light Amplification by the Stimulated Emission of Radiation
LD	:	Laser diode
LIDAR	:	Light detection and ranging
MCVD	:	Modified chemical vapor deposition
MIR	:	Mid-infrared

Nd	:	Neodymium
NiO	:	Nickel oxide
NLDR	:	Nonlinear Dispersive Regime
NOLM	:	Nonlinear optical loop mirror
NPR	:	Nonlinear polarization rotation
OC	:	Output coupler
PC	:	Polarization controller
PDC	:	Pulse duty cycle
PVA	:	Polyvinyl alcohol
QD	:	Quantum dots
RF	:	Radio frequency
SA	:	Saturable absorber
SAM	:	Self-amplitude-modulation
Sc-DF	:	Scandium-doped fiber
SCG	:	Spent coffee ground
SDS	:	Sodium dodecyl sulphate
SESAM	:	Semiconductor saturable absorption mirror
SMF	:	Single mode fiber
SNR	:	Signal-to-noise ratio
SWCNT	:	Single-wall carbon nanotubes
TBP	:	Time bandwidth product
TDF	:	Thulium-doped fiber
TDFL	:	Thulium-doped fiber laser
TI	:	Topological insulators
Tm	:	Thulium
TMD	:	Transition metal dichalcogenides

VOA	:	Variable optical attenuator
WDM	:	Wavelength division multiplexing
XRD	:	X-ray diffraction

CHAPTER 1: INTRODUCTION

1.1 Background

Over the last two decades, photonics technology has significantly advanced especially in communication applications, where many optical devices have been developed and commercialized (Haynes, Bland-Hawthorn, Large, Klein, & Nelson, 2004). Recently, the photonic research has changed its focus to other areas including industrial applications. One of the recent focuses is the development of fiber laser. There has been a lot of tremendous progress in fiber laser technology since 1961, when the first demonstration of laser oscillation in glass was made (Koester & Snitzer, 1964). Fiber lasers continue to be of interest due to the significant advantages that have revolutionized the laser market over the last decade (Mary, Choudhury, & Kar, 2014; Shi, Schulzgen, Amezcua, Zhu, & Alam, 2017). These advantages include the high quality of the laser beam, and fiber lasers generally offer improved device characteristics including compactness, better stability, and efficiency compared to bulk solid-state lasers. Fiber lasers have evolved into an important device for laser light sources, enabling advancements in various fields such as laser processing in manufacturing (Miranda, Lopes, Quintino, Rodrigues, & Williams, 2008), microscopy (Moneron et al., 2010), spectroscopy (Zhao et al., 2016), and medical applications (Pierce et al., 2001), etc. Basically, a fiber laser uses optical fiber as the active gain medium. The optical fiber is doped with rare earth elements such as ytterbium, erbium, thulium, dysprosium, and neodymium to operate in different wavelength region. There are numerous advantages to utilizing optical fiber as the gain medium. For instance, the pump and light signal in the active gain medium are perfectly overlapping due to the optical fiber's waveguide nature. The fiber laser's construction is also completely alignment-free, as there are no free-space components in its design. The large ratio of the surface area to the volume of the fiber also eliminates the need for water cooling of the gain medium. Furthermore, optical

fiber's single mode properties ascertain great beam quality. In practice, fiber lasers are typically less expensive than solid-state lasers, allowing laser technology mobility that enables the system to be adopted more widely, particularly beyond the confines of specialized laboratories.

Fiber lasers advanced dramatically in the 1980s, owing primarily to the availability of powerful semiconductor lasers, which promoted diode-pumped laser technology. The superiority of fiber lasers has outperformed other types of lasers such as dye, gas, chemical, solid state, and semiconductor, and they are regarded as the most promising laser technology (L. Dong & Samson, 2016). Compared to the conventional dye, gas, chemical and solid- state lasers, fiber lasers are advantageous due to their compactness, flexibility, and efficiency. Because of their high durability and excellent heat management to carry high optical powers, these lasers are capable of performing as powerful industrial high power fiber lasers (Sugioka & Cheng, 2014a). Fiber lasers can be operated in either continuous wave (CW) or pulse mode. A continuous wave (CW) laser provides a continuous power with time. The phase and amplitude of the CW laser oscillate randomly which makes it more preferable in welding, cutting, and manufacturing (Zervas & Codemard, 2014).

Pulsed lasers offers a much higher peak power, which can be realized by either Q-switching or mode-locking operation (Nishizawa, 2014). Q-switching is a technique that produced a pulse duration in the range of milliseconds to microseconds by modulating the Q-factor and loss in the laser cavity (Zulkipli, Batumalay, et al., 2020). On the other hand, a mode-locked laser is realized by inducing the fixed-phase relationship between the longitudinal modes in the resonant cavity. Interference between these modes, resulting in a continuous train of extremely short pulses (Zulkipli, Jafry, et al., 2020). Q-switched and mode-locked fiber lasers can be realized by either active or passive techniques (M. Wang, Chen, Huang, & Chen, 2014; Y. Wang et al., 2019). The

active technique employs an acousto-optic or electro-optic modulator to generate pulses by modulating the loss of the resonator or changing the resonator round-trip phase (Nikodem, Sergeant, Kaczmarek, & Abramski, 2008). It necessitates frequent alignments and has significant signal loss between components. On the other hand, the passive technique, in general uses a saturable absorber (SA) device. This device could modulate the resonator loss quicker than the modulator to generate shorter pulses (Hofer, Ober, Haberl, & Fermann, 1992). Compared to the active technique, the passive methods are preferable due to their many advantages in terms of simplicity, compactness, flexibility, and cost (Sun et al., 2022).

In this thesis, both Q-switched and mode-locked fiber lasers operating in 1550 nm region are demonstrated using newly developed SAs. Two types of SAs are developed based on transition metal carbide materials. The EDF is employed as a gain medium in conjunction with 980 nm pumping for laser operation in 1550 nm region.

1.2 Motivation of Study

Fiber laser technology has advanced significantly during recent decades to meet the needs of industry and medical applications (Shi et al., 2017). The fiber laser is a low-cost system that produces high beam quality while being environmentally friendly. Fiber lasers are also preferred because they have a smaller geometry size, higher intensity and peak powers, a more durable system, and require near zero maintenance (Pierce et al., 2001). Compared to the CW fiber lasers, Q-switched and mode-locked fiber lasers have become a subject of growing interest and rapid development in recent years due to their wide applications in different fields including biomedical, optical communication, remote sensing, high-precision material cutting and drilling, cold ablation, micro marking, and military applications (Mary et al., 2014). For instance, Ilina et al. have proposed novel

techniques of laser- based embryo marking and controlled laser-assisted embryo hatching (Ilina, Khramova, Ivanova, Filatov, & Sitnikov, 2021). In another work, Anthony et al. reported on laser processing of minerals where they have shown that short, low-power pulses can efficiently produce thin, deep holes, and long, high-power pulses are more energy efficient at removing the most amount of material (Anthony et al., 2021).

SA is often used for passively generating Q-switched and mode-locked pulses as it allows pulse generation in a simpler way compared to the active technique (Wu et al., 2018). The active technique employs a costly and complex electrically-driven modulator that ultimately limits the pulse durations achievable directly from the laser source (Nikodem et al., 2008). The SA devices can be broadly classified into two categories: artificial and real SA. Artificial SA exploits nonlinear effects within the laser cavity to mimic the action of a real SA by inducing an intensity-dependent transmission while real SA is based on various materials that exhibit an intrinsic nonlinear decrease in absorption with increasing light intensity. This work is restricted to real SA, considering they are cheap, compact, flexible, easy to build and use. The real SA is mainly composed of carbon and boron group elements and compounds. These include nanomaterials such as carbon nanotubes (CNTs) (H. H. Liu, Chow, Yamashita, & Set, 2013), graphene (Xie et al., 2012), black phosphorus (BP) (Sotor, Sobon, Macherzynski, Paletko, & Abramski, 2015), and transition metal dicalcogenides (TMDs) (Tiu, Ooi, Guo, Zhang, & Ahmad, 2019). CNT-based SAs are easy and inexpensive to manufacture, but have a short spectral bandwidth and are strongly influenced by the diameter of the nanotubes. Graphene-based SAs provide a high absorption spectrum, but with lower modulation and damage thresholds. BP-based SAs typically have a wide wideband spectral range, but have low nonlinear absorption, low optical thresholds, and complex manufacturing processes. SAs based on TMD materials such as SnS_2, WS_2, and MoSe have been shown to have excellent absorption properties (Manzeli, Ovchinnikov, Pasquier, Yazyev, & Kis, 2017). However,

they are hampered by low optical damage thresholds and complex manufacturing. Therefore, the surge for a new SA material which is not only easy to prepare, yet preserve the excellent nonlinear optical properties, wide operating bandwidth, and high damage threshold is still essential.

Recently, transition metal carbides including MAX phases have also gained great interest due to their excellent optical and electrical properties (Z. M. Sun, 2011). They have a hexagonal polycrystalline form made of carbide and nitride. The general formula is $M_{n+1}AX_n$, where M is an early transition metal, A is an A-group element in the periodic table (usually IIIA and IVA), X is carbide or nitride, and *n* is an integer. This ternary compound has unique characteristics that combine merit properties of metals and ceramics (Sokol, Natu, Kota, & Barsoum, 2019). Like metals, it has excellent thermal (~37 W/m·K) and electrical (~$4.5 \times 10^6\ \Omega^{-1}\,m^{-1}$) conductivities, relatively low hardness (~4 GPa) which makes it easy to machine like common metal or graphite, high Young modulus (~325 GPa), and moderate flexural strength (260–600 MPa), it is not susceptible to thermal shock, and it has damage tolerance at high temperatures (Gonzalez-Julian, 2021; Hoffman et al., 2012). It also duplicates several ceramic properties such as good oxidation resistance of up to 1400°C, relatively low density (~4.52 g/cm^3), and high decomposition temperature (~1700°C), and some researchers have also reported that its melting temperature is up to 3000°C (Jin, Su, Hu, & Zhou, 2020; Perevislov, Sokolova, & Stolyarova, 2021; Silvestroni, Melandri, & Gonzalez-Julian, 2021). These properties are beneficial for many applications including biosensors, electrochemical capacitors, catalysts, and optical devices (Gonzalez-Julian, 2021). On the other hand, another ternary metal carbide/nitride so-called MXene was also gained interests as a new member for 2D material class (Naguib et al., 2011). It has a general formula of Mn+1XnTx, where M is transition metal, X is a carbon or nitrogen with n = 1, 2, 3. . . , and T is a face-termination group likes oxygen or fluorine. MXene can be

produced by selectively etching of MAX layer (Alhabeb et al., 2018). The MXene has been previously utilized in various photonic applications due to its excellent optical, thermal, and physical properties (X. Jiang et al., 2018). It has many advantages such as small band gap size, metallic conductivity, and hydrophilic nature of its surface. Mxene also has an excellent saturable absorption characteristic, which is suitable for photonic diodes (Y. Dong et al., 2018). It is also reported that the MXene also exhibits the zero-bandgap structure, which can be potentially used for the broadband optical device (Zhenhong Wang et al., 2020).

In this thesis, Q-switched and mode-locked fiber lasers operating in 1.55 region are demonstrated using two new transition metal carbides-based SAs: titanium silicon carbide (Ti_3SiC_2) MAX phase and titanium carbide ($Ti_3C_2T_x$) MXene. These materials are chosen due to their high optical damage tolerance, which makes it a preferable SA, in comparison to other nano materials (Zhenhong Wang et al., 2020).

1.3 Research objectives

The work aims to develop new SA device based on transition metal carbide material for Q-switching and mode-locking applications in 1550 nm wavelength region. Two new materials; titanium silicon carbide (Ti_3SiC_2) MAX phase and titanium carbide ($Ti_3C_2T_x$) MXene are explored as a passive SA in this work. To achieve this, the following objectives have been proposed to guide the research direction. The research objectives are outlined as:

1. To fabricate new passive SA devices based on Ti_3SiC_2 MAX phase and $Ti_3C_2T_x$ MXene materials.
2. To characterize the newly developed Ti_3SiC_2 and $Ti_3C_2T_x$ based SAs.

3. To demonstrate various Q-switched and mode-locked pulse generations in Erbium-doped fiber laser (EDFL) cavity using the new SAs.

1.4 Thesis Outline

This thesis contains 5 chapters in which a comprehensive study on Q-switched and mode-locked pulse generations by using the newly developed transition metal carbide material based SAs is presented. This chapter presents the background, motivation, and objectives of this study. Chapter 2 is intended to present a thorough literature review on fiber laser technologies and provides details of fundamentals of optical fibers and pulse formation in fiber laser cavities.

In chapter 3, two new SAs are developed based on Ti_3SiC_2 MAX phase and $Ti_3C_2T_x$ MXene materials. The SA thin films were fabricated based on liquid exfoliation technique using PVA as a host polymer. The physical and optical characterizations of these SAs are also described in this chapter. Field Emission Scanning Electron Microscope (FESEM) and Energy-dispersive X-ray spectroscopy (EDS) were used to characterize the physical properties of the prepared thin film. The optical properties of the SA were analyzed using homemade linear and nonlinear absorption set-ups. The linear absorption set-up consists of a white light source that connected to an OSA while a twin balance detector technique was used to examine the nonlinear absorption.

Chapter 4 demonstrates the Q-switched and mode-locked EDFLs operating in 1.55 μm region using both types of thin film based SAs: Ti_3SiC_2 MAX phase and $Ti_3C_2T_x$ MXene materials. The newly developed SA is inserted between two optical fiber ferrules in the EDFL cavity to act as a Q-switcher and mode-locker for microsecond and picosecond pulse generation, respectively.

Chapter 5 concludes the thesis and presents a summary of the research findings. The future direction of this work is also discussed in this chapter.

CHAPTER 2: LITERATURE REVIEW

2.1 Introduction

The acronym LASER stands for light amplification by stimulated emission of radiation. The laser principle was first described by Albert Einstein in 1917 while the first working laser was demonstrated by Theodore Maiman in 1960. Theodore Maiman successfully generated red laser using a ruby crystal as a gain medium and flash lamp as a pumping light. Since then, the development of laser technology including fiber laser has tremendously progressed. Elias Snitzer invented the fiber laser in 1961 and demonstrated its application in 1963 (Snitzer, Hoffman, & Crevier, 1963). Serious commercial applications only emerged in the 1990s, due to unavailability of high-power pump laser. Fiber lasers are everywhere in the modern world, and they are widely used in industrial environments to perform cutting, marking, welding, cleaning, texturing, drilling and a lot more. They are also used in other fields such as telecommunication and medicine. Fiber lasers use an optical fiber cable made of silica glass to guide light and thus they are alignment-free types of lasers. The resulting laser beam is more precise than with other types of lasers because it is smaller and straighter. They also have a small footprint, low maintenance, good electrical efficiency, and low operating costs. Up to date, the progress on fiber laser works continuous to improve where many active and passive mode-locking techniques such as the ones using semiconductor saturable absorber mirror (SESAM), Kerr Mode-locking, and soliton mode-locking have been proposed in recent years (Y. Zhang et al., 2021).

Q-switching is a technique for short pulse generation, from modulation of Q-factor laser resonator. Active Q-switched technique theory was first reported in 1963's (Wagner & Lengyel, 1963) based on ruby laser. A saturable absorber (SA) was proposed

in the passive Q-switched operation a year later using reversibly bleachable dye (Soffer & Hoskins, 1964). A decade later, a mode-locked operation was also demonstrated using dye SA (Ippen, Shank, & Dienes, 1972). Initially, mode-locked laser was achieved by applying active technique utilized optical modulator. However, such technique requires complicated electronic circuit and has limited gain bandwidth. Optical fibers were first used for telecommunications, realizing low attenuation, high-capacity channels as a substitute for conventional copper wires. However, they experienced rapid development in producing various optical amplifiers and fiber lasers. The core of optical fiber was doped in rare-earth ions such as Thulium (Tm), Holmium (Ho), Ytterbium (Yb), Erbium (Er) and Neodymium (Nd) for these applications.

Over the years, numerous efforts have been made by scientists around the world to produce a reliable and powerful laser for a multitude of industrial and scientific applications (Addanki, Amiri, & Yupapin, 2018; Dubey & Yadava, 2008). In the past few decades, the laser produced is mainly based on a bulk solid-state gain medium (Ursula Keller, 2003a). However, the limitations of this laser bring the research on another type of laser based on rare-earth doped fiber as the gain medium. The fiber laser employs a passive saturable absorber (SA) for generating pulses train. The problem of bulky, alignment-dependent set up, and expensive maintenance operation has been successfully overcome by the deployment of the fiber laser with passive SA. Conventionally, the pulse generation in fiber laser is normally achieved using semiconductor saturable absorber mirrors (SESAMs) as the SA (Bonaccorso & Sun, 2014; U. Keller et al., 1996). In addition, the fiber laser is proven better than the conventional bulk laser as it covers a wider operating bandwidth (ranging from 1 to mid-infrared wavelength region). An erbium-doped fiber laser (EDFL) is the most widely investigated fiber laser. It operates at a 1.55 μm regime and thus is suitable for telecommunication applications.

This research work aims to develop Q-switched and mode-locked lasers operating in 1.5 μm region using new passive SAs based on transition metal carbide material. This chapter presents thorough literature reviews on fiber lasers, pulse generation and metal carbide materials.

2.2 Optical Fiber

Optical fiber is a type of cylindrical waveguide in which light can propagate along its main axis. It is usually made of fused silica and has a core with a refractive index higher than that of the surrounding cladding. Since the first attempts to realize low loss light propagation in an optical fiber in 1970s, optical fibers have undergone several breakthroughs especially in the fabrication and design. To date, optical fibers have reached a mass-production level and are now widely used for telecommunication to transmit information (Arumugam, 2001). Other applications include illumination, optical imaging, sensing, spectroscopy, or even power transmission. On the other hand, optical fibers are also used in fabrication of optical amplifiers and lasers.

The propagation of light in an optical fiber can be described using a ray optics approach or electromagnetic theory (Keiser, 2003). Optical fiber consists of a core of high refractive index (n_1) where the light propagates, surrounded by a cladding of low refractive index (n_2) that traps the light through total internal reflection. As the light is launched into the optical fiber, it propagates mainly in the core region though the intensity distribution may extend beyond the core. Due to the guidance and the low propagation losses, the optical power can be maintained in the fiber for long propagation distance. For a step-index optical fiber, the refractive indices are constant for both the core and the cladding. The difference in refractive index between the core and the cladding is often very small: $(n_1 - n_2)/n_1 \ll 1$. It is realized by a slight modification of chemical doping.

Fig. 2.1 shows the light transmission in a step index optical fiber based on multiple total internal reflection at the boundary between the core and the cladding. If $n_1 > n_2$, the total internal reflection occurs at incident angle $\alpha > \alpha_{min} = \sin^{-1}(n_2/n_1)$ based on Snell's law of refraction. The acceptance cone is defined by the minimum incidence angle α_{min} allowing the light to be transmitted through the fiber after multiple reflections. The rays of light entering the fiber from outside this cone escapes through refraction in the cladding. This cone of light defines the numerical aperture (NA) of the optical fiber. It quantifies the strength of fiber guidance and is given as:

$$NA = n \sin\left(\frac{\pi}{2} - \alpha_{min}\right) = \sqrt{(n_1^2 - n_2^2)} \qquad (2.1)$$

Typical NA values are ~0.1 for conventional SMFs while large mode-area SMFs can have low NA below 0.05.

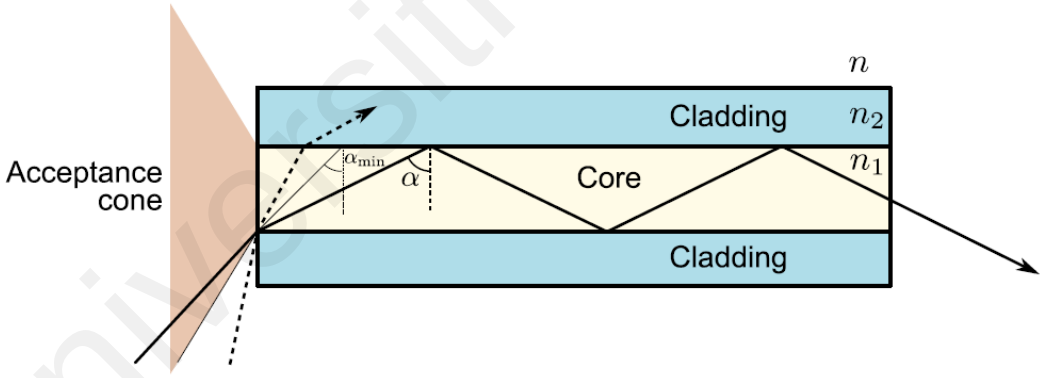

Figure 2.1: Light propagation inside an optical fiber.

2.3 Erbium-doped Fiber Lasers

If the core of an optical fiber is doped with rare-earth ions, such as erbium, ytterbium, and thulium, it can be used as a gain medium for optical amplifier and laser applications. These rare-earth doped fiber lasers offer very narrow infrared beam laser

output with high beam quality and high optical-to-optical efficiency. These rare-earth ions are optically active, and thus they can absorb light at one wavelength and emit light at a longer wavelength. Typically, they are doped in the silica glass host. For instance, Erbium (Er^{3+}) ion is usually used as an active element since it can operate at low loss region of 1.55-micron which suitable for optical communication application. An Erbium-doped fiber can provide small signal gain up to >40 dB in 1550 nm region as it is pumped by a 980 nm laser diode. The invention of rare-earth doped fiber has opened the door for the development of many new active devices such as generating ultra-short pulses, which have many potentials for many applications. The fiber laser offers large optical alignment tolerance and reduces the complexity of opto-mechanic system construction. Ultrafast fiber lasers are widely used in many areas of optical science and technology, including modern ophthalmology, optical microscopy, laser micromachining, optical communication, and precision metrology (M'Sallem et al., 2011; Sugioka & Cheng, 2014a). This section introduces Erbium-doped fiber laser (EDFL) and discusses its working mechanism.

Over the years, numerous efforts have been made by scientists around the world to produce a reliable and powerful laser for a multitude of industrial and scientific applications (Addanki et al., 2018; Dubey & Yadava, 2008). In the past few decades, the laser produced is mainly based on a bulk solid-state gain medium (Ursula Keller, 2003a). However, the limitations of this laser bring the research on another type of laser based on rare-earth doped fiber as the gain medium. The fiber laser employs a passive saturable absorber (SA) for generating pulses train. The problem of bulky, alignment-dependent set up, and expensive maintenance operation has been successfully overcome by the deployment of the fiber laser with passive SA. Conventionally, the pulse generation in fiber laser is normally achieved using semiconductor saturable absorber mirrors (SESAMs) as the SA (Bonaccorso & Sun, 2014; U. Keller et al., 1996). In addition, the

fiber laser is proven better than the conventional bulk laser as it covers a wider operating bandwidth (ranging from 1 to mid-infrared wavelength region). An erbium-doped fiber laser (EDFL) is the most widely investigated fiber laser. It operates at a 1.55 μm regime and thus is suitable for telecommunication applications.

The progress of optical communication has commenced a series of research works in fiber lasers and amplifiers (C Randy Giles & Desurvire, 1991; Saglamyurek et al., 2015). The communication bandwidth ranging from 1.3 to 1.6-μm can be accomplished by implementing several rare-earth ions as the active medium in silica glasses as host materials (Desurvire, Giles, Simpson, & Zyskind, 1991). For instance, an erbium-doped fiber (EDF) has a high absorption and emission coefficient in 1.55-μm region. In general, the variation of host materials provides different spectroscopic characteristics for erbium ion, as such its emission and absorption cross-section differ for each of the glass hosts. On the other hand, the amplification characteristic of the EDF decreases with the increase of dopant concentration (Ainslie, 1991; Wagener, Wysocki, Digonnet, Shaw, & DiGiovanni, 1993). This is attributed to an ion-ion interaction between nearby Er^{3+} ions, resulting in an excited-state population loss in its energy band (Becker, Olsson, & Simpson, 1999). A straightforward method to enhance the amplification efficiency is by employing low dopant concentrations of Er^{3+} (<100 ppm), but this makes a few applications impossible, such as planar waveguides amplifiers and single frequency fibers (Lumholt, Rasmussen, & Bjarklev, 1993). Therefore, Quimby et al. introduced a novel method to mitigate the ion-ion interaction without reducing the dopant concentration (Quimby, Miniscalco, & Thompson, 1994). The device's efficiency can be improved by introducing an aluminium (Al) element to the core glass, which minimizes the clustering effect between Er^{3+} ions.

Figure 2.2 shows a typical energy level diagram of Er^{3+} ions. It indicates various absorption lines spanning from 980 to 1600 nm with the transition from the ground energy

state of $^4I_{15/2}$ to the upper energy state of the Er^{3+} energy-band diagram. 980 and 1530 nm are two dominant absorptions within the spectral regions covered by Er^{3+} ions, which are important for various telecommunications applications. Various optical amplifier devices have been demonstrated based on a core pumping approach using those absorption regions (C. R. Giles, Burrus, DiGiovanni, Dutta, & Raybon, 1991; "Optimizing the pumping configuration for the power scaling of in-band pumped erbium doped fiber amplifiers," 2012). Figure 2.3 shows the emission and absorption spectra of Er^{3+} ions at the $^4I_{13/2} \rightarrow {}^4I_{15/2}$ transition, which represents the strong line for zero-phonon vibration. The luminescence span from 1450 to 1650 nm.

Erbium as a gain medium follows the stimulated emission mechanism that allows the photon to emit from the quantum system. Initially, Er^{3+} ion absorbs the pumped photon and get excited to the upper-energy state of $^4I_{13/2}$ or $^4I_{11/2}$. If the photons pumped by a 980 nm laser diode (LD), the ion jumps to the $^4I_{11/2}$ state. However, the 1480 nm pumped photon resulting in the excitation of the electron at $^4I_{13/2}$ state. In the erbium-doped fiber, the excited electron stays at the upper energy state for ~10 ms. The relaxation time of the Er^{3+} ion determines its quantum efficiency. The longer the relaxation time, the lower the input pump supplied into the laser system, thus increasing the device's efficiency (C Randy Giles & Desurvire, 1991). In this work, a 980 nm LD is used as an optical pump for the gain medium to achieve amplified spontaneous emission (ASE) of the system. The chosen LD was due to its quantum efficiency, which is twice the value of 1480 nm LD (Pedersen, Thompson, Zemon, Miniscalco, & Wei, 1992).

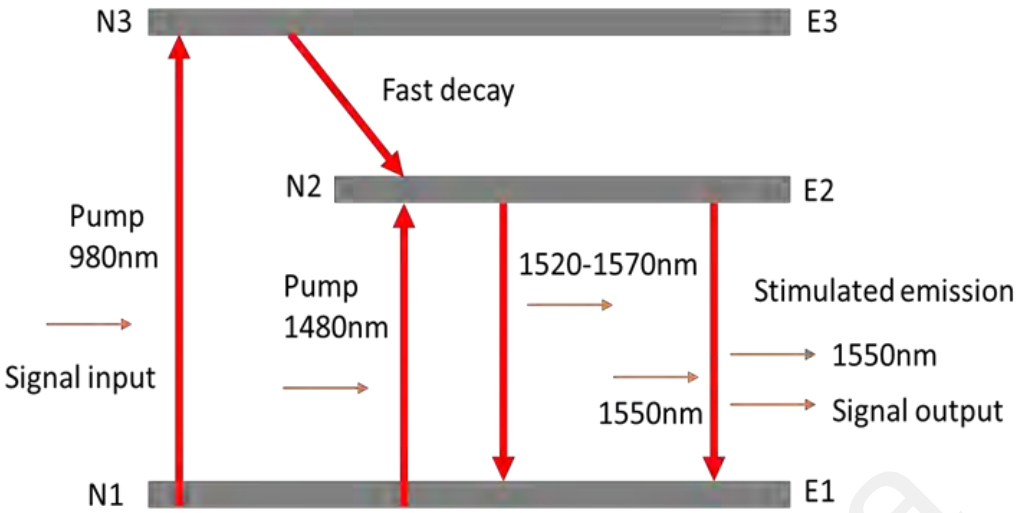

Figure 2.2: Energy level diagram of Er^{3+} ions in silica fibres (Babu et al., 2007).

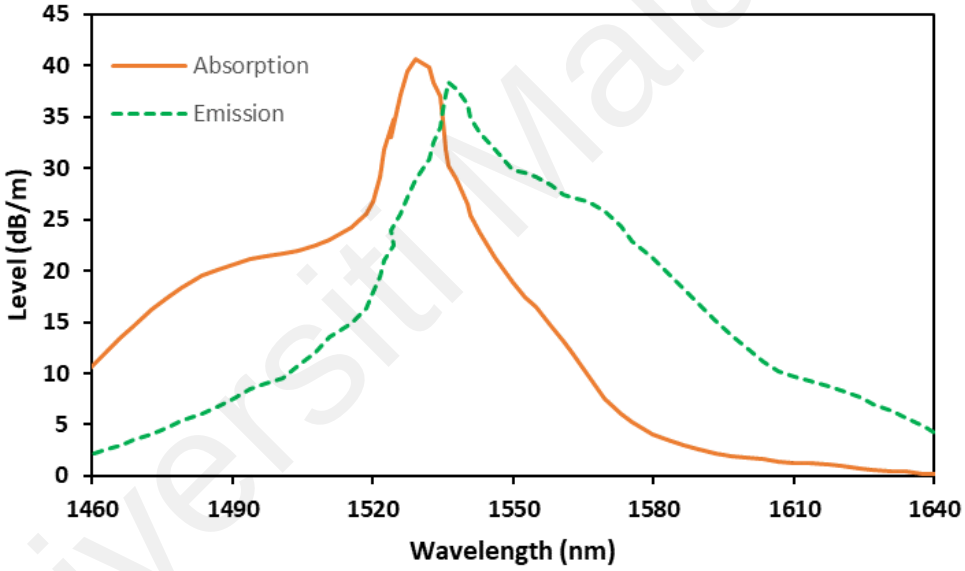

Figure 2.3: The typical absorption and emission cross sections of EDF (due to the $^4I_{15/2} \rightarrow {}^4I_{13/2}$ and $^4I_{13/2} \rightarrow {}^4I_{15/2}$ transitions).

2.4 Q-switching

Pulse generation in the nanosecond to microsecond regime of time domain can be realized by modulating the intracavity losses in a laser resonator. This method is also known as a Q-switching. This technique is capable to produce pulse train with a few hundred nanojoule energy. Q-factor generally refers to the strength of the resonator modes

damping while in the energy storage term, it is the ratio between energy stored and dissipated energy in one complete oscillation (Paschotta, 2008). However, the term became slightly different in lasing with two significant characteristics, which are the round-trip losses and a laser gain to compensate for the loss during continuous-wave operation.

The mechanism of Q-switching starts by pumping the gain medium to keep the resonator losses high (low Q-factor), this simultaneously avoids the energy to be extracted from the resonator. Then, the Q-factor is increased which is the result of a higher gain compared to resonator losses. As such, the intracavity power rises exponentially until the power drops and the gain saturates. The generated light energy produced from this process originates from the energy stored in a gain medium. Therefore, gain medium plays a significant role in producing a Q-switched laser with high pulse energy. A few factors that needed attention when selecting a gain medium are high laser-active ions population, slow upper-state lifetime, and moderate gain efficiency. This is important, since a high-efficiency gain medium may trigger an excessive amplified spontaneous emission which in turn limits the initial loss and energy stored of Q-switch laser.

For a better understanding of Q-switched laser operation, let consider the following mechanism. Fig. 2.4 illustrates the single pulse energy of Q-switched laser. First, consider a saturable absorber with bleach '*0*', unbleached conditions 'q_0', saturable absorber loss coefficient '*q(t)*', and total cavity loss per round trip '*l*'. Refer to phase 1 of Figure 2.13, when the total cavity loss (low Q) and gain are the same, the pulse will emerge at the saturable absorber unbleached conditions. Then, as the laser intensity increase, the gain starts to bleach the absorber. This instantly promotes the increment of intracavity power *P(t)* when the gain *g(t)* becomes similar to *l*, thus saturates the absorber and allowing it to grow significantly.

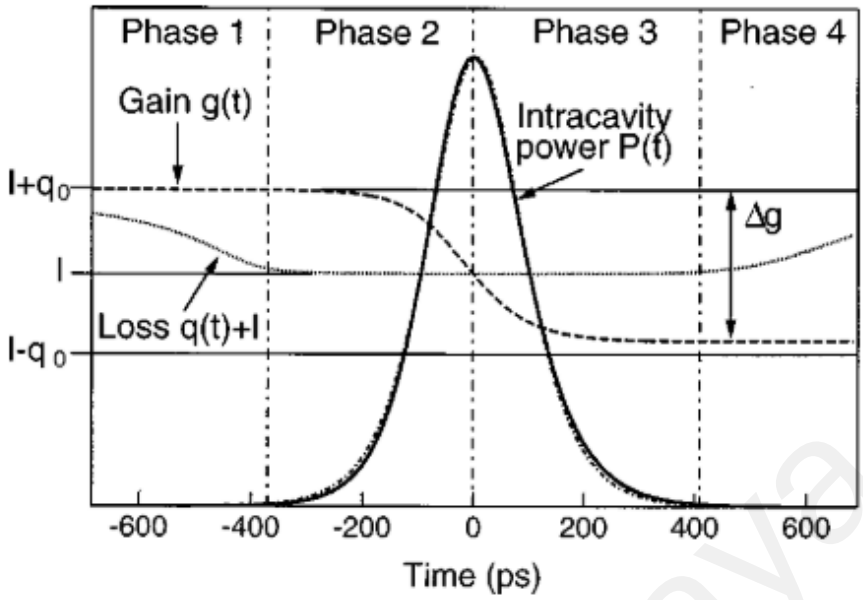

Figure 2.4: Evolution of loss, gain, and power on the time scale of pulse width plotted from the numerical integration of the rate equation (Spühler et al., 1999).

At phase 2, upon increasing the pump power, the absorber becomes fully bleach when the gain is kept at high Q. Further, the gain is depleted to the loss level of *q(t) + l*. When the gain *g(t)* is equal to the total cavity loss *l* at the bleach condition, the maximum pulse is obtained. Later at phase 3, the gain continues to decrease and eventually reaches the negative value, this leads to the decrease in the intracavity power *P(t)*. In the last phase, which is phase 4, the absorber is restored to its unbleached states attributed to the shorter recovery time of the absorber in comparison to the gain. Then, the pumped gain medium will continue to provide gain to the laser, which allows the next cycle of pulse to starts. The gain medium stored the source of energy for the entire lasing operation, which is expressed by the following expression,

$$E_{stored} = AL_G N_2 h\nu_1 \tag{2.2}$$

where $h\nu_1$ is a photon energy at the pumping wavelength, N_2 is the excitation energy in

the gain medium, and AL_G is the volume of pumped gain medium.

Repetition rate is defined as how many pulses are formed per second or simply an inverse of pulses' time interval. In a passively Q-switched fiber laser, the repetition rate is usually in the range of 1 to 100 kHz. However, a few works have successfully achieved Q-switched with a repetition rate of more than 100 kHz (Sobon et al., 2012; L. Wang et al., 2019). This leads to the formation of a pulsed laser that produces a high pulse energy operation. The repetition rate is a laser parameter that depends on the optical intensity of the laser diode pump. Upon increasing the pump power, the repetition rate increase, however, it is limited to the maximum value that the laser diode can achieve. This limit varies according to the laser diode pump and controller. Figure 2.5 shows the typical two pulse envelop of a passively Q-switched laser. It indicates how the pulse's width and repetition rate are measured.

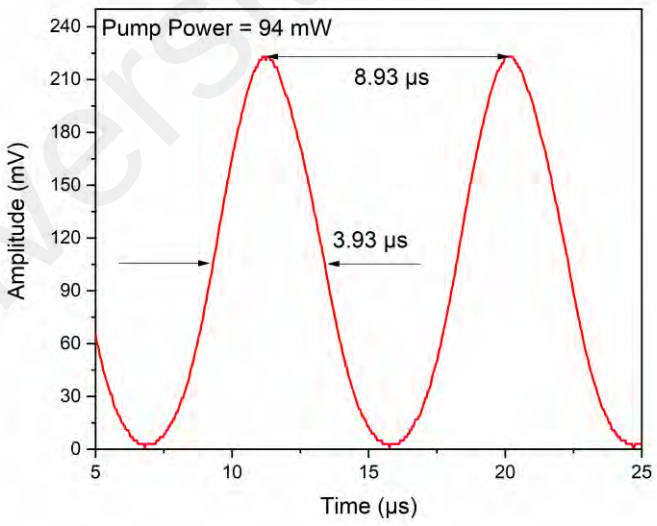

Figure 2.5: The typical oscilloscope trace from a Q-switched fiber laser showing a pulse period of 8.93 µs and pulse width of 3.93 µs.

As shown in Fig. 2.6, the pulse period or interval between two consecutive pulses (T) is measured at 8.93 µs, which can be translated to a repetition rate, *f* of 112 kHz, based on the following expression:

$$f = \frac{1}{T} \tag{2.3}$$

The laser frequency can also be verified by measuring the frequency spectrum using a radio frequency spectrum analyser. The stability of the generated pulses can also be evaluated from the RF spectrum. In case of a Q-switched laser, the RF spectrum exhibits a series of harmonic peaks with different heights as shown in Fig. 2.6. This figure also indicates that the peaks become shorter as the frequency span increases, which is a typical Q-switching behaviour. An important parameter that determines the pulse's stability is a signal-to-noise ratio (SNR) of the fundamental frequency. It can be defined as the distance between the peak and the floor of the fundamental peak (the first peak on the spectrum). For a passively Q-switched operation, the value above 30 dB indicates that the laser is stable. This is closely related to the suppression of noise in a laser cavity and the pulses' resonant relaxation oscillation frequency (Yue, Wang, Xiong, Wang, & Qiu, 2013). Note that the repetition rate of the fundamental peak must match the calculated repetition rate from equation 2.38.

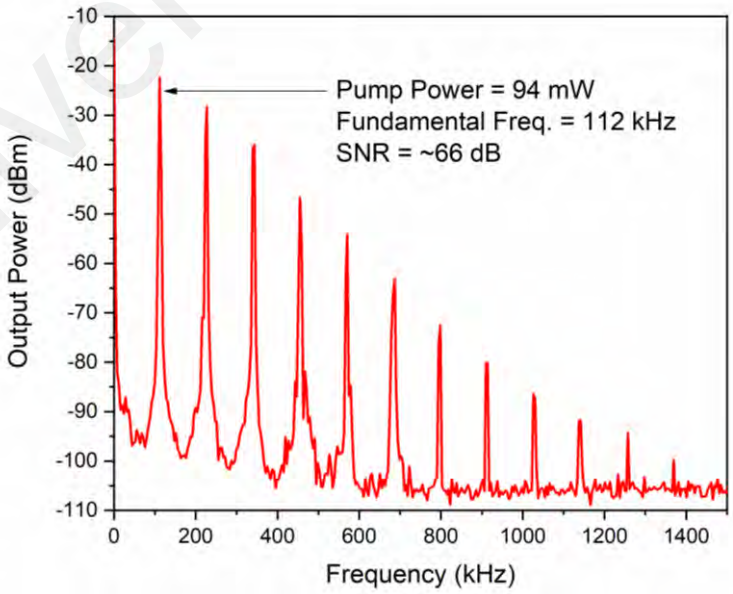

Figure 2.6: The typical RF spectrum captured from a Q-switched fiber laser.

Pulse width τ is defined as the width of the pulse within which the power is at the half peak power. In the other word, full width at half maximum (FWHM). From Fig. 2.5, the pulse width is measured as 3.93 μs based on a captured oscilloscope trace. Usually, the pulse width is around a few nanoseconds to microseconds for a Q-switched laser (S. Salam, W. R. Wong, A. H. H. Al-Masoodi, & S. W. Harun, 2019b). In a typical Q-switched operation, the pulse width decreases with the increase in pump power. The following expression yields the relationship between pulse width (τ_p), laser cavity, and saturable absorption properties,

$$\tau_p = \frac{S_p T_r}{q_0}\left[\frac{\delta(1+\delta)\eta}{\Delta - \ln(1+\delta)}\right] \qquad (2.4)$$

where S_p or the pulse shape factor is approximately 0.88, T_r is the cavity's round-trip time, η is the energy extraction efficiency, and δ is the ratio of saturable to non-saturable loss. Therefore, the following assumptions can be obtained, where the pulse width is proportional to the round-trip time of cavity and inversely proportional to the saturable loss of a SA material.

When measuring the power-dependent laser performance of Q-switched, the optical intensity is adjusted from the lowest possible value to the laser diode limit. For every 10^{th} pump intensity, the measurement of average power is obtained with an optical power meter. The pulse energy is defined as average power divided by repetition rate. During Q-switching, the value of pulse energy is calculated based on the following expression.

$$E_p = \frac{P_{avg}}{f} \qquad (2.5)$$

With P_{avg} as average power, E_p as pulse energy, *f* as repetition rate, those parameters are related to each other, and they also change with the change in optical intensity. Pulse energy is dependent on the amount of energy stored in the gain medium (Spühler et al., 1999). Therefore, it is important to ensure that the gain medium used owns a high device

efficiency. The two properties that influence pulse energy are the gain medium lifetime and absorber's saturation loss.

Peak power (P_p) is defined as the highest attainable optical power of a pulse. Peak power is related to pulse energy and pulse duration. Hence, if the pulsed laser has a short pulse width, it will consume high peak power. The following expression relates the relationship between the three parameters,

$$P_p = \frac{P_E}{\tau} \tag{2.6}$$

where P_E is pulse energy while τ is a pulse width or FWHM. The significance of a high pulse intensities laser or a laser with high peak power is a low heat affected zone that can produce a good laser ablation procedure. There is a multitude of applications that manipulates a pulsed laser with high brightness such as micromachining of material, optical data storage, and waveguide production (Balling & Schou, 2013; Jiang, Wang, Li, Cui, & Lu, 2018).

The passive Q-switching generation can be realized by using either an artificial saturable absorber (nonlinear polarization rotation (NPR) or nonlinear optical loop mirror (NOLM)) or real saturable absorber (SA) techniques. Up to date, various real-SAs have been implemented such as semiconductor saturable absorber mirrors (SESAMs) (Okhotnikov, Grudinin, & Pessa, 2004) and two-dimensional (2D) materials (graphene, topological insulators, transition-metal dichalcogenides) (Tiu et al., 2019; ZT Wang, Chen, Zhao, Zhang, & Wen, 2012; Xu, Ming, Han, Man, & Zhang, 2019) for Q-switching generation in various EDFL cavities. However, the applications of these SAs are restricted due to their drawbacks such as complex optical alignments, environmental sensitivity, complicated fabrication, and limited operating bandwidth. Therefore, there is many new attempts in recent years to develop new SAs with better performance for Q-switching laser operation.

2.5 Mode-locking

The simple meaning of mode-locking techniques is the phase-locking of many longitudinal cavity modes. It was created to induce self-amplitude-modulation (SAM) effect on the propagation of pulse. Mode-locked laser, in contrast to Q-switched one, possessed a few distinctions in terms of output pulse characteristics. First, it can produce a desirable optical pulse train with narrower pulse width, higher peak power and higher repetition rate compared to a Q-switched laser. Secondly, the laser beam produced from such a laser is diffraction limited. The term describes the ability of any laser beam to produce a precise and focused laser beam, which in turn reduces the possible beam divergence on a surface of laser illumination. Those characteristics come from the properties of fiber laser and mode-locked optical pulse.

In a laser resonator, an electromagnetic wave owns two modes of oscillation which are transverse and longitudinal. Normally, those modes are said to not correlate with each other. However, under certain circumstances, adjacent longitudinal modes are locked into constant phase differences. This so-called mode-locking process starts from a series of short pulses with irregular phases in the form of noise. The pulses produced travel back and forth between the two end mirrors, further, the amplification of pulses occurs through the laser light that bounces off the mirrors.

In a mode-locking regime, two competing mechanisms that lead to optical pulses are the laser gain and modulator. The first factor contributing to the bandwidth-limited gain factor leads to the spectral bandwidth shortening and broadening of pulse width in each round-trip. The second factor causes the pulse width to shorten attributed to the time varying transmission of the laser modulator. Both pulse width and spectral bandwidth are the two important characteristics of mode-locked pulses. The temporal width of the pulsed laser relied on the equilibrium state of the two contributing factors. However, the

amplitude modulator's modulating frequency decides the pulses' spectral characteristics. Fig. 2.7 shows the schematic of a mode-locked laser resonator, which consists of a gain and loss elements. It works by modulating the intracavity loss and collecting the laser light with short pulses, which is around the minimum of the loss modulation. An output coupler transmits a small portion of the laser pulse out of the resonator. The period of that pulse, T_R is given by the cavity round-trip time as follows:

$$T_R = \frac{2L}{V_g} \tag{2.7}$$

where L is the laser cavity length and V_g is the group velocity inside the laser resonator. Mode-locked pulses are formed in a fiber laser when several different phases are locked together as shown in Fig. 2.8.

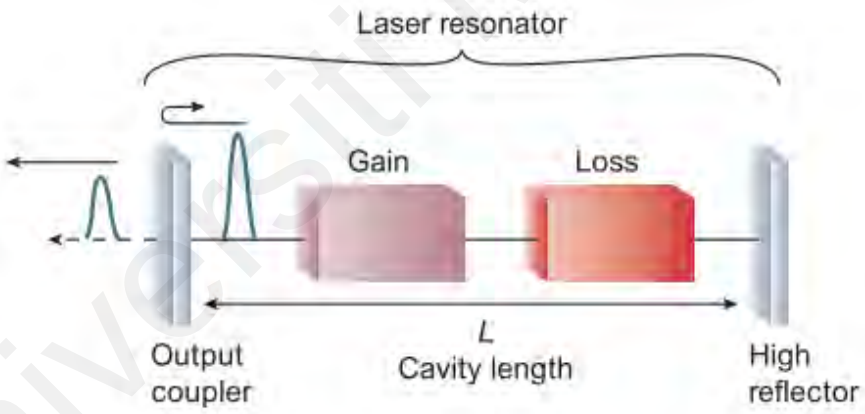

Figure 2.7: A schematic diagram of a mode-locked laser resonator (Ursula Keller, 2003b)

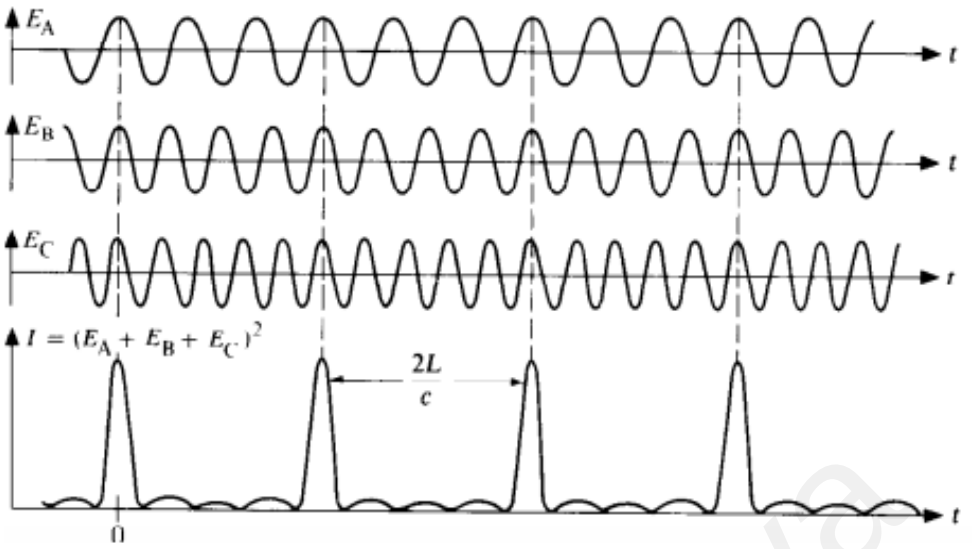

Figure 2.8: Mode-locked pulse generation through phase-locking.

The mode-locked pulse shape can be represented by a bell-shaped function, such as a Gaussian and Hyperbolic secant ($sech^2$) function. According to Haus' master equation, the mode-locked laser operating in anomalous dispersion regime such as soliton laser produces $sech^2$ pulse shape while Gaussian pulse shape is produced in a laser cavity operating in normal dispersion regime. Table 2.1 details the pulse shape function parameters for both pulse shapes. These functions fittings are used in the autocorrelation of the pulse to describe the pulse shape, where the FWHM intensity autocorrelation pulse is represented as τ_{AC}. The pulse width of a mode-locked laser is typically obtained in few picoseconds to femtoseconds regime.

Table 2.1: Pulse characterization.

Pulse shape	$\tau.\Delta\lambda_{3dB}$	τ/τ_{AC}
Gaussian	0.441	0.7071
$Sech^2$	0.315	0.6482

Since actual FWHM quantities are easier to be measured by using auto-correlator, the relationship between the pulse width and 3-dB spectral bandwidth of laser pulse can be written as

$$\tau . \Delta\lambda_{3dB} \geq TBP \tag{2.8}$$

where τ is the FWHM from single pulse envelope, $\Delta\lambda_{3dB}$ is the 3-dB spectral bandwidth measure from optical output spectrum in Hz, and TBP is the time-bandwidth product which refer to Fourier-transform limit. If the equality is achieved in Equation (2.8), the measured pulse width reaches a transform limit and the attainable pulse width meets the minimum possible pulse width that could produce from this condition of laser. Thus, to achieve an ultrashort laser pulse in time domain, the developed laser in this thesis should generate a broad spectral bandwidth laser. On the other hand, the minimum possible pulse width of a pulse can be calculated by giving a spectrum with $\Delta\lambda_{3dB}$ (nm) at FWHM, central peak wavelength λ_o (nm), and the speed of light (m/s) c:

$$\tau \geq TBP \frac{{\lambda_o}^2}{\Delta\lambda_{3dB} . c} \tag{2.9}$$

Fig. 2.9 shows the autocorrelation pulse envelope and oscilloscope pulse train with pulse width of 6.85 ps. Pulse energy (E_p) is basically the total optical energy content of a single pulse or the integral of its optical power against time. For a mode-locked fiber laser, the typical pulse energy is within the range of picojoules and nanojoules. Typically, the pulse energy is calculated by dividing the average output power by the repetition rate as

$$E_p = \frac{P_o}{f_r} \tag{2.10}$$

where P_o is the average output power and f_r is the repetition rate.

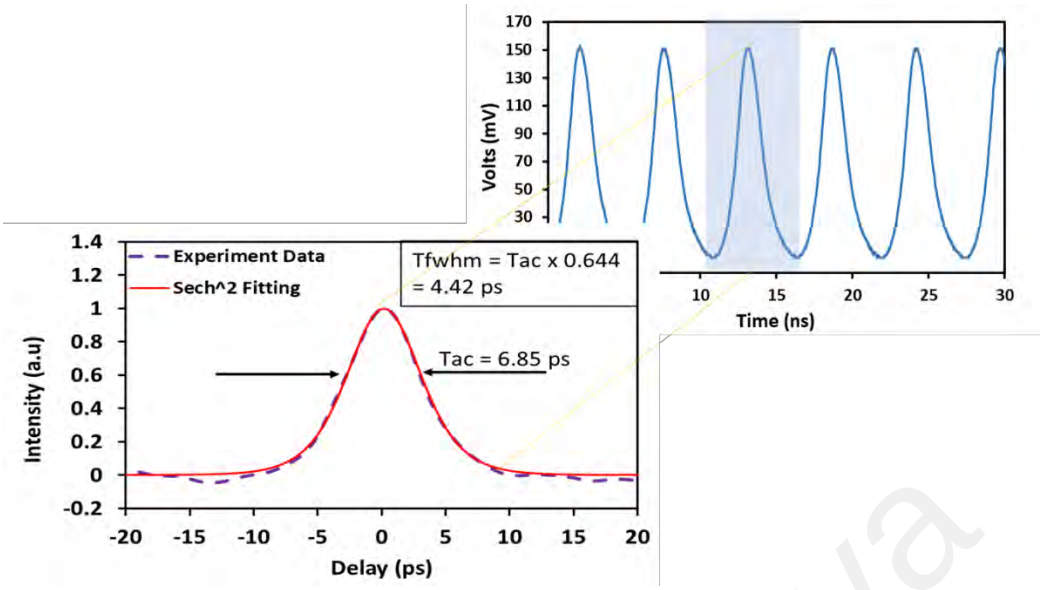

Figure 2.9: Typical autocorrelation pulse envelope of a mode-locked fiber laser. The inset figure shows the corresponding oscilloscope pulse train.

Peak power P_p is the highest instantaneous optical power level in the pulses. It is also defined as a rate of energy flow in every pulse envelope. A short pulse width can generate higher peak power even for the moderately energetic pulses. By dividing the pulse energy by the pulse width, the peak power can be written as:

$$P_p[W] = \frac{Q}{\tau} \tag{2.11}$$

where Q is the pulse energy and τ is the pulse width. The conversion of the peak power depends on the temporal shape of the pulse. As discussed earlier, the transform limit of the single envelope is only represented in Gaussian function or Sech^2 function.

Mode-locking can be realized based on two main techniques: active and passive techniques. An active mode-locking happened when an optical modulation device was inserted into the cavity to make the round-trip phase change and reduce modulation losses. Acoustic-optic and electro-optic modulator are the popular optical modulation devices used in the cavity to generate active mode-locking (Malmström, Margulis,

Tarasenko, Pasiskevicius, & Laurell, 2012). A passive mode-locking pulse is produced using SA or self-synchronization using polarization controller (PC) (Nelson, Jones, Tamura, Haus, & Ippen, 1997). The role of SA in the passive technique is to absorb linearly the light enter the cavity until it reaches at certain intensity. When the laser power is achieved at certain level of intensity, the SA becomes saturated and behaves nonlinearly to support pulse production over CW. The passive technique is advantageous in terms of simplicity in fabrication, able to generate pulse without external control devices, and cheaper compared to that of active approaches.

2.6 Saturable absorber

A saturable absorber (SA) is a material in which the absorption of light decreases nonlinearly with increasing incident light intensity. It is incorporated into a laser cavity for pulse generation. Most of the earlier SAs are fabricated using a semiconductor material where the resonant nonlinearities that involve carrier transitions from the valance to conduction band produces the saturable absorption effect (Okhotnikov & Pessa, 2004). To explain this phenomenon, one often employs simple qualitative arguments based on a two-level electronic model, for which saturable absorption is symmetrical to gain saturation. Fig. 2.10 illustrates the complete process of the SA working mechanism based on a two-level model in the particle form. As shown in the figure, the electrons in the ground state of the lower energy level or valance band (E_1) can absorb photons when their photon energy is the same as the difference between the two levels and be excited to higher energy level or conduction band (E_2) if there is no electron at the upper state. As all the excited electrons populated E_2, the material reaches saturation level whereby it is unable to further absorb the photons according to the Pauli blocking principle. After reaching the E_2 lifetime, electrons decay to the ground state and the saturable absorption process continuously repeated.

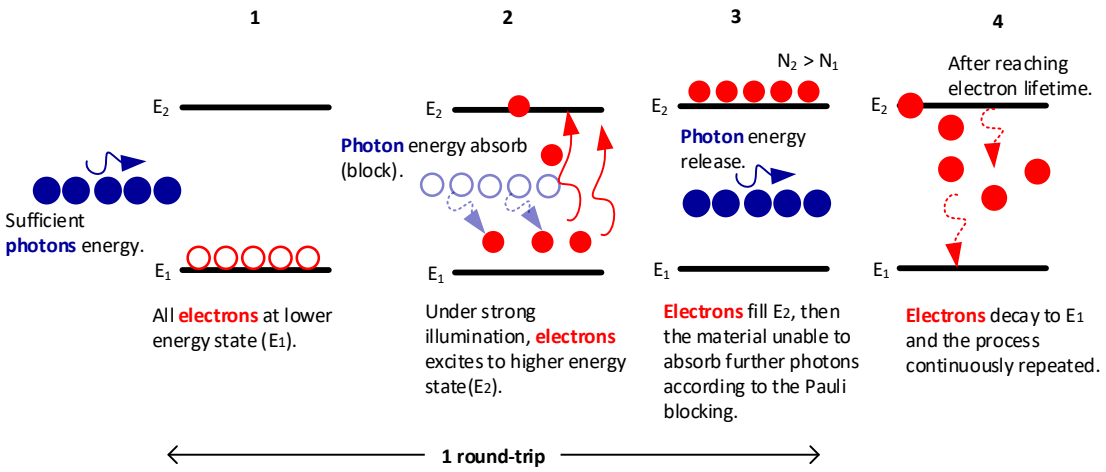

Figure 2.10: Illustration of saturable absorber working mechanism based on a two-level model in particle form.

Up to now, a variety of materials have been proposed and demonstrated for SA applications. SAs are mostly made of elements and compounds of Carbon and Boron groups. They include nanomaterials such as SESAM, graphene, carbon nanotube (CNT), black phosphorus (BP), and transition metal dichalcogenides (TMD). The SESAM is a saturable absorber that operates in reflection; thus, the reflectivity increases with higher incoming pulse intensity. It has gained tremendous interest for commercial mode-locked fiber lasers due to its ultrafast operation. Furthermore, the device design, fabrication process and long-term device reliability have been improved in recent years. However, SESAM device is expensive and is not really reliable for long-term operation (Y. Zhang et al., 2021). Graphene based SAs offer a high absorption spectrum but suffer from a low modulation depth and damage threshold (Z. Dong et al., 2012). CNT based SAs can be easily fabricated at low cost (Hasan et al., 2009; X. Li et al., 2014), but they have a short spectral band, that is heavily influenced by the diameter of the nanotubes (J. Wang et al., 2015). BP based SAs usually have a wide broadband spectrum range but a low nonlinear absorption, low optical threshold and complex fabrication process (Y. Chen, G. Jiang, S. Chen, Z. Guo, X. Yu, C. Zhao, H. Zhang, Q. Bao, S. Wen, D. Tang, et al., 2015). SAs

based on TMD materials such as WS_2 (Mao, Zhang, et al., 2015; Yingying Yang, Yang, Li, & Lin, 2019), SnS_2 (K. Niu, R. Sun, Q. Chen, B. Man, & H. Zhang, 2018a), and $MoSe_2$ (W. Liu et al., 2018) have been shown to have a good absorption property. However, they are affected by a low optical damage threshold and complex fabrication. Therefore, the search for alternative SAs is still ongoing. Table 2.2 summaries the advantage and disadvantages of few SAs. The SA could be integrated into a fiber laser cavity by several approaches such as sandwiching the material in between the fiber ferrules or depositing the SA onto the side-polished fiber (Nizamani et al., 2020).

Table 2.2: Advantages and disadvantages of few types of SAs.

SA	**Advantages**	**Disadvantages**
Semiconductor saturable absorber mirror (SESAM)	• Strongly reduces the tendency for self Q-switching instabilities • Effective saturable absorption • Compact optical setup • Low production volume • Generate high quality pulse	• Expensive electronics • Structure is complicated and difficult to produce • Average power level is low • Long and complex laser cavities
Graphene	• Good, condensed matter properties • Prevent lattice dislocation and crystal imperfection at high temperature • Ultrafast relaxation time	• Limitation of bandgap alteration ability • Low modulation depth
Carbon nanotube (CNT)	• Extraordinary optical, mechanical, electrical and chemical properties • Sub-picosecond recovery time • Low saturation intensity • Ultrafast respones time	• Defect causes electronic properties to modify drastically • CNT from entangled morphologies causing strommng scattering and substantial nonsaturable losses • Ultrashort pulse radiation multiphoton effect oxidation occurs • Degrades long-term stability of absorber

SA	**Advantages**	**Disadvantages**
Transition-metal dichalcogenides (TMDCs)	• Layer-dependant bandgap • High nonlinear optical response	• Difficult to control number of layers • Too low in productivity • Requires specific types of equipment to produce • Expensive and difficult to handle

MAX-phases are polycrystalline materials that contain hexagonal ternary carbides and nitrides. M stands for the front metal element of the transition group; A represents the elements of the main group, mainly the elements of the third group and the fourth group; X is for carbon or nitrogen. Ti_3SiC_2 is one of the most widely studied MAX phase materials (Perevislov et al., 2021). It has been widely concerned by material scientists and physicists due to its unique electronic and optical properties. Ti_3SiC_2 has the characteristics of metal and ceramics. It has the same excellent high-temperature mechanical properties, oxidation resistance and high elastic modulus as ceramic, but also has the same heat conduction and good conductivity capability as metal (Silvestroni et al., 2021).

Recently, a new family of 2D materials called MXenes has gained a tremendous interest for optoelectronics applications due to their excellent electronic and optical properties. MXenes are typically produced by etching their precursor, MAX Phases with strong etching solutions such as ammonium bifluoride (NH_4HF_2), hydrofluoric acid (HF), or a mixture of hydrochloric acid (HCl) and lithium fluoride (LiF) (Ghidiu, Lukatskaya, Zhao, Gogotsi, & Barsoum, 2014; Halim et al., 2014). For instance, a MXene of $Ti_3C_2T_x$ can be obtained by selectively removing the aluminum (Al) atoms from the MAX-phase Ti_3AlC_2 using a HF solution (Halim et al., 2016). Recently, the saturable absorption properties of MXenes, such as Ti_3CT_x and $Ti_3C_2T_x$, have been extensively investigated and their excellent performance comparable to those of other 2-dimensional

(2-D) materials has been well demonstrated (X. Jiang et al., 2018). However, there are remaining questions whether MAX-phase, the seed material for MXene synthesis, by itself possesses saturable absorption properties, which are suitable for implementation of Q-switching and mode-locking. Compared to MXenes, MAX phases do not require the use of strong etching solutions, thus simplifying fabrication process and minimizing the cost. In this thesis, the experimental investigation of the saturable absorption properties of the MAX-phase Ti_3SiC_2 and MXene $Ti_3C_2T_x$ are carried out and reported.

CHAPTER 3: PREPARATION AND CHARACTERIZATION OF SATURABLE ABSORBERS

3.1 Introduction

The generations of Q-switched and mode-locked pulses have received tremendous interests in recent years due to their potential applications in many areas such as metrology, material processing, biochemistry, and optical communication (Sharma, Kim, & Kang, 2004; Shi, Fang, Zhu, Norwood, & Peyghambarian, 2014; Sugioka & Cheng, 2014a). This is attributed to their ability to produce a high beam quality in an alignment-free and compact structure. Active and passive approaches are two important methods to produce Q-switching and mode-locking pulses. The active technology is complex and needs external bulk laser devices such as electro-optic modulators to be used in the laser cavity (Nikodem et al., 2008). On the other hand, the passive techniques require saturable absorber (SA) and more attractive due to their advantages of simplicity, compactness, and implementation flexibility (X.-X. Shang, L.-G. Guo, H.-N. Zhang, D.-W. Li, & Q.-Y. Yue, 2020). The SA functions to modulate the laser light by exploiting its inherent linear and non-linear optical absorption properties. They are cheap, compact, flexible, and easy to construct and use. SAs are mostly made of elements and compounds of carbon and boron groups. They include nanomaterials such as graphene, carbon nanotube (CNT), black phosphorus (BP), and transition metal dichalcogenides (TMD). Graphene-based SAs offer a high absorption spectrum but suffer from a low modulation depth and damage threshold (Martinez & Sun, 2013). CNT based SAs can be fabricated easily and cheaply (M. Ahmed et al., 2015), but they have a short spectral broadband that is heavily influenced by the diameter of the nanotubes. BP based SAs usually have a wide broadband spectrum range but a low nonlinear absorption, low optical threshold, and

complex fabrication process [9]. SAs based on TMD materials such as WS_2 (Yingying Yang et al., 2019), SnS (Niu et al., 2018a) and $MoSe_2$ (W. Liu et al., 2018) have been shown to have a good absorption property. However, they are affected by a low optical damage threshold and complicated fabrication.

Recently, MAX phases and corresponding 2D derivative MXenes have also attracted considerable interests due to their unique properties that have metallic and ceramic elements (Barsoum, 2000; Z. M. Sun, 2011; Xue, Zhang, Tang, & Li, 2014). This can be seen in the large number of publications that appear annually on these materials and their applications. In this thesis, the use of Ti_3SiC_2 MAX phase and $Ti_3C_2T_x$ MXene thin film as SA device are explored for pulse generation. In this chapter, the preparation and characterization of these SAs are thoroughly described.

3.2 Preparation of Saturable Absorber

Two materials used in this study are Ti_3SiC_2 MAX phase and $Ti_3C_2T_x$ MXene. In this section, the fabrication and characterization of these materials are described.

3.2.1 Ti3SiC2 MAX phase

SA operation is based on light absorption saturation due to Pauli's blocking principle. It has commonly been fabricated by using III-V compound semiconductors. Despite widespread implementation of III-V semiconductor-based SAs, there are still many practical and technical issues with these materials, such as their complicated and expensive fabrication processes. To overcome these drawbacks, alternative SA materials have been intensively investigated as previously discussed.

More recently, transition metal carbides including MAX phases have also gained great interest due to their excellent optical and electrical properties. They have a

hexagonal polycrystalline form made of carbide and nitride. The general formula is Mn +1AXn, where M is an early transition metal, A is an A-group element in the periodic table (usually IIIA and IVA), X is carbide or nitride, and n is an integer (Sokol et al., 2019). This ternary compound has unique characteristics that combine merit properties of metals and ceramics. Like metals, it has excellent thermal (~37 W/m·K) and electrical (~4.5 × 106 Ω−1 m−1) conductivities, relatively low hardness (~4 GPa) which makes it easy to machine like common metal or graphite, high Young modulus (~325 GPa), and moderate flexural strength (260–600 MPa), it is not susceptible to thermal shock, and it has damage tolerance at high temperatures (Radovic & Barsoum, 2013). It also duplicates several ceramic properties such as good oxidation resistance of up to 1400°C, relatively low density (~4.52 g/cm^3), and high decomposition temperature (~1700°C), and some researchers have also reported that its melting temperature is up to 3000°C (Z. Sun, 2011). These properties are beneficial for many applications including biosensors, electrochemical capacitors, catalysts, and optical devices (Gonzalez-Julian, 2021). MAX-phases have a hexagonal polycrystalline form made of carbide and nitride.

This dissertation aims to experimentally demonstrate the generation of Q-switched and mode-locked laser pulses using a titanium-silicon carbide (Ti_3SiC_2) material as SA. Ti_3SiC_2 is a ternary layered carbide known as MAX phase compound. It is a low-cost and bulk material, which exhibits performance comparable to the ones based on 2-D materials. Herein, we report the preparation of a fiberized SA based on Ti_3SiC_2 polyvinyl alcohol (PVA) composite thin film.

To fabricate a saturable absorber for this experimental demonstration, commercially available titanium silicon carbide Ti_3SiC_2 powder (99.9%, Shanghai Winfay Industry Ltd.) was used with polyvinyl alcohol (PVA) to form a composite. Ti_3SiC_2 powder (10 mg) was first dissolved in isopropyl alcohol (IPA) solution. After stirring for 24 hours, 10 ml of this solution was mixed with 10 ml of PVA solution, which was obtained by

dissolving 10 mg of PVA into 20 ml of distilled water. After stirring the mixture solution for 24 hours, a small amount of the composite solution was directly poured into a Petri-dish and left for 3 days to dry at room temperature. Finally, the dried Ti_3SiC_2/ PVA thin film was then peeled out and cut to a tiny piece. The preparation of the SA thin film is summarized in Fig. 3.1.

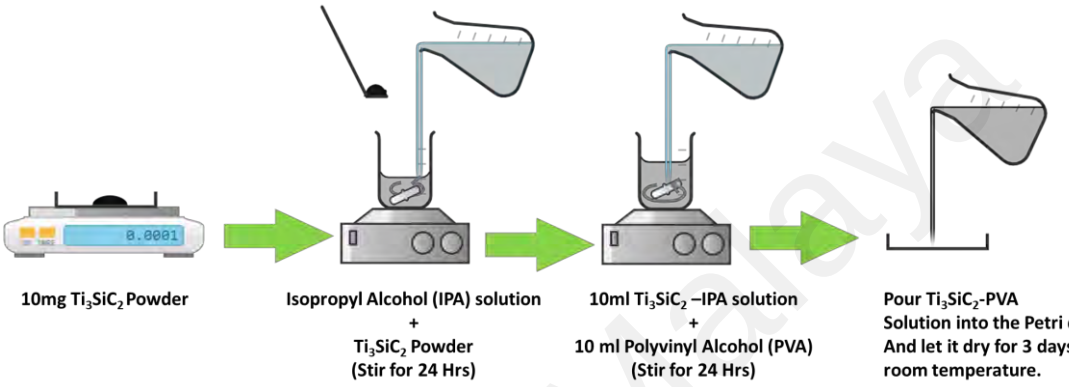

Figure 3.1: Preparation of Ti_3SiC_2/ PVA thin film

The developed thin film was then characterized using a Scanning Electron Microscope (SEM) as shown in **Figure 3.2**. It clearly showed that the Ti_3SiC_2 powder was thoroughly mixed with a PVA host polymer. A high density of micro-grains was also clearly seen on the film's surface. The micro-grains are in irregular shapes and distributed randomly on the surface. The average size of these grains is less than 100 nm.

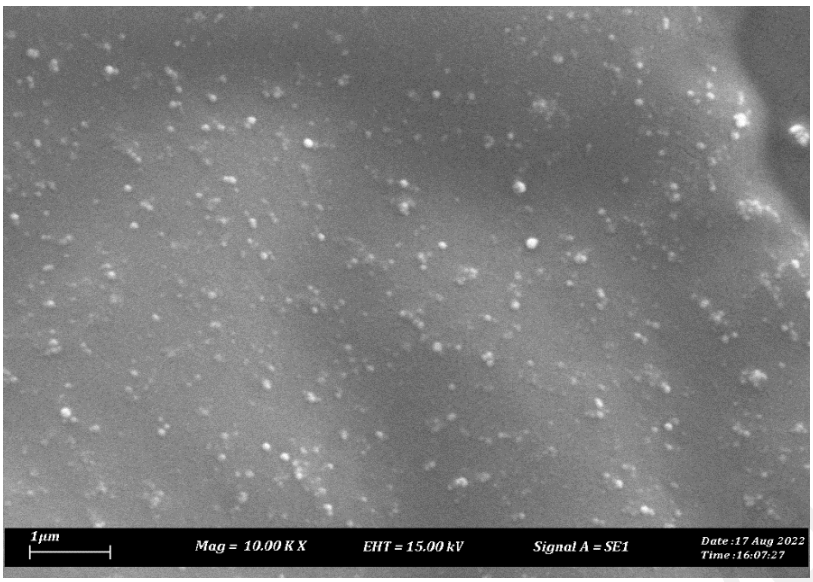

Figure 3.2: The SEM image of the thin film

The elemental constituent of the Ti_3SiC_2 used in this work was then analysed using an Energy Dispersive X-ray Spectroscopy (EDS) as shown in Figure 3.3. Strong peaks that correspond to carbon (C), silicon (Si) and titanium (Ti) were clearly visible in the EDS profile. It indicates that the material consists of 84.07 weight % of carbon, 4.40 weight % of silicon and 11.53 weight % of titanium.

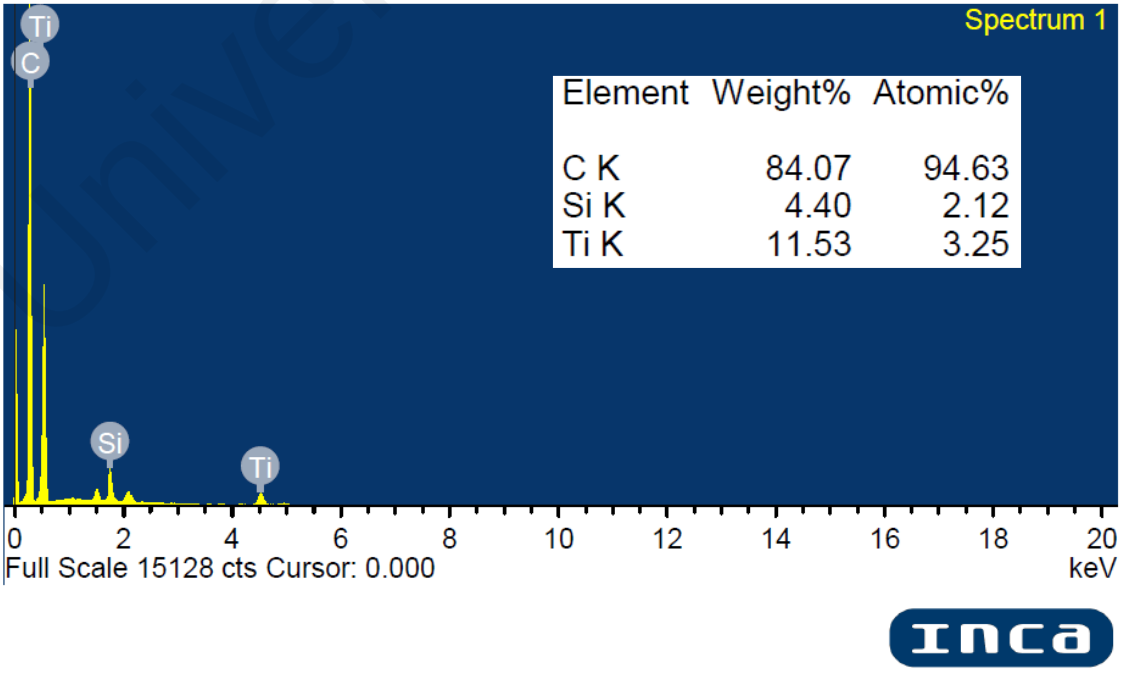

Figure 3.3: EDS analysis for the Ti_3SiC_2 MAX phase compound used in this study

3.2.2 Ti3C2Tx MXene

Recently, a ternary metal carbide/nitride so-called MXene was also gained interests as a new member for 2D material class (Zhenhong Wang et al., 2020). It has a general formula of Mn+1XnTx, where M is transition metal, X is a carbon or nitrogen with n =1,2,3…, and T is a face-termination group likes oxygen or fluorine. MXene can be produced by selectively etching of MAX layer. The MXene has been previously utilized in various photonic applications due to its excellent optical, thermal, and physical properties (Y. Dong et al., 2018). It has many advantages such as small band gap size, metallic conductivity, and hydrophilic nature of its surface. Mxene also has an excellent saturable absorption characteristic, which is suitable for photonic diodes (Y. Dong et al., 2018). It is also reported that the MXene also exhibits the zero-bandgap structure, which can be potentially used for the broadband optical device (Y. Dong et al., 2018). One of the objectives of this dissertation is to demonstrate the generations of Q-switched and mode-locked laser pulses using a MXene material as SA. MXene owns the ability to erase the procedure obstacle of tunable bandgap and monolayer dispersion. The titanium carbide ($Ti_3C_2T_x$) was chosen as the main compound due to its graphene-like but highly tunable and tailorable electronic/optical properties (X. Jiang et al., 2018). Furthermore, it was reported to have a high optical damage tolerance, which makes it a preferrable SA, in comparison to other 2D-based materials. In this subsection, the preparation of the $Ti_3C_2T_x$ is discussed.

The MXene material was prepared from the layered ternary carbides and/or nitrides (MAX phases). The titanium carbide Ti_3AlC_2 MAX phase used was obtained from Shanghai Winfay Industry Ltd. We performed selective etching of Ti_3AlC_2 MAX phase with 50% wt% hydrofluoric acid to fabricate MXene $Ti_3C_2T_x$. The method took place at

room temperature for 6 hours. Then, we obtained the sample of $Ti_3C_2T_x$ through vacuum-assisted filtration by polyvinyl difluoride filter membrane. It was dried with a vacuum oven at 80 ° C for 24 hours for formation of clay. The powder was collected and put into a clean beaker. Next, 20 mg of $Ti_3C_2T_x$ MXene powder was mixed with 10 mg of polyvinyl alcohol (PVA) powder and 40 ml of distilled water. The mixture was then agitated at room temperature for 24 hours. We used the ultrasonic bath for 2 hours to separate the agglomerate of $Ti_3C_2T_x$ particles by cavitation. Consequently, about 5 mL of the $Ti_3C_2T_x$ solution was placed inside a clean petri dish and left for 48 h to dry. At last, the dried $Ti_3C_2T_x$ MXene film was peeled out and cut to a tiny piece. Fig. 3.4 shows FESEM image of the developed MXene $Ti_3C_2T_x$, showing the $Ti_3C_2T_x$ particle distribution in the film. Inset of Fig. 1 shows the actual image of the film, which has a thickness of around 50 µm.

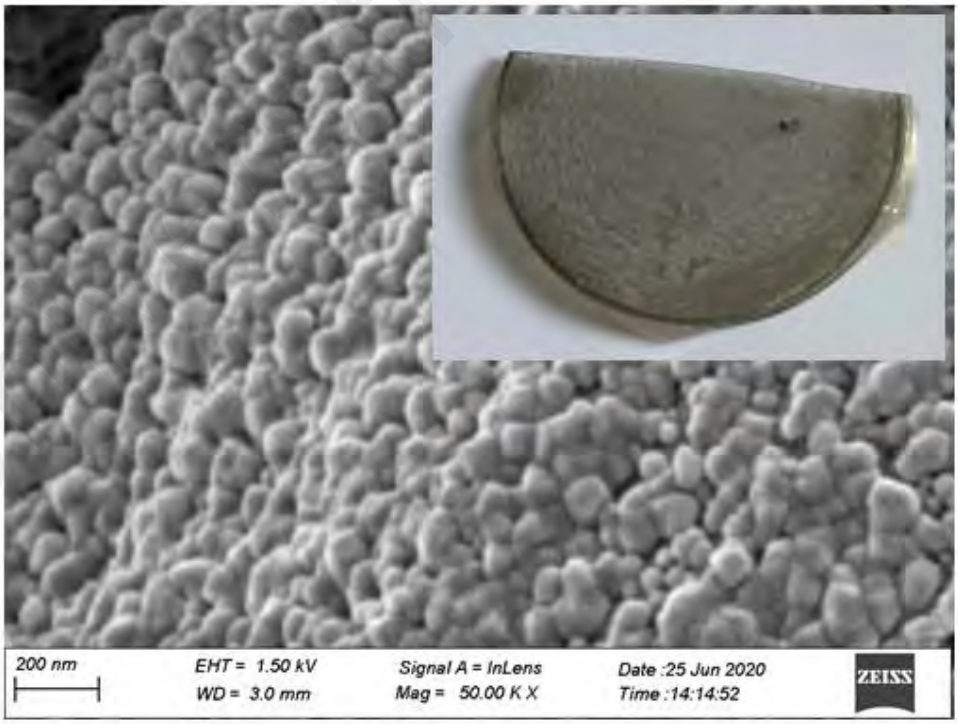

Figure 3.4: FESEM image of the prepared MXene $Ti_3C_2T_x$ film. Inset shows the actual image

Energy Dispersive X-ray Spectroscopy (EDS) analysis was then conducted to investigate the elemental constituent of the prepared MXene $Ti_3C_2T_x$ film. The result is shown in Figure 3.5. The elemental analysis indicates that only 5.61 weight % of carbon was detected, whereas oxygen represents 34.34 weight % of the material. The content of aluminium and titanium element was 2.66 weight % and 57.39 weight %, respectively. Hence, it confirmed the elemental distribution of the $Ti_3C_2T_x$ SA.

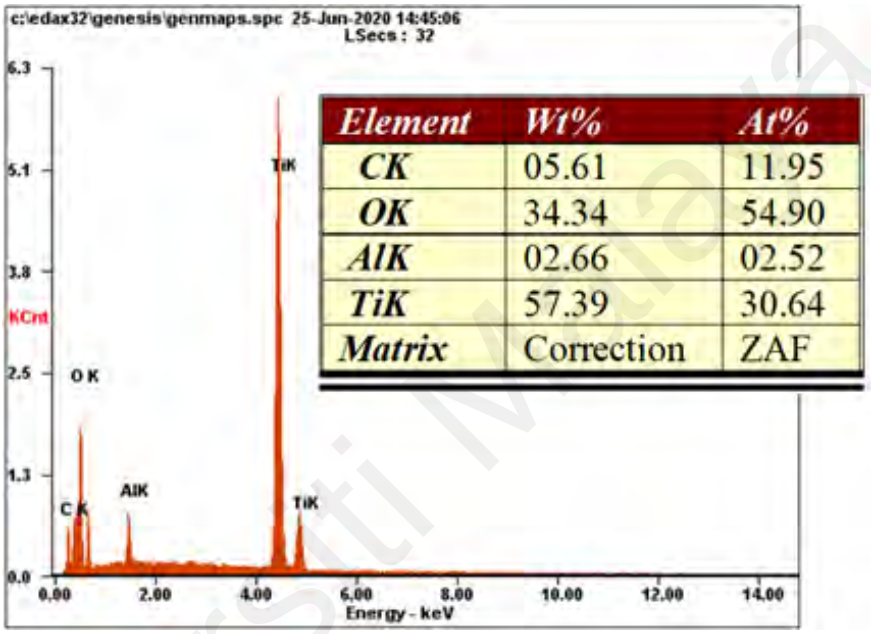

Figure 3.5: EDS analysis for the prepared MXene $Ti_3C_2T_x$ film

3.3 Linear and Nonlinear Absorption Characteristics of The Fabricated Thin Films

In this section, the linear and nonlinear characteristics of two fabricated SA thin films: Ti_3SiC_2/PVA and $Ti_3C_2T_x$/PVA thin films are presented. the optical properties of fabricated SA thin films are analyzed using self-constructed linear and nonlinear absorption set-ups. The linear absorption set-up consists of a white light source that is connected to an OSA as shown in **Fig. 3.6**. The OSA was set to cover a broad near-infrared region, extending from 600 nm to 1700 nm wavelength span.

The nonlinear absorption of the prepared thin film was then characterized by utilizing a twin balance detection technique as shown in Fig. 3.7. The light source was a home-built mode-locked laser operating at 1561.1 nm with a repetition rate of 0.9 MHz and a pulse width of ~6.4 ps. The output port of the laser was connected to the erbium-doped fiber amplifier (EDFA), and then to the variable optical attenuator (VOA) to tune the output intensity of the laser. A 3 dB coupler was used after the attenuator to split the beam power equally into two portions. The first portion was directly connected to the optical power meter as a reference power. The other portion passed through thin film, and the transmission power was recorded by another optical power meter.

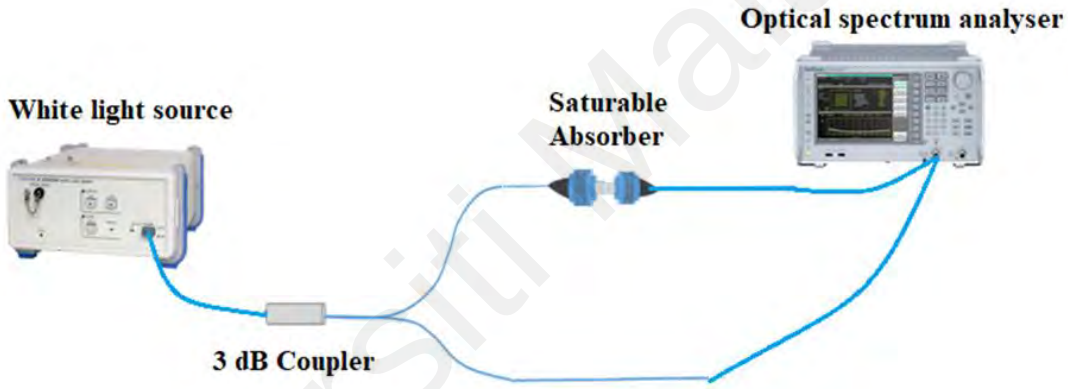

Figure 3.6: Measurement setup for linear absorption

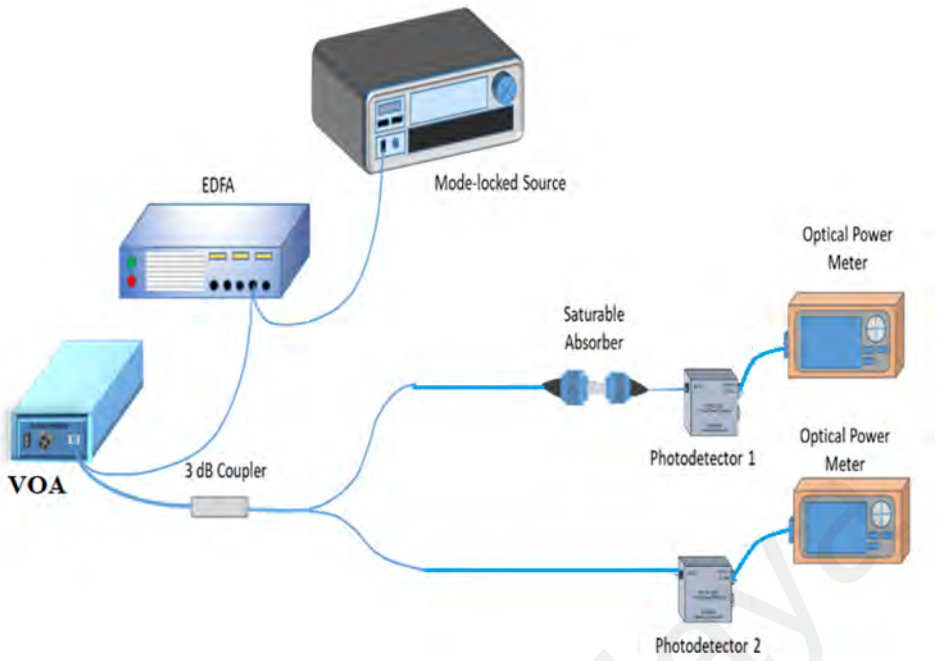

Figure 3.7: Measurement setup for nonlinear absorption

3.3.1 Ti_3SiC_2/PVA

The linear absorption of the fabricated Ti_3SiC_2/PVA thin film was also investigated using a broadband light source and optical spectrum analyzer (OSA) in the range of 1000 nm to 1600 nm, see Fig. 3.8. The absorption spectrum shows a constant loss which implies that the film holds a broadband resonance wavelength like graphene. As shown in Fig. 3.8, the SA thin film exhibits linear absorption of around 3.7 dB at 1550 nm wavelength region. Fig. 3.9 shows the nonlinear optical absorption of the Ti_3SiC_2/PVA thin film, which is obtained by utilizing a balanced twin detector technique as described previously. The results of the saturable absorption (α_0), the saturation intensity (I_{sat}) and the non-saturable absorption loss (α_{ns}) were fitted by the following saturation model formula (Wu et al., 2018):

$$\alpha(I) = \frac{\alpha_0}{1+\frac{I}{I_{sat}}} + \alpha_{ns} \qquad (3.1)$$

The saturable absorption, saturation intensity, and non-saturable absorption of the Ti_3SiC_2 film were estimated to be 51%, 0.03 MW/cm^2, and 30%, respectively. The strong saturable-absorption property of the fabricated Ti_3SiC_2/PVA thin film at 1550 nm regime indicates that this device could be used as a SA to modulate the cavity loss for Q-switching pulse generation.

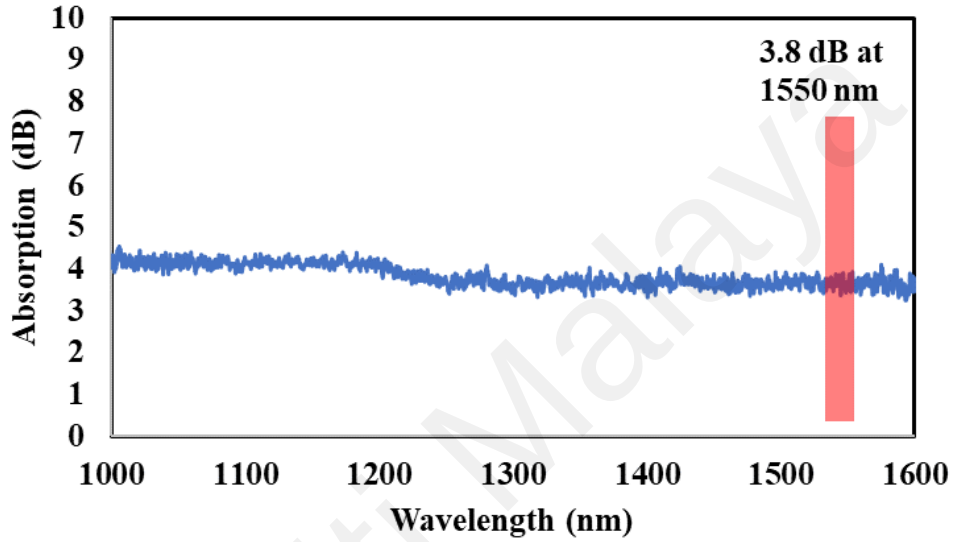

Figure 3.8: Linear absorption curve for the Ti_3SiC_2/PVA thin film

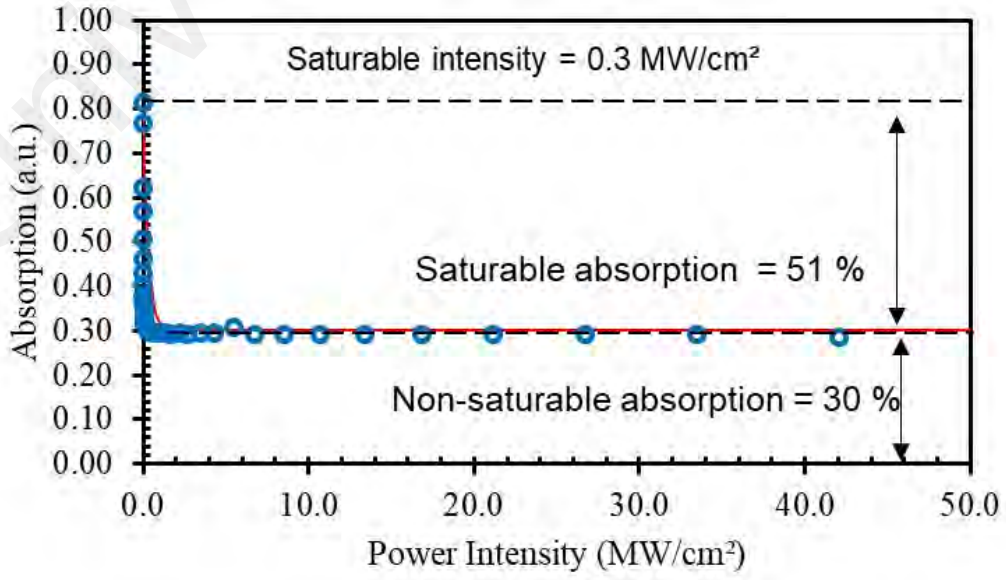

Figure 3.9: Nonlinear absorption curve for the Ti_3SiC_2/PVA thin film

3.3.2 $Ti_3C_2T_x$/PVA

To experimentally validate our theoretical prediction for the outstanding photonic performance of highly stacked $Ti_3C_2T_x$ MXene, the intensity-dependent optical absorption behaviour of the thin film was also investigated. The linear absorption of the prepared $Ti_3C_2T_x$/PVA film was also characterized by using the wide light source in conjunction with OSA as previously described and the result is shown in Fig. 3.10. It has an absorption of about 2.2 dB at 1550 nm region. The MXene has a 2D stacking layer and thus its absorption loss is lower compared to the bulk Ti_3SiC_2. It shows that the Ti_3SiC_2 thin film can be readily used in implementations requiring SA operating in 1550 nm region.

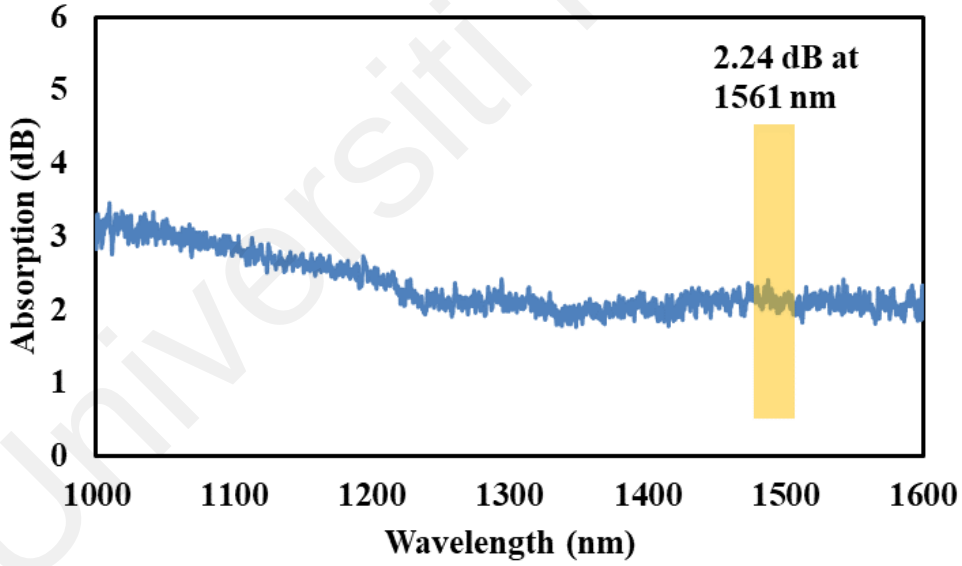

Figure 3.10: Linear absorption curve for the $Ti_3C_2T_x$/PVA thin film

The nonlinear absorption of the prepared $Ti_3C_2T_x$/PVA thin film was then characterized by utilizing a twin balance detection technique. Equation (3.1) was used for the fitting of the nonlinear optical absorption curve of the $Ti_3C_2T_x$ SA device. Noticeably, significant nonlinear optical absorption has occurred in the $Ti_3C_2T_x$/PVA thin film. Fig.

3.11 shows the nonlinear optical profile for the MXene film, which was obtained by comparing the output power spectrum with and without the SA. The saturable intensity, saturable absorption and non-saturable absorption of the film were measured to be about 20 MW/cm^2, 4.8%, and 3.6%, respectively. The measured saturable absorption or modulation depth is examined to be comparable with the others SA (Liu et al. 2014; Wang et al. 2016). The strong saturable-absorption property of the $Ti_3C_2T_x$/PVA film at 1550 nm region indicates that this device could be used as a fast optical switch for Q-switched and mode-locked pulse generation.

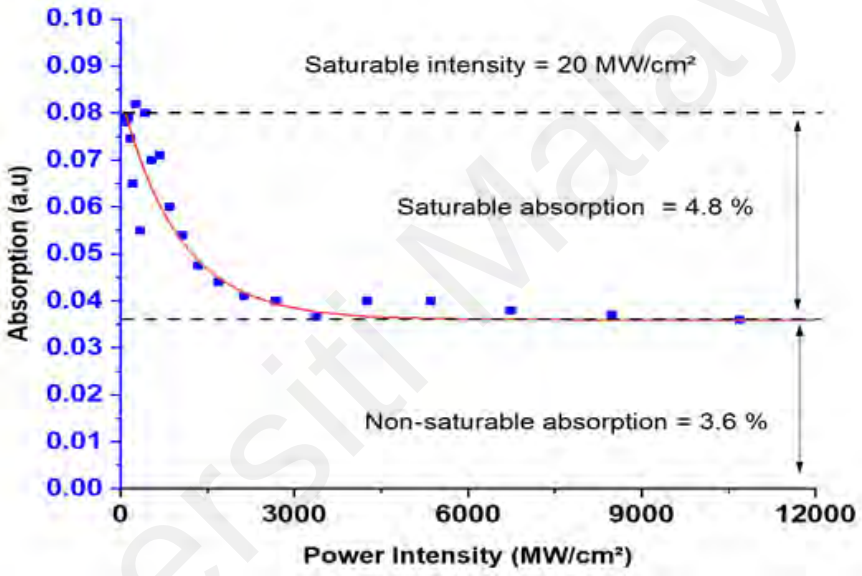

Figure 3.11: Nonlinear absorption curve for the $Ti_3C_2T_x$/PVA thin film

3.4 Summary

Two types of thin film-based SA were successfully developed based on drop casting technique. Transition metal carbide materials of Ti_3SiC_2 MAX phase and $Ti_3C_2T_x$ MXene were selected as a base material and PVA was used as a host polymer. These thin films were also successfully characterized in terms of linear and nonlinear absorption. The Ti_3SiC_2 and $Ti_3C_2T_x$ thin films have a modulation depth of 51 %, 4.8 %, respectively and thus suitable for Q-switching and mode-locking applications.

CHAPTER 4: RESULTS AND DISCUSSION

4.1 Introduction

Q-switched and mode-locked fiber lasers have become mature technology, facilitating a broad range of applications, including remote sensing, material processing, medicine, range finding and telecommunications. This is attributed to their ability to produce a high beam quality in an alignment-free and compact structure. Q switching is obtained by modulating the loss of optical resonator cavity loss or the quality factor (Q-factor. On the other hand, mode-locking is realized by locking the multiple axial modes in the laser cavity. It generates a train of high pulse repetition rate usually in MHz regime by enforcing coherence between the phases of different modes. This process also produces extremely narrow pulses separated by equal time intervals. Active and passive approaches are two important methods to achieve both types of lasers. The active technology is complex and needs external bulk laser devices such as electro-optic modulators to be used in the laser cavity (H. Chen, Chen, Jiang, & Hou, 2015). On the other hand, the passive techniques require saturable absorber (SA) and more attractive due to their advantages of simplicity, compactness, and implementation flexibility (Ursula Keller, 2003c). The SA functions to modulate the cavity loss or to assist in enforcing coherence between the phases of different axial modes for generating Q-switched or mode-locked pulse, respectively (S. Salam, W. R. Wong, A. Al-Masoodi, & S. W. Harun, 2019a). They are cheap, compact, flexible and easy to construct and use (Ursula Keller, 2003b).

In the previous chapter, two types of thin film based SAs: Ti_3SiC_2 MAX phase and $Ti_3C_2T_x$ MXene were successfully developed based on drop casting technique. In this

chapter, Q-switched and mode-locked fiber lasers are demonstrated by incorporating the newly developed SAs in an Erbium-doped fiber laser (EDFL) cavity.

4.2 Q-switched Pulse Generation with Ti_3SiC_2 MAX phase

Q-switched fiber lasers have attracted much attention in recent years for wide-range of applications including metrology, material processing, biochemistry and optical communication (Sugioka & Cheng, 2014b). This is attributed to their ability to produce a high beam quality in an alignment-free and compact structure. Active and passive approaches are two important methods to achieve Q-switching for generating short pulses. The active technology is complex and needs external bulk laser devices such as electro-optic modulators to be used in the laser cavity (H. Chen et al., 2015). On the other hand, the passive techniques require saturable absorber (SA) and more attractive due to their advantages of simplicity, compactness, and implementation flexibility (Ursula Keller, 2003c). The SA functions to modulate the Q-factor of a laser cavity to produce Q-switched pulse (Salam et al., 2019a). They are cheap, compact, flexible and easy to construct and use (Ursula Keller, 2003b). SAs are mostly made of elements and compounds of Carbon and Boron groups. They include nanomaterials such as graphene, carbon nanotube (CNT), black phosphorus (BP), and transition metal dichalcogenides (TMD). Graphene based SAs offer a high absorption spectrum but suffer from a low modulation depth and damage threshold (Z. Dong et al., 2012). CNT based SAs can be fabricated easily and cheaply (Hasan et al., 2009; X. Li et al., 2014), but they have a short spectral broadband that is heavily influenced by the diameter of the nanotubes (J. Wang et al., 2015). BP based SAs usually have a wide broadband spectrum range but a low nonlinear absorption, low optical threshold and complex fabrication process (Y. Chen, G. Jiang, S. Chen, Z. Guo, X. Yu, C. Zhao, H. Zhang, Q. Bao, S. Wen, D. Tang, et al., 2015). SAs based on TMD materials such as WS_2 (Mao, Zhang, et al., 2015; Yingying Yang et al., 2019), SnS_2 (Niu et al., 2018a), and $MoSe_2$ (W. Liu et al., 2018) have been shown to

have a good absorption property. However, they are affected by a low optical damage threshold and complicated fabrication.

More recently, transition metal carbides including MAX phases have also gained great interest due to their excellent optical and electrical properties (Radovic & Barsoum, 2013). They have a hexagonal polycrystalline form made of carbide and nitride with a general formula of $M_{n+1}AX_n$,; M is an early transition metal, A is an A-group element (usually IIIA and IVA), X denotes either nitride or carbide (Sokol et al., 2019). The MAX phase is a useful material for high temperature, nuclear and aerospace applications due to its unique properties that combine the merits of ceramics and metals (Hoffman et al., 2012). It duplicates metal properties like excellent electrical and thermal conductivities, relatively low hardness, high modulus of elasticity, insensitive to thermal shock, moderate flexural strength, and high damage tolerance at high temperatures (Jin et al., 2020). Like ceramic, it has a good oxidation resistance of up to 1400°C, relatively low density, and high decomposition and melting temperature (Silvestroni et al., 2021). These properties are beneficial for many applications including electrochemical capacitors, sensors, catalysts, and optical devices (Gonzalez-Julian, 2021). MAX-phases have a hexagonal polycrystalline form made of carbide and nitride.

In this section, the demonstration of Q-switched pulse generation is reported utilizing a titanium-silicon carbide (Ti_3SiC_2) material as SA. Ti_3SiC_2 belongs to a ternary layered carbide or MAX phase material (Perevislov et al., 2021). It was chosen as the SA to investigate whether a low cost and bulk material could be used to realize Q-switched pulses with performance comparable to the previous 2D nanomaterials. Herein, we demonstrated the use of a fiberized SA based on Ti_3SiC_2 polyvinyl alcohol (PVA) composite thin film for generating Q-switched pulses operating at 1.5-μm wavelengths. By integrating the proposed SA into an Erbium-doped fiber laser (EDFL) cavity, self-

started Q-switched pulses operating at 1561.8 nm were successfully realized.

Fig. 4.1 shows the experimental schematic of the proposed Q-switched fiber laser configuration. The laser cavity comprises of a 980/1550 nm wavelength division multiplexer (WDM), a 2.4 m long Erbium-doped fiber (EDF) (Fibercore, I25), an optical isolator, an optical coupler (OC), and SA device. The EDF used as a gain medium has an absorption coefficient of 23.9 dB / m at 979 nm. The numerical aperture, core diameter and clad diameter of the fiber are 0.24, 5.8 μm, and 125.4 μm, respectively. A 980-nm laser diode was employed as a pumping source. It was coupled into the gain medium through a WDM. The isolator was deployed after EDF to obtain unidirectional light propagation within the laser cavity. The laser output was extracted via the 20% port of an 80:20 OC. The prepared Ti_3SiC_2-based SA was placed after the OC as a Q-switcher. It was constructed by slotting a tiny piece of the prepared Ti_3SiC_2/PVA thin film in between two fiber ferrules. The analysis of the Q-switched pulses was executed by employing an oscilloscope (OSC) (GWINSTEK: GDS-3352), and a radio frequency spectrum analyzer (RFSA) (Anritsu: MS2683A) in conjunction with a photo detector (Thorlabs: DET01CFC). The OCS, RFSA and photodetector have a bandwidth of 350 MHz, 7.8 GHz and 1.2 GHz, respectively. The output power and spectrum of the Q-switched laser were measured by utilizing an optical power meter (OPM) (Thorlabs: PM100D) and an optical spectrum analyzer (OSA) (MS9710C), respectively.

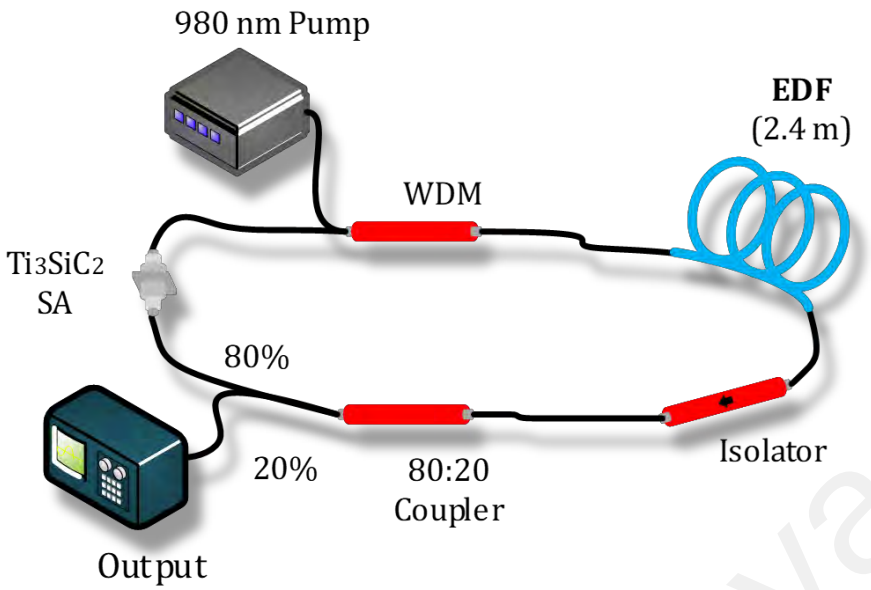

Figure 4.1: The EDFL cavity set-up with Ti_3SiC_2/PVA thin film-based SA for the Q-switching experiment.

The output pulses generated by the EDFL setup were investigated and characterized at various incident pump powers. When the incident pump was raised to 35 mW, stable self-started short pulses were successfully generated, and the Q-switching operation was maintained up to a maximum pump power of 71.5 mW. Fig. 4.2 (a) illustrated the optical spectrum of the output pulses when the pump power is fixed at 35 mW. The laser operated at a center wavelength of 1561.8 nm with a 3-dB bandwidth of about 1.4 nm. Both pulse repetition rate and pulse width were observed to change with the variation of pump power. Above 71.5 mW pump power, Q-switched pulses became unstable and reverted to CW operation. This is most probably due to the excessive heat accumulation under the strong laser signal. It is observed that the Q-switched pulse operation could be recovered when the power was reduced to 71.5 W, demonstrating the superior structural stability of the Ti_3SiC_2/PVA thin film. Mode-locking was not realized in the current experimental setup. This is attributed to the large insertion loss of the prepared SA film. Fig. 4.2 (b) shows the measured output pulse train at 71.5 mW pump power. It indicates a uniform pulse train with a peak-to-peak separation of about 23 μs, which corresponds

to a repetition frequency of 43.5 kHz. The minimum pulse width was obtained at 5.6 µs as shown in the inset figure. The radio frequency (RF) spectrum was also obtained at an input pump power of 35.0 mW, see Fig. 4.2 (c). It indicates a fundamental RF peak at 23.6 kHz, which corresponds well with the oscilloscope trace. The signal-to-noise ratio (SNR) of the fundamental peak is measured to be larger than 46 dB, which attested that the Q-switched EDFL was stable.

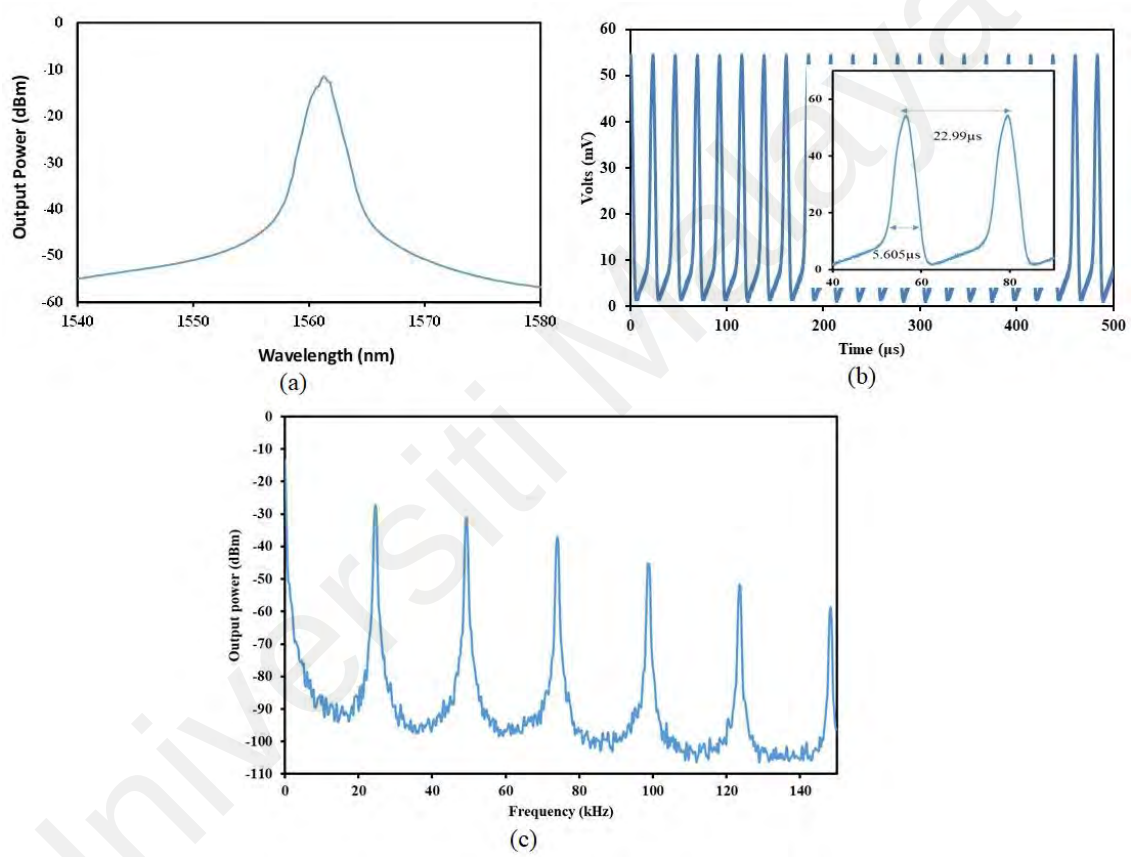

Figure 4.2: Q-switched laser performances with Ti_3SiC_2 based SA. (a) OSA spectrum at the threshold pump power of 35.0 mW (b) oscilloscope trace at the repetition frequency of 43.5 kHz. Inset displays two pulses envelop with a period of about 23 µs (d) RF spectrum at the incident pump of 35.0 mW.

Fig. 4.3 (a) depicts the measured repetition rate and pulse width as a function of the incident pump power. As the incident pump rose from 35.0 mW to 71.5 mW, the repetition rate was increased from 23.6 kHz to 43.5 kHz, whereas the pulse width

decreased from 10.16 µs to 5.61 µs conversely due to a strong pumping-induced gain compression effect. The phenomenon obeys with the typical features of Q-switched fiber lasers (Lee, Kwon, & Lee, 2019; Wu et al., 2018). Fig. 4.3 (b) displays the average output power and calculated pulse energy under different pump powers. As the incident pump power grew from 35.0 mW to 71.5 mW, the average output power was increased from 1.37 mW to 4.38 mW, which attested that the laser efficiency is about 8.27 %. The pulse energy also increased with increase to pump power; the maximum pulse energy was obtained at 100.7 nJ

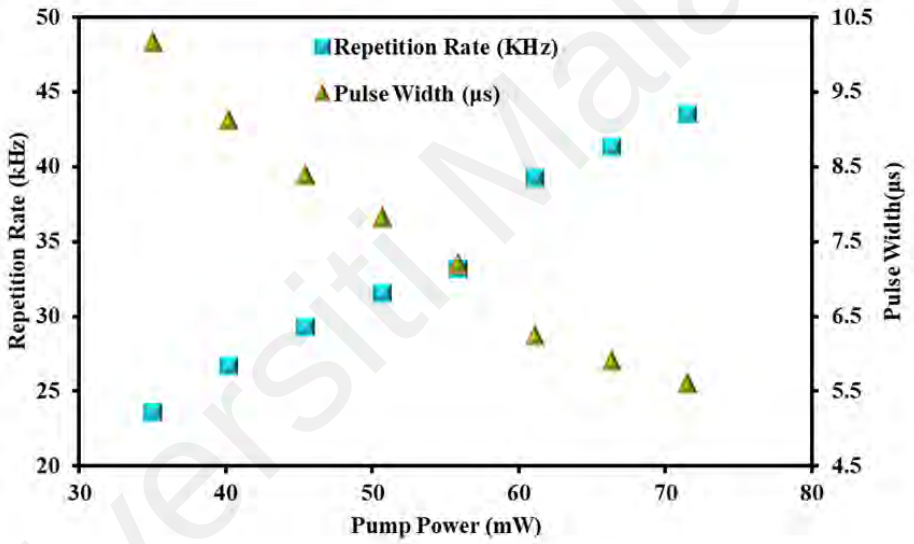

(a)

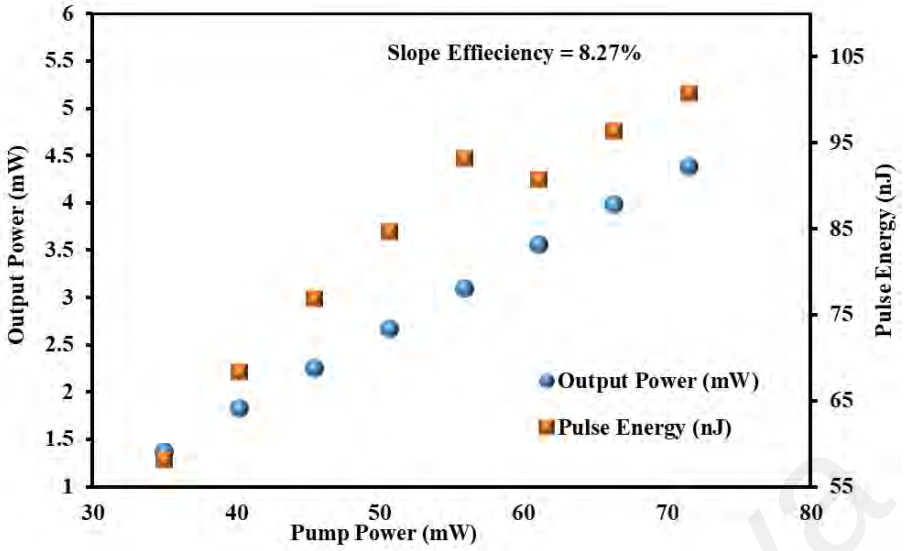

(b)

Figure 4.3: The output characteristics of repetition rate, pulse width, average output power and pulse energy as functions of incident pump power (a) repetition rate and pulse width (b) average output power and pulse energy.

The performance of the proposed Ti_3SiC_2 based Q-switched fiber laser was also compared with that of recently reported, passively Q-switched EDFL using other SA materials, see Table 4.1. The result shows that Ti_3SiC_2 MAX phase has the highest modulation depth, and we obtained the highest pulse energy of 100.7 nJ in the passively Q-switched EDFL. It is apparent from this comparison table that the performance of Ti_3SiC_2-based SA is comparable to other 2D materials. We believe that the improvement of Q-switching performance and the mode-locking operation could be obtained by further optimization of the fiber cavity and SA parameters.

Table 4.1: Performance comparison of several reported Q-switched EDFLs based on 2D material SAs.

SA materials	Modulation depth (%)	Wavelength (nm)	Max. Repetition Rate (kHz)	Min. Pulse Width (μs)	Max. Pulse Energy (nJ)	Ref.
Graphene	NA	1522~1555	103	2	40	(Popa et al., 2011)
Bi_2Te_3	4.1	1558.1	47.1	1.58	17.8	(Lee et al., 2016)
$MoSe_2$	NA	1562.3	32.8	30.4	57.9	(Chen et al., 2015)
WSe_2	3.5	1560	49.6	3.1	33.2	(Woodward et al., 2015)
BP	18.55	1562.87	15.75	10.32	94.3	(B. Chen et al., 2016)
Ti_2AlC	6.3	1559.5	27.45	4.88	22.58	(Lee et al., 2019)
Ti_3SiC_2	51	1561.8	43.5	5.6	100.7	This work

4.3 Mode-locked Pulse Generation with Ti_3SiC_2 MAX phase

Recently, optical pulse train generation via mode-locking has gained notable attention owing to their high peak power and ultrashort pulses. The mode-locked fiber laser can be achieved with the use of saturable absorber (SA) (Yusoff et al., 2020), nonlinear optical loop mirror (NOLM) (Ilday, Wise, & Sosnowski, 2002), and nonlinear polarization rotation (NPR) (Gao et al., 2019). One of the early devices used to generate pulse laser is semiconductor SA mirrors (SESAMs) (Okhotnikov et al., 2004). It was widely used due to its ultrafast recovery time and rate of absorption. After a while, its popularity began to dwindle as it suffers from low damage threshold and narrow bandwidth. It is also expensive to manufacture. The mode-locking can also be realized by using SAs made of different nanomaterials like black phosphorus (Sotor et al., 2015), transition metal dichalcogenides (Wu et al., 2018), graphene (H. Zhang et al., 2010), topological insulator (Yan et al., 2015), and carbon nanotubes (Set, Yaguchi, Tanaka, & Jablonski, 2004). However, these materials also pose their own limitations which restrict

their wide scale implementations. More recently, 2D materials like titanium disulfide (TiS_2) (X.-X. Shang et al., 2020), perovskite (P. Li et al., 2017), and antimonene (Song et al., 2017) have also been employed as SAs for the generation of various optical pulse trains. The TiS_2 SA effectively minimizes the ratio of signal to noise of the generated pulses whereas perovskite possesses low lasing threshold, the thickness of unit cell is low, and its modulation depth is high. The stability of the laser is also improved with the use of antimonene as SA due to their excellent optical response.

Recently, transition metal carbides including MAX phases have drawn attention due to their unique electronic and optical properties, these properties are useful for applications such as electrochemical capacitors, catalysts, water purifiers, biosensors, and photonic devices. In the previous section, a Q-switched pulse generation was demonstrated using Ti_3SiC_2-based SA. Here, we presented a mode-locked EDFL using MAX phase, Ti_3SiC_2-PVA as a SA.

The EDFL cavity used in this study is shown in Fig. 4.4, which comprises a 980 nm laser diode (LD), a wavelength division multiplexer (WDM), an erbium-doped fiber (EDF), an optical isolator, an output coupler, a 100 m long single-mode fiber (SMF) spool, and SA device. The SA device was constructed by slotting a tiny piece of the prepared Ti_3SiC_2 PVA thin film in between two fiber ferrules. The LD pumps in a continuous 980 nm laser to the cavity via a WDM. The WDM is connected to 2.4 m long EDF gain medium that provides lasing in 1.5 μm region. The EDF has a coefficient absorption of 23.9 dB/m at 979 nm. The numerical aperture is 0.24, and the core diameter and clad diameter of the fiber are 5.8 and 125.4 μm, respectively. The isolator maintains a unidirectional laser beam propagation while the OC lets 20% of the laser to be taken out of the cavity for analysis and keeps 80% of it in circulation. The analysis of the mode-locked pulses is executed using a photo detector (Thorlabs: DET01CFC) with a bandwidth of 1.2 GHz, an oscilloscope (OSC) (GWINSTEK: GDS-3352), and a radio

frequency spectrum analyzer (RFSA) (Anritsu: MS2683A). The OSC has a bandwidth of 350 MHz and the RFSA has a bandwidth of 7.8 GHz. In addition, an optical power meter (OPM) (Thorlabs: PM100D) is used to check the output power of the laser, and its spectrum is examined by an optical spectrum analyzer (OSA) (MS9710C). Mode-locked laser requires the phase locking of propagating longitudinal modes within the fiber laser cavity. To achieve mode-locking in EDFL, a 100 m long SMF spool having group velocity dispersion (GVD) of -21:7 ps^2/km was added to the EDFL cavity to balance between the nonlinearity and dispersion. The total cavity length was estimated to be around 106 m, and the total cavity dispersion of this cavity was calculated to be around -2:94 ps^2.

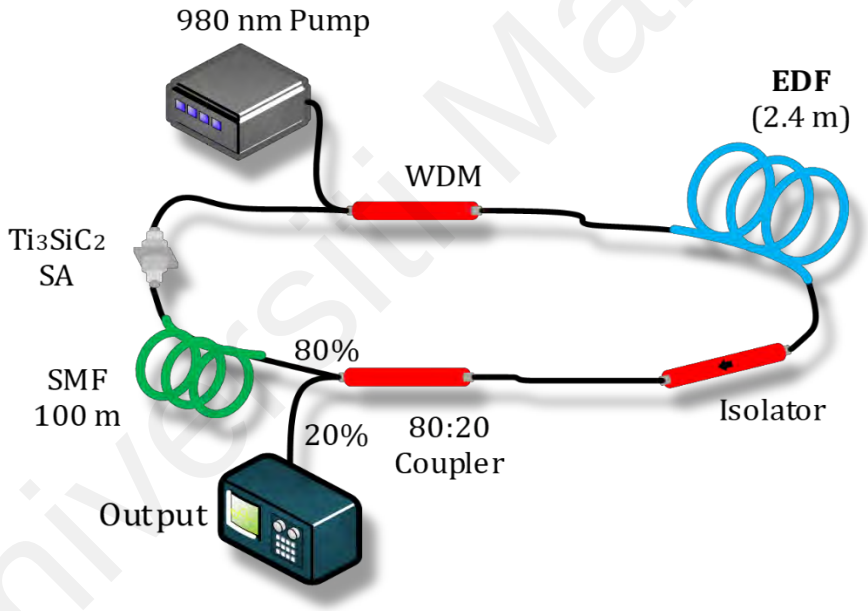

Figure 4.4: The EDFL cavity setup for mode-locked pulse generation.

As the Ti_3SiC_2-PVA is sandwiched between two fiber connectors and incorporated into the laser with addition of 100 m long SMF, a stable mode-locked pulse is realized when the pump power is increased to an appropriate level. The SMF provides a sufficient intracavity dispersion and nonlinearity effect for mode-locking operation. It

is also worthy to note that no pulse train could be obtained without the Ti_3SiC_2-PVA thin film. This suggests that the Ti_3SiC_2-SA plays a major role in starting and stabilizing the pulses. Self-starting mode-locked pulse trace was observed in an oscilloscope when the pump power reached 123.7 mW. The pump power could be increased up to 181.1 mW without losing the mode locking.

Fig. 4.5 (a) depicts the typical output spectrum of the mode-locked laser, which operated at a wavelength of 1559 nm with a 3 dB spectral bandwidth of 1.0 nm. The typical oscilloscope trace at 181.1 mW is depicted in **Fig. 4.5 (b)**. It indicates a stable pulse train with repetition time of 531 ns, which is equivalent to 1.88 MHz repetition frequency. The fundamental cavity frequency of 1.88 MHz well corresponded to a total cavity length of 106 m. The pulse width is measured to be around 100 ns from the oscilloscope trace. The actual pulse duration could not be measured due to low sensitivity of the device. Therefore, the commercial autocorrelator was used for measurement of the autocorrelation of the mode-locked pulse. Fig. 4.5 (c) shows the measured autocorrelation trace alongside a $sech^2$ fit; the corresponding pulse duration is 3.03 ps. The time-bandwidth product (TBP) was calculated to be 0.374, which is 1.18 times larger than that of the transform-limited pulse, indicating that the pulse is slightly chirped. **Fig. 4.5 (d)** displays the RF spectrum measured with 1 MHz resolution bandwidth. It indicates the fundamental repetition frequency of 1.88 MHz, which matches very well with the oscilloscope measurement. This confirms that one pulse is produced per round trip. The signal to noise ratio (SNR) was shown to be more than 74 dB in the inset of Fig. 4.5 (d). It suggests low-amplitude fluctuation and stable mode-locking operation.

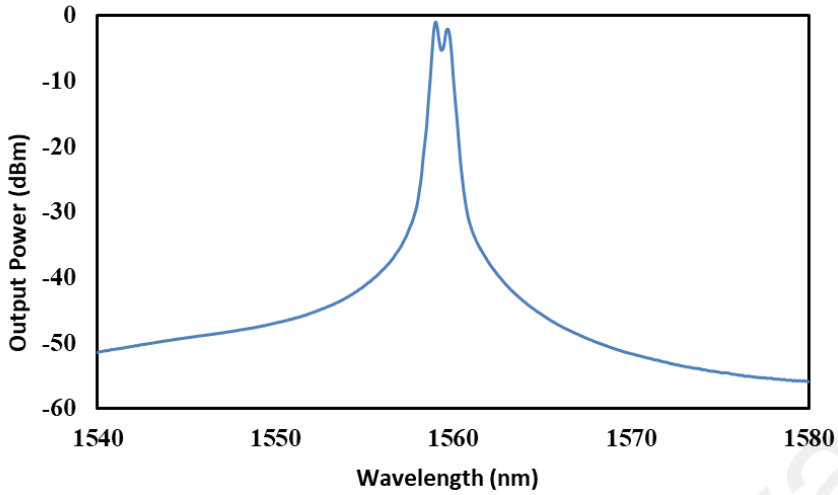

(a)

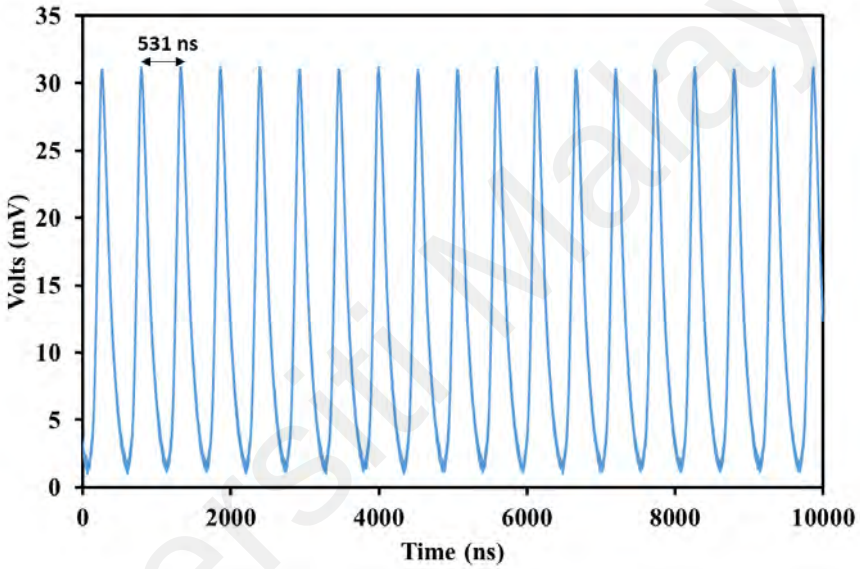

(b)

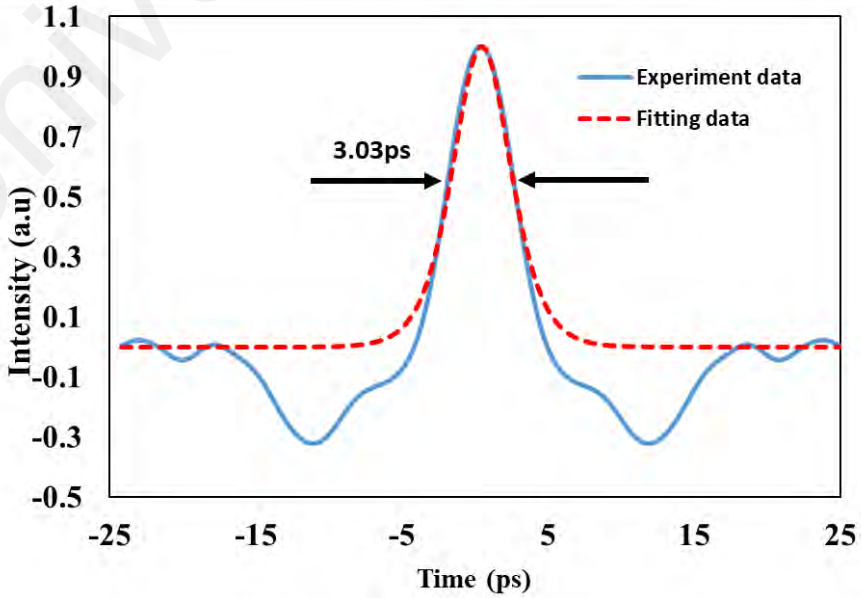

(c)

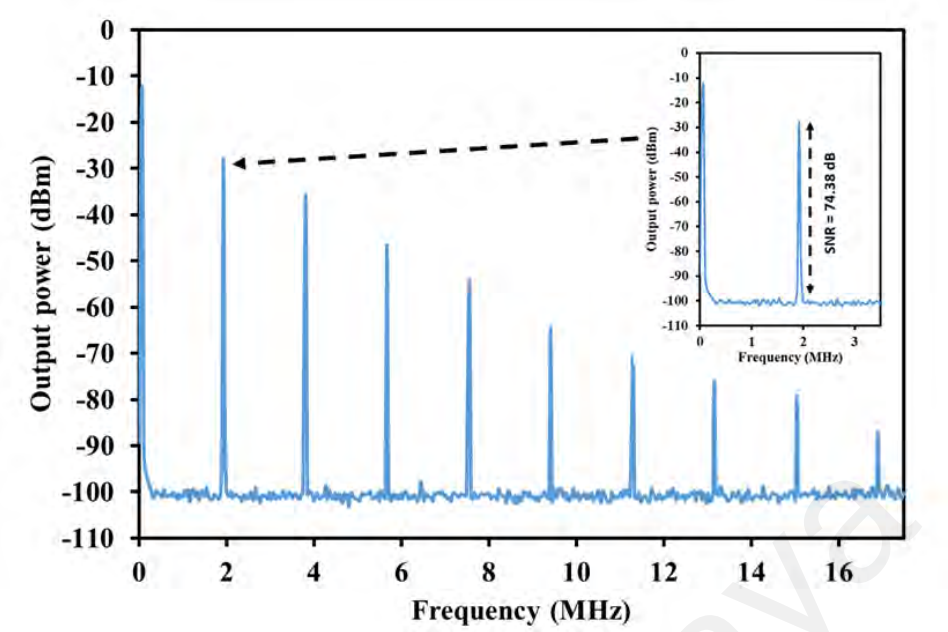

(d)

Figure 4.5: Output performance of the mode locked EDFL based on Ti_3SiC_2 MAX phase SA (a) measured optical spectrum with a 3 dB spectral width of 1.0 nm at 1559 nm (b) typical output pulse train at 181.1 mW showing a repetition time of 531 ns (b) autocorrelation trace of the 3.303 ps output pulses together with a $sech^2$ fit; (d) RF spectrum showing the fundamental frequency at 1.88 MHz with a SNR of 74.38 dB.

Fig. 4.6 (a) shows the change of average output power and pulse energy as the launched pump power was varied. The output power improved linearly from 7.38 to 11.26 mW as the pump power increased from 123.7 to 181.1 mW. It corresponds to an optical conversion efficiency of 6.78 %. The pulse energy also improved from 3.9 to 6.0 nJ as the pump power was increased within the same range. As the pump power increased beyond 181.1 mW, the mode-locked pulse disappeared, and the laser operation became CW. Fig. 4.6 (b) illustrates the relationship between the peak power and the launched pump power. As the pump power increases, the peak power of the mode-locked pulse increases almost linearly. The maximum peak power is measured to be 2 kW at the pump

power of 181.1 mW. Table 4.2 compares the performance of the Ti_3SiC_2 film with other materials as it was employed in EDFL for mode-locking. As seen, the Ti_3SiC_2 SA performance is comparable with other SAs. A mode-locked pulse with improved temporal performance is expected to be achieved by getting the laser cavity shorter.

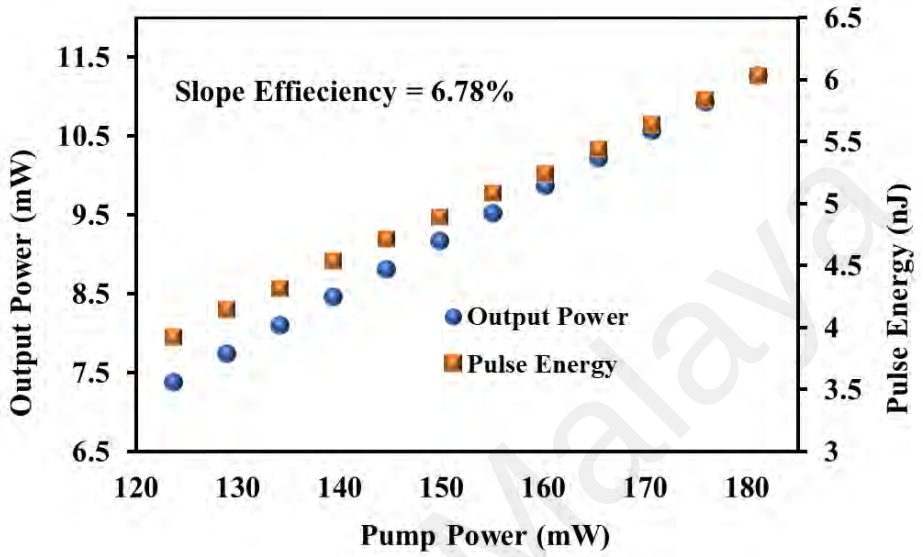

(a)

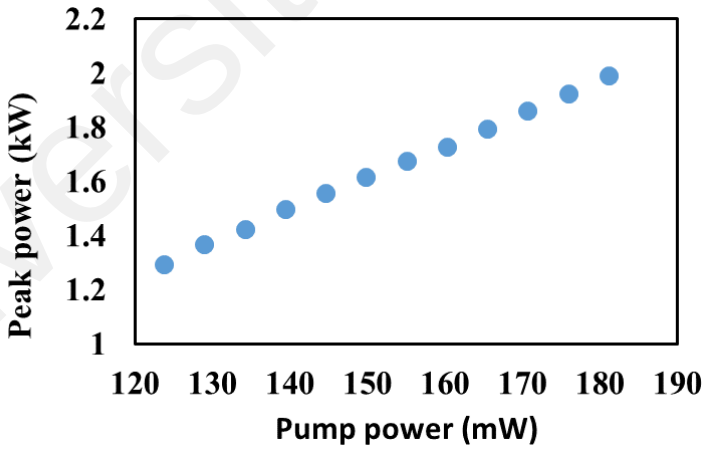

(b)

Figure 4.6: The relationship of (a) the average output power, pulse energy and (b) peak power with the launched pump power.

Table 4.2: Comparison of mode locked EDFL performance with different SAs

SA material	Wavelength (nm)	Repetition rate (MHz)	Pulse duration (ps)	Max. Output Power (mW)	Mod. depth, %	Ref.
CNTs	1550	4.5	1.28	NA	NA	(Cheng et al. 2013)
Graphene	1561	9.9	1	10.5	3.2	(Yang et al., 2014)
Bi_2Te_3	1557	8.6	1.08	NA	2	(Mao et al., 2015)
$MoTe_2$	1559	1.8	2.46	NA	0.62 – 1.46	(Wang et al, 2017)
BP	1586.5	15.2	1.12	NA	4.9	(Wang et al., 2016)
PdS_2	1533.6	7.7	1.83	5.4	6.2	(Wang, et al., 2020)
Tellurene	1574	12.2	8.3	23.6	5.1	(Xu, Ma, et al., 2020)
SnS_2 nanosheet	1562	29.3	0.62	1.2	4.6	(Niu et al., 2018b)
PbS/CdS	1562.5	3.3	54	2.7	7	(Ming et al., 2018)
TiS_2	1531.7	3.43	2.36	3.3	13.2	(Shang et al., 2020)
Ti_3SiC_2	1559	1.88	3.03	11.26	51	This work

4.4 Q-switched Pulse Generation with $Ti_3C_2T_x$ MXene

Recently, a ternary metal carbide/nitride so-called MXene was also gained interests as a new member for 2D material class (Naguib et al., 2011). It has a general

formula of Mn+1XnTx, where M is transition metal, X is a carbon or nitrogen with n =1,2,3…, and T is a face-termination group likes oxygen or fluorine. MXene can be produced by selectively etching of MAX layer (Enyashin & Ivanovskii, 2013; Ivanovskii & Enyashin, 2013). The MXene has been previously utilized in various photonic applications due to its excellent optical, thermal and physical properties (X. Jiang et al., 2018). It has many advantages such as small band gap size, metallic conductivity, and hydrophilic nature of its surface. Mxene also has an excellent saturable absorption characteristic, which is suitable for photonic diodes (Y. Dong et al., 2018). It is also reported that the MXene also exhibits the zero-bandgap structure, which can be potentially used for the broadband optical device (Jhon et al., 2017). In this section, the generation of Q-switched laser pulses is experimentally demonstrated using a newly developed thin-film SA that belongs to the MXene family. The titanium carbide ($Ti_3C_2T_x$) was chosen as the main compound due to its graphene-like but highly tunable and tailorable electronic/optical properties (X. Jiang et al., 2018).

In constructing the SA, $Ti_3C_2T_x$ powder obtained through a selective etching process is dispersed in PVA solution before the mixture is dried to form a thin film as described in the previous chapter. The tiny piece of the prepared $Ti_3C_2T_x$ PVA thin film was slot in between two fiber ferrules and integrated into a ring EDFL cavity to function as a Q-switcher. The insertion loss of the SA device is measured to be around 1.0 dB. The EDFL cavity used in this study is same as Fig. 4.1, which comprises of a 980 nm LD, a WDM coupler, a 2.4 m long EDF, an optical isolator and a 20:80 OC. The LD pumps in a continuous 980 nm laser to the laser cavity via a WDM to provide lasing in 1.5 μm region. The isolator maintains a unidirectional laser beam propagation while the OC lets 20% of the laser to be taken out of the cavity for analysis and keeps 80% of it in circulation. The analysis of the Q-switched pulses is executed using similar equipment and approaches as explained in section 4.2.

In this work, the initial threshold input laser diode power to continuous wave (CW) is 10 mW. As we further incremented input pump power, a stable passively Q-switched EDFL pulse train was spotted at threshold of power of 29.8 mW. The Q-switching process was preserved in cavity configuration as the pump power was incremented up to 66.3 mW. As the input LD power incremented beyond 66.3 mW, the Q-switching pulses became unstable and disappear, the laser output changed to CW operation. On the contrary, no pulse train was observed upon removal of the SA from the cavity configuration, which confirmed that $Ti_3C_2T_x$ MXene film is necessary to initiate Q-switching operation.

Fig. 4.7 shows the typical pulse characteristics of the Q-switched EDFL that has been produced via $Ti_3C_2T_x$ MXene film as SA at input LD power of 66.3 mW. Fig. 4.7 (a) illustrates the oscilloscope pulse train of the stable Q-switched laser. The pulse train shows uniform peak intensity without any distortion or inconsistency which demonstrates the high stability of the Q-switching operation. The dual-pulse envelop of the Q-switched laser is shown in the inset of Fig. 4.7 (a). It exhibits a pulse width of 3.11 μs and a pulse interval of 15.25 μs, which corresponds to a repetition frequency of 65.59 kHz. The typical output spectrum gained via the proposed SA film and was gauged via OSA with resolution of 0.2 nm, see Fig. 4.7 (b). The Q-switched EDFL operated at 1561 nm with a 3 dB spectral bandwidth of 2.6 nm at input pump power 66.3 mW. The radio frequency (RF) spectrum was also obtained at an input pump power of 66.3 mW to prove the stability of the Q-switched system. The Q-switched laser has a signal-to-noise ratio (SNR) of up to 57 dB with the fundamental RF peaks at 65.59 kHz, see Fig. 4.7 (c).

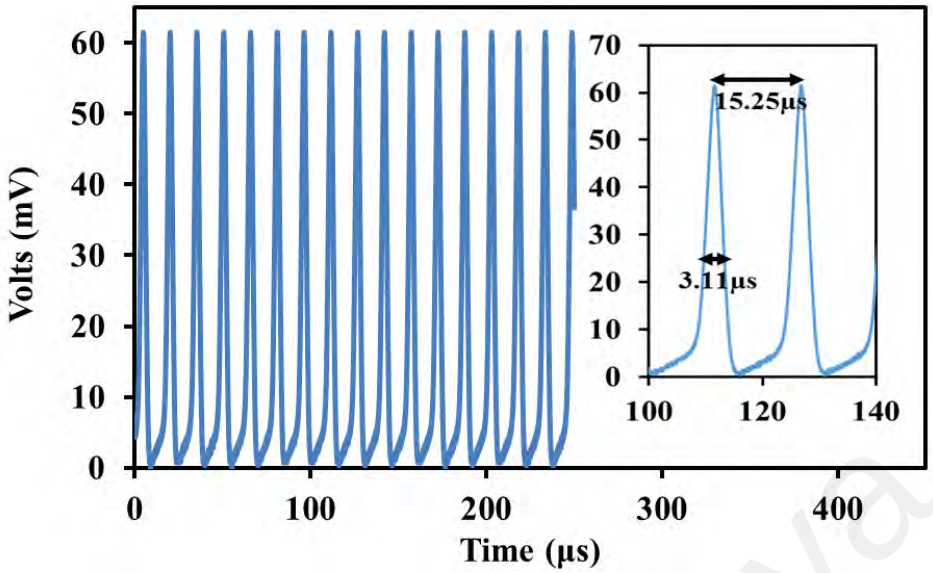

(a)

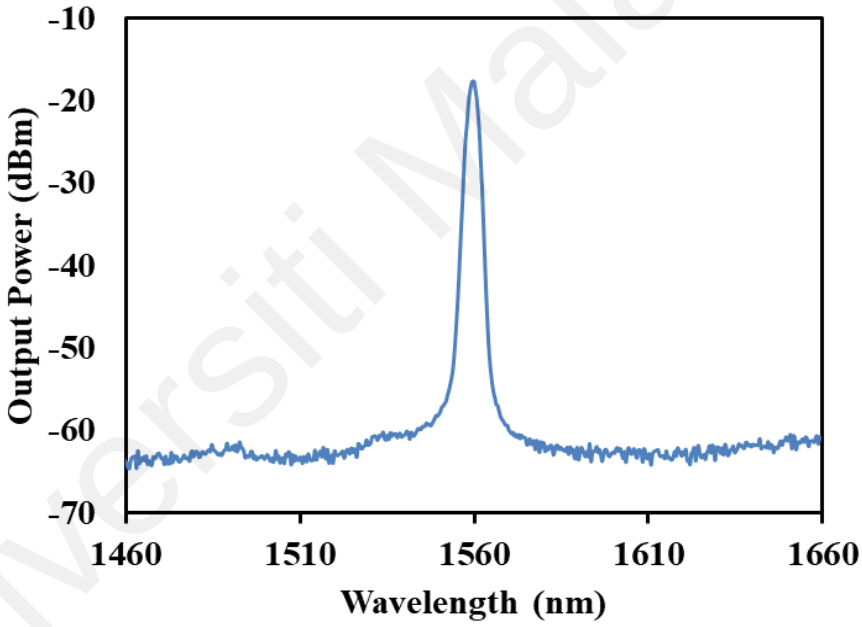

(b)

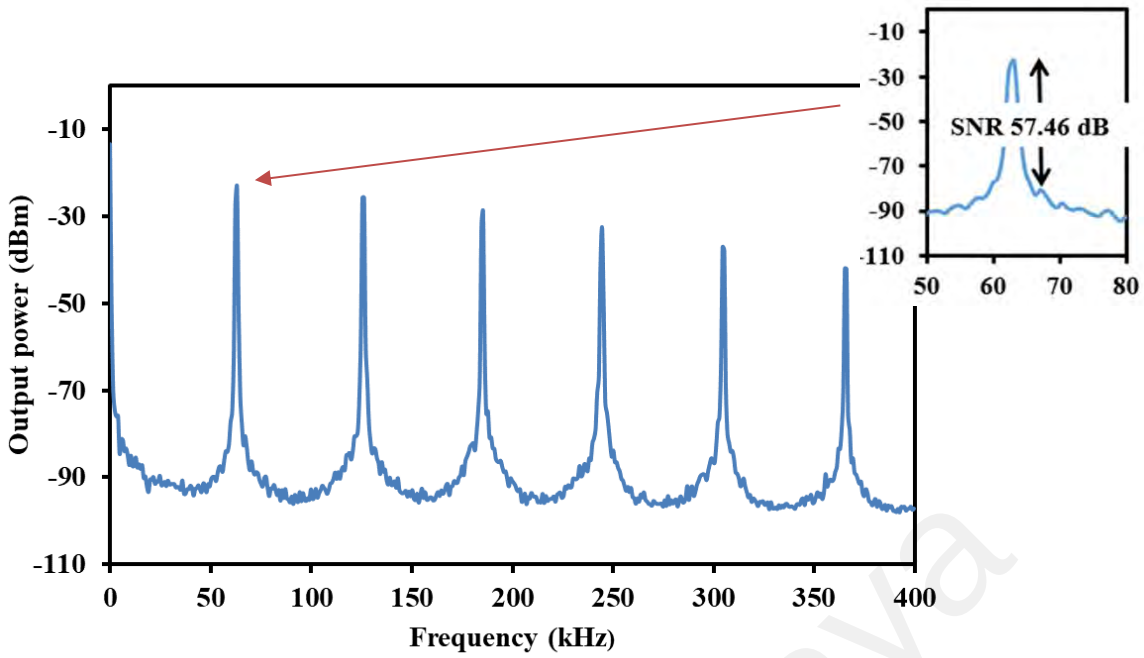

(c)

Figure 4.7: The typical characteristics of the Q-switched EDFL with $Ti_3C_2T_x$ MXene film- based SA at 66.3 mW pump power (a) typical pulse train. Inset shows the dual pulse envelop (b) optical spectrum (c) RF spectrum.

Fig. 4.8 (a) summarizes the relations between the pump power, and the repetition rate and pulse width. The repetition rate increases from 45.25 to 65.59 kHz, the pulse width decreases from 5.04 to 3.11 μs as the pump power rises gradually from 29.8 mW to 66.3 mW. This trend is expected because the higher pump power generated a greater population inversion and hence incremented the accessibility obtain in laser configuration. The higher gain, in turn, increases the laser intensity. Then, the Q-switched pulses falling times become narrower because of the SA saturation. The performance of average output power and pulse energy of the proposed MXene based Q-switched laser were measured as shown in **Fig. 4.8 (b)**. Average output power and pulse energy increased in a range from 3.68 to 8.17 mW and 81 nJ to 125 nJ, respectively, as the pump power was raised from 29.8 mW to 66.3 mW. The slope efficiency of the laser was obtained at 12.3%. As the pump power was further increased beyond 66.3 mW, the Q-

switched pulse generated became unstable and eventually vanished. This is most probably due to the oversaturation of the $Ti_3C_2T_x$ SA and the instability of laser cavity in the high pump power. However, the Q-switched pulses were regained their stable operation when the pump power was decreased back to 66.3 mW due to the high saturation absorption of the SA. We believe that reducing the loss associated with the SA and adjusting the coupling ratio might improve the pulse width, output power, and optical efficiency. Table 4.3 compares the performance of the $Ti_3C_2T_x$ SA with the previously reported SAs made of other materials. The proposed $Ti_3C_2T_x$ SA exhibits a good performance in terms of pulse energy and output power. In addition, the Q-switched laser was working continuously for 3 days without any interruption during the period. Based on that, we can conclude the new SA device can withstand long-term illumination while maintaining the stability of the output pulses.

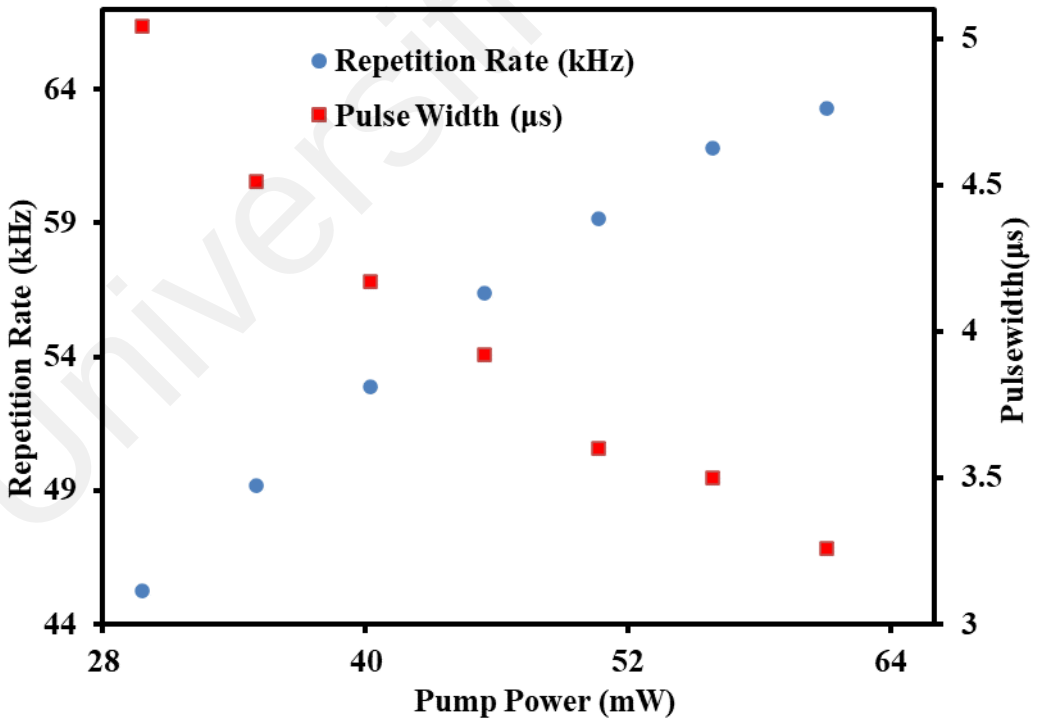

(a)

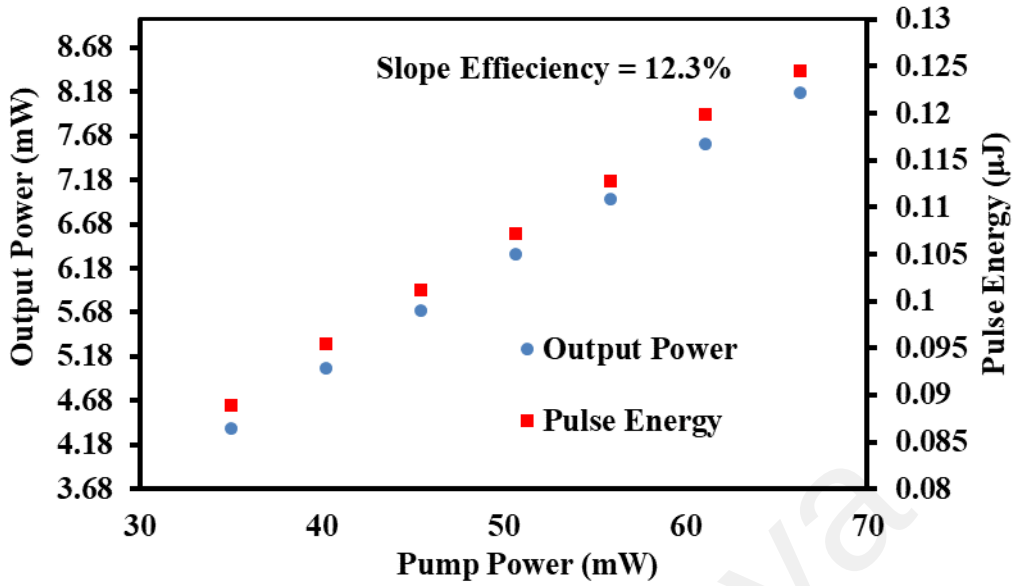

(b)

Figure 4.8: The Q-switching performance (a) repetition rate and pulse width against pump power (b) output power and pulse energy against pump power

Table 4.3: Performance for various SA materials

SA	Max pump power (mW)	Rep. rate (kHz)	Pulse width (µs)	Pulse energy (nJ)	Output Power (mW)	λ (nm)	Ref
Graphite	273	46.1	1.98	58.9	2.7	1559.3	(Lee et al., 2016)
Graphene	151.47	67.8	6.02	206	32	1558.3	(Zuikafly et al., 2018)
CNT	209.6	70.4	4.5	81.3	5.7	1563.1	(Liu et al., 2013)
BP	170	44.33	7.04	134	5.94	1552.9	(Ahmed et al., 2017)
MoS_2	170	38.43	5.02	141.3	5.43	1551.4	(Ahmed et al., 2017b)
MoS_2	170	41.4	13.5	184.7	0.7	1560	(Chen et al., 2015)

SA	Max pump power (mW)	Rep. rate (kHz)	Pulse width (μs)	Pulse energy (nJ)	Output Power (mW)	λ (nm)	Ref
WSe_2	300	49.6	3.1	33.2	1.23	1560	(Chen et al., 2016)
Ti_2AlN	106	41.55	2.52	7	0.291	1557	(Kwon, Lee, & Lee, 2021)
Ti_3AlC_2	94	112	3.93	75	8.4	1560.2	(Jafry et al., 2020)
Ti_2AlC	74	27.45	4.88	22.58	0.62	1560.4	(Lee et al., 2019)
$Ti_3C_2T_x$	66.3	65.59	3.11	125	8.17	1561	This work

4.5 Mode-locked Pulse Generation with $Ti_3C_2T_x$ MXene

Recently, optical pulse train generation via mode-locking has gained notable attention due to their many applications in material processing, biomedicine, remote sensing (Wu, Zhang, Wang, Li, & Chen, 2015). As previously discussed, the mode-locked fiber laser can be achieved with the use of various SA devices. In this section, the generation of mode-locked laser pulses is experimentally demonstrated using a MXene material as SA. MXene owns the ability to erase the procedure obstacle of tunable bandgap and monolayer dispersion (X. Jiang et al., 2018). The titanium carbide ($Ti_3C_2T_x$) was chosen as the main compound due to its graphene-like but highly tunable and tailorable electronic/optical properties (X. Jiang et al., 2018). Furthermore, it was reported to high optical damage tolerance, which makes it a preferrable SA, in comparison to other 2D-based materials (Jhon, Lee, Jhon, & Lee, 2021).

In constructing the SA, titanium carbide ($Ti_3C_2T_x$) powder obtained through a selective etching process is dispersed in polyvinyl alcohol (PVA) solution before the mixture is dried to form a thin film. A small piece of the $Ti_3C_2T_x$ PVA film is placed

between two fiber ferrules to form a fiber compatible SA device and added to an erbium-doped fiber laser (EDFL) cavity to produce mode-locked pulses. The EDFL cavity is same as the previous experiment of Fig. 4.4. The fiber laser was constructed using a 2.4 m long EDF, which has a group velocity dispersion (GVD) of 27.6 ps^2/km as a gain medium. The EDF was co-pumped by a 980 nm laser diode through a 980/1550 WDM. The isolator enables a unidirectional propagation of laser light. A fiber optical coupler (OC) with a split ratio of 20:80 was used, so that 20% of the power was used to measure the output of the fiber laser in the time and frequency domains. To achieve mode-locking in EDFL, a 100 m long SMF spool having group velocity dispersion (GVD) of -21.7 ps^2/km was used in the EDFL cavity to balance between the nonlinearity and dispersion. The total cavity length is about 106 m and the net cavity dispersion is calculated to be around -2.94 ps^2. The performance of the mode-locked fiber laser was measured using an OSA, an oscilloscope, an RF analyzer and an autocorrelator with a high-speed photodetector.

In the proposed EDFL cavity, the initial threshold input laser diode power for continuous wave (CW) operation is 16 mW. As we further increase the input pump power, a stable passively mode locked EDFL pulse train was spotted at threshold of power of 40.2 mW. The mode-locking operation was maintained up to pump power of 87.2 mW. Fig. 4.9 (a) shows the output spectrum of the mode-locking operations, which indicates a lasing centered at 1561.2 nm with 3-dB bandwidth of 0.3 nm. However, the 3-dB spectral bandwidth is relatively narrow, and the Kelly sidebands did not appear in the emission spectrum of the mode-locked laser because of the nonlinearity that has been generated from 106 m cavity length. The pulses are periodically stretched and recompressed in every resonator round trip in the cavity and thus increased the average pulse width of the laser. The shorter pulse duration can be expected by further reducing the total cavity length and enhancing the modulation depth of the SA. The modulation

depth may be increased by improving the SA's preparation process. Fig. 4.9 (b) illustrates a uniform pulse train of the mode-locked operation, which was measured using an oscilloscope at 87.2 mW pump power. The dual-pulse envelop of the mode-locked laser is shown in Fig. 4.9 (c). It exhibits a pulse duration of 154 ns and a pulse interval of 530 ns, which can be translated to a repetition rate of 1.89 MHz. The repetition rate corresponded well with the cavity length of 106 m. The radio frequency (RF) spectrum was also obtained at an input pump power of 87.2 mW to prove the stability of the mode-locking operation. The mode-locked laser has a signal-to-noise ratio (SNR) of up to 70.57 dB with the fundamental RF peaks at 1.89 MHz, see Fig. 4.9 (d). Nonlinear polarization evaluation (NPE) can also produce passively mode-locked lasers [24, 25]. To validate that only the proposed SA was responsible for the generation of pulsed laser. We first removed the SA, cleaned the fiber ferrules, and tuned the laser pump power at all the possible ranges. However, there was no pulse formed without the SA in EDFL cavity. Further, by replacing the SA with a pure PVA thin film could also not produce any traces of pulses in the laser cavity. Thus, the mode-locked laser was produced only by $Ti_3C_2T_x$ thin film SA in our experimental setup.

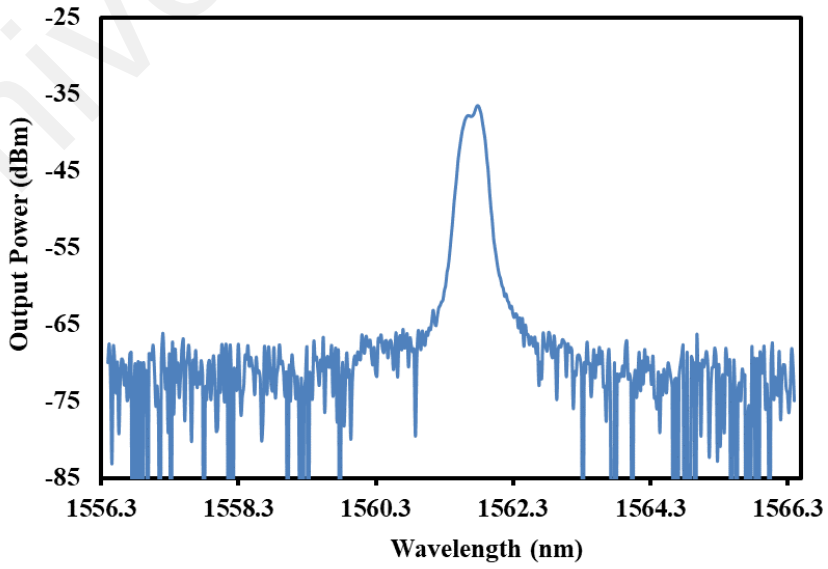

(a)

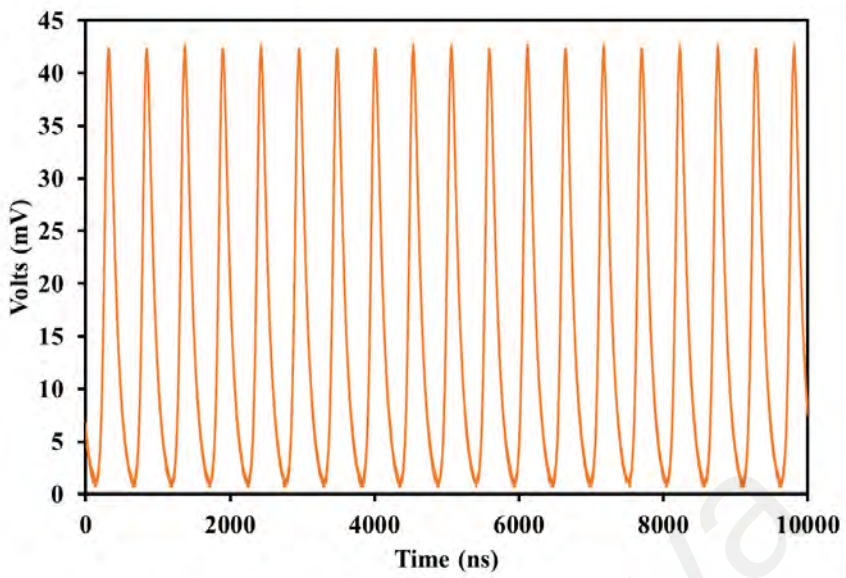

(b)

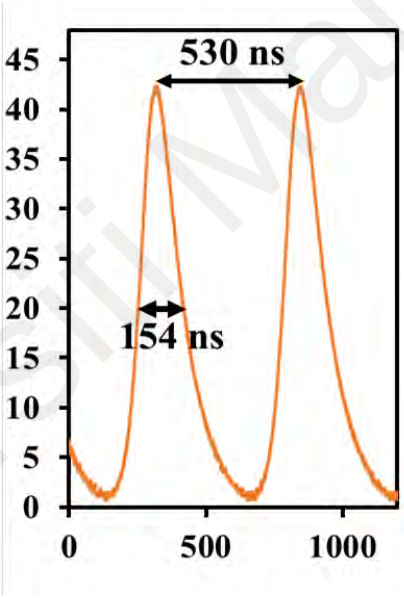

(c)

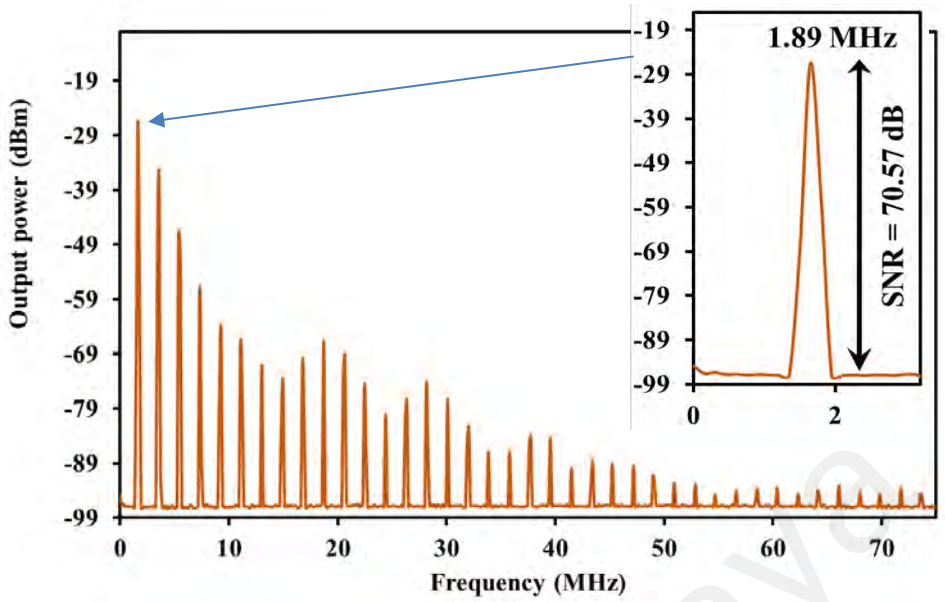

(d)

Figure 4.9: Spectral and temporal performances of the mode-locked laser at the pump power of 87.2 mW (a) OSA spectrum (b) oscilloscope trace, (c) two pulses envelops, and (d) RF spectrum

Fig. 4.10 (a) plots the linear relationship between the obtained average output power and pulse energy versus the power of input pump. The average output power and pulse energy were increased from 5.69 mW to 11.85 mW and 3.01 nJ to 6.24 nJ, respectively as the pump power was raised from 40.2 to 87.2 mW. The slope efficiency of the laser is analyzed to be about 13.16, which is relatively high due to the low loss of the SA. As the input LD power incremented beyond 87.2 mW, the mode-locking pulses became unstable and disappear, the laser output changed to CW operation. The pump intensity-dependent peak power performance was plotted in Fig. 4.10 (b). The peak power has increased from 19.5 mW to 40.7 mW as the pump power varied from 40.2 to 87.2 mW. We believe the damage threshold of our proposed thin-film SA is beyond our operating regime of 185 mW pump power because, when the pump power was swelled to maximum and then reduced back to 87.2 mW, the mode-locking was recovered,

confirming that the SA was not burnt. The optimizing of film thickness can improve the performance of the laser.

The developed mode-locked laser has applications in many scientific and industrial fields. For instance, it can be used to generate supercontinuum light source, which is important for sensing and imaging applications.

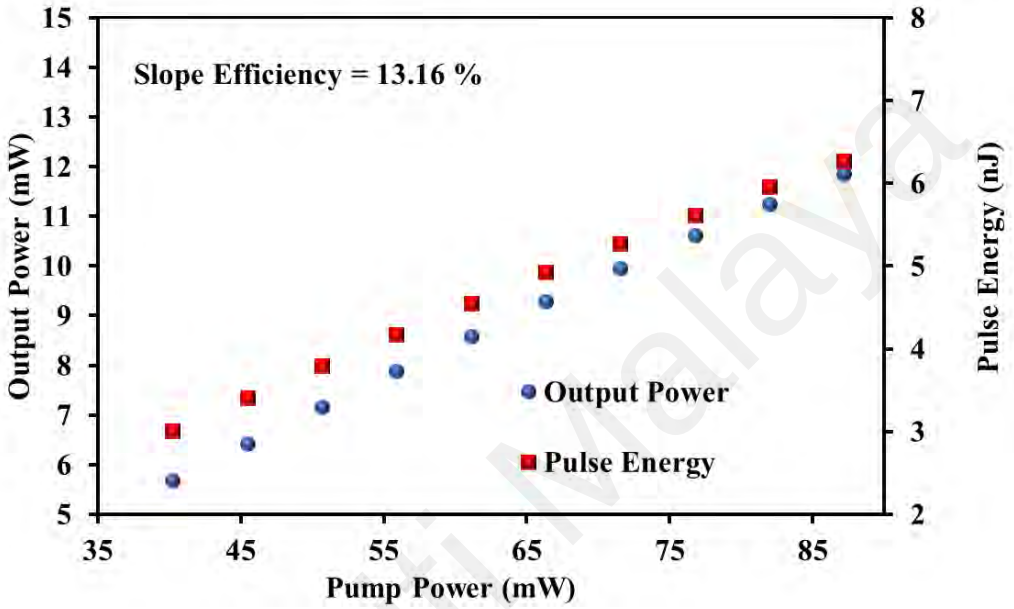

(a)

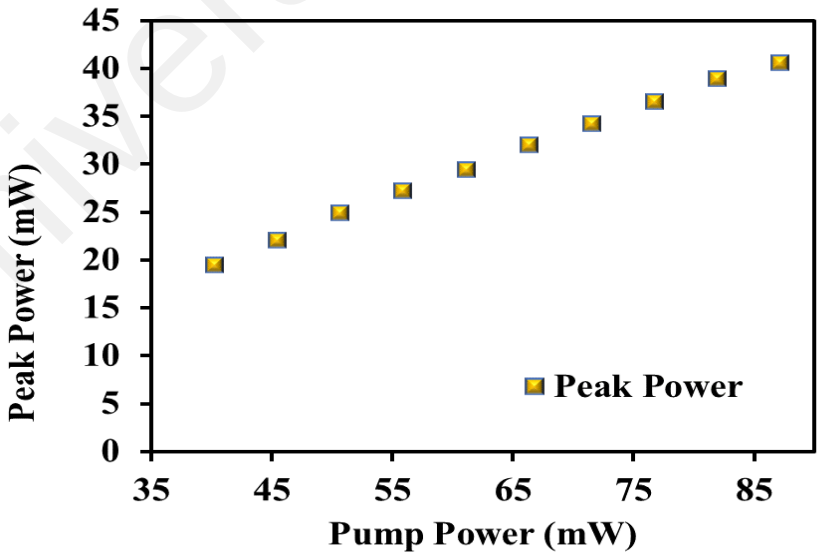

(b)

Figure 4.10: Mode-locking performance of the $Ti_3C_2T_x$ film SA (a) output power and pulse energy performances (b) Peak power performance against pump power.

4.6 Summary

Q-switched and mode-locked EDFLs have been successfully demonstrated using two types of thin film based SAs based on transition metal carbide: Ti_3SiC_2 MAX phase and $Ti_3C_2T_x$ MXene. By integrating the prepared Ti_3SiC_2/PVA thin film into an EDFL cavity, stable Q-switched pulses operating at 1561.8 nm were obtained and the maximum energy of 100.7 nJ was achieved at a repetition rate of 43.5 kHz. The minimum pulse width of the output pulses was 5.6 μs at a pump power of 71.5 mW. The Ti_3SiC_2 PVA thin film exhibited 51 % saturable absorption and thus capable of achieving picosecond pulse when integrated with the extended EDFL ring cavity with a length of 106 m. The proposed mode locked EDFL operated at repetition frequency of 1.88 MHz, pulse width of 3.03 ps as the pump power was adjusted within 123.7 to 181.1 mW. The laser achieved the maximum pulse energy of 6.0 nJ and the maximum peak power of 2.0 kW. This study also successfully demonstrated the use of a $Ti_3C_2T_x$ MXene SA for Q-switched pulse generation in 1550 nm region. The results show that the SA successfully produces Q-switched laser pulses with a pulse width of 3.11 μs and repetition rate of 65.59 kHz at the input pump power of 66.3 mW. At the same pump power, the pulse energy is 125 nJ and the maximum output power is 8.17 mW. The use of a $Ti_3C_2T_x$ MXene compound is finally demonstrated as a passive SA in an EDFL cavity to produce nanosecond pulses via mode-locking. It is found that the $Ti_3C_2T_x$ PVA SA successfully produces mode-locked pulses within a pump power from 40.2 mW to 87.2 mW. It operates at 1561.2 nm with a repetition rate of 1.89 MHz and pulse width of 154 ns. At 87.2 mW pump power, the average output power, pulse energy and peak power is 11.85 mW, 6.24 nJ, and 40.7 mW, respectively. These results validated the simplicity and feasibility of both SAs for producing a stable Q-switched and mode-locked pulse train.

CHAPTER 5: CONCLUSION AND FUTURE WORK

5.1 Conclusion

Fiber lasers which represent third-generation lasers have obtained significant interests in recent years due to their promising applications many scientific and industrial fields. They have occupied a large share of the commercial laser market and can be divided into two types depending on the mode of operation: continuous and pulsed. The pulsed fiber laser has high pulse energy and short pulse width, greatly expanding the application of lasers in optical communication, micromachining, automotive manufacturing, medical devices, and other fields. Q-switching and mode-locking are the two main techniques enabling pulsed laser, both of which can be implemented actively or passively. The passive approach has gained increasing interest in the recent years owing to its simplicity, compactness, flexibility, and low implementing cost. Unlike the active approach, the passive one does not rely on bulky and complex optical modulators and electronic drivers, which can achieve laser pulse output simply by placing a saturable absorber (SA) in the resonant cavity. Therefore, the SA plays a crucial role in the passive Q-switched and mode-locked lasers. The development of passive pulsed lasers relies heavily on SA materials. Up to date, many materials have been examined and reported as SA such as semiconductor saturable absorber mirror (SESAM), graphene, carbon nanotubes (CNTs), black phosphoros, topological insulators (TIs) and transition metal dichalcogenides (TMDs). These materials, however, have many limitations and thus finding a new material to be used as a high-performance SA has been of great interest in recent years.

Motivated by the progress of the previous SA, another type of 2D material, transition-metal carbides have also attracted rising attention due to their high nonlinear

optical response and high temperature operation. Erbium-doped fiber (EDF) has been widely used in many fiber laser systems due to its operation in a 1550 nm region and low cost for the components. Therefore, this thesis aimed to develop new SA devices based on transition metal carbide for Q-switching and mode-locking applications in 1550 nm wavelength region.

Three objectives have been outlined in this research. The first one is to fabricate new passive SA devices based on titanium silicon carbide (Ti_3SiC_2) MAX phase and titanium carbide ($Ti_3C_2T_x$) MXene materials. Ti_3SiC_2 and $Ti_3C_2T_x$ thin film based SAs were successfully developed based on drop casting technique as described in Chapter 3. The SA was fabricated by a simple processing technique; simply by embedding the material into the polyvinyl alcohol (PVA) film.

The second objective is to characterize the newly developed Ti_3SiC_2 and $Ti_3C_2T_x$ thin film based SAs. These SAs were successfully characterized in terms of SEM or FESEM image, Energy Dispersive X-Ray Analysis (EDX), etc. These thin films were also successfully characterized in terms of linear and nonlinear absorption as also discussed in Chapter 3. Table 5.1 depicted the optical properties of the prepared SA devices from this work. The Ti_3SiC_2 and $Ti_3C_2T_x$ thin films have a modulation depth of 51 %, 4.8 %, respectively and thus suitable for Q-switching and mode-locking applications. It is found that Ti_3SiC_2 film exhibits higher modulation depth and non-saturable loss due to its bulk structure.

Table 5.1: Optical properties of the prepared SA devices.

SAs	Linear Absorption at 1550 nm region (dB)	Modulation Depth (%)	Saturable Intensity (MW/cm^2)	Non-Saturable Loss (%)
Ti_3SiC_2	3.8	51	0.3	30
$Ti_3C_2T_x$	2.24	4.8	20	3.6

The third objective is to demonstrate various Q-switched and mode-locked pulse generations in Erbium-doped fiber laser (EDFL) cavity using the new SAs. Q-switched and mode-locked EDFLs operating in 1550 nm region have been successfully demonstrated using all two types of thin film based SAs: Ti_3SiC_2 and $Ti_3C_2T_x$ as described in Chapter 4. Using the Ti_3SiC_2/PVA thin film-based SA within an EDFL ring cavity, a self-started and stable Q-switched pulse train was achieved at a wavelength of 1561.8 nm. It exhibited a maximum pulse energy of 100.7 nJ, maximum repetition rate of 43.5 kHz, minimum pulse width of 5.6 μs at a pump power of 71.5 mW. A picosecond pulse train was also successfully demonstrated when the Ti_3SiC_2 PVA thin film was integrated into an extended EDFL ring cavity with a length of 106 m. The proposed mode locked EDFL operated at repetition frequency of 1.88 MHz, pulse width of 3.03 ps as the pump power was adjusted within 123.7 to 181.1 mW. The laser achieved the maximum pulse energy of 6.0 nJ and the maximum peak power of 2.0 kW.

With $Ti_3C_2T_x$ MXene SA, a Q-switched EDFL operating at 1561 nm was also succesfully demonstrated. The repetition rate of the Q-switched pulses can be varied between 45.25 and 65.59 kHz with the corresponding pulse width of 5.04–3.11 μs when the pump power is increased from 29.8 to 66.3 mW. At the maximum output power of 8.17 mW, the highest pulse energy of 125 nJ is obtained. The $Ti_3C_2T_x$ thin film can also be used to realize mode-locked pulse in an EDFL cavity with a length of 106 m. The

mode-locked laser operates at 1561.2 nm with a repetition rate of 1.89 MHz and pulse width of 154 ns as the pump power is fixed within a range from 40.2 to 87.2 mW. At 87.2 mW pump power, the maximum average output power, pulse energy, and peak power were measured to be 11.85 mW, 6.24 nJ, and 40.7 mW respectively. This study also successfully demonstrated the use of a $Ti_3C_2T_x$ MXene SA for both Q-switched and mode-locked pulse generation in 1550 nm region. These results verified that all the objectives were fulfilled.

5.2 Recommendation for Future Work

All the proposed objectives have been successfully implemented. However, the study of both materials (Ti_3SiC_2 and $Ti_3C_2T_x$) for generating Q-switched and mode-locked pulses can be further explored. Further work should be devoted to enhancing the performance of the proposed fiber laser in terms of shorting the pulse width, increasing the repetition rate, output power and pulse energy. This can be achieved by addressing a shorter cavity length, enhanced cavity gain, and improved nonlinear characteristic of the SA.

Additionally, a future work should also focus on exploring the developed SAs in other wavelength regions such as 1 μm, 2.0 μm and 3.0 μm using Ytterbium-doped fiber (YDF), Thulium-doped fiber (TDF) and ZBLAN Erbium-doped fiber, respectively, as the active gain medium. Q-switched and mode-locked fiber lasers operating in mid-infrared (MIR) region will be a very interesting area to investigate because of their advantages for application in variety of fields such as military, remote sensing, spectroscopy and medical. In addition, these lasers operate in eye-safe wavelength regions that suite for free space applications such as light detection and ranging (LIDAR) and telecommunication systems.

As to the best of our knowledge, there is still a lack of research work on addressing the organic materials-based SA. Developing new organic materials for ultrashort pulse generations will be interesting research as well.

REFERENCES

Addanki, S., Amiri, I. S., & Yupapin, P. (2018). Review of optical fibers-introduction and applications in fiber lasers. *Results in Physics, 10*, 743-750. doi:https://doi.org/10.1016/j.rinp.2018.07.028

Ahmed, M., Ali, N., Salleh, Z., Rahman, A. A., Harun, S. W., Manaf, M., & Arof, H. (2015). Q-switched erbium doped fiber laser based on single and multiple walled carbon nanotubes embedded in polyethylene oxide film as saturable absorber. *Optics & Laser Technology, 65*, 25-28.

Ahmed, M. H. M., Al-Masoodi, A. H. H., Latiff, A. A., Arof, H., & Harun, S. W. (2017). Mechanically exfoliated 2D nanomaterials as saturable absorber for Q-switched erbium doped fiber laser. *Indian Journal of Physics, 91*(10), 1259-1264.

Ainslie, B. J. (1991). A review of the fabrication and properties of erbium-doped fibers for optical amplifiers. *Journal of Lightwave Technology, 9*(2), 220-227.

Alhabeb, M., Maleski, K., Mathis, T. S., Sarycheva, A., Hatter, C. B., Uzun, S., . . . Gogotsi, Y. (2018). Selective etching of silicon from Ti3SiC2 (MAX) to obtain 2D titanium carbide (MXene). *Angewandte Chemie, 130*(19), 5542-5546.

Anthony, N., Frostevarg, J., Suhonen, H., Wanhainen, C., Penttilä, A., & Granvik, M. (2021). Laser processing of minerals common on asteroids. *Optics & Laser Technology, 135*, 106724.

Arumugam, M. (2001). Optical fiber communication—An overview. *Pramana, 57*(5), 849-869.

Babu, P., Seo, H. J., Jang, K. H., Balakrishnaiah, R., Jayasankar, C., Lim, K.-S., & Lavín, V. (2007). Optical spectroscopy, 1.5 μm emission, and upconversion properties of Er 3+-doped metaphosphate laser glasses. *Journal of the Optical Society of America B, 24*(9), 2218-2228.

Balling, P., & Schou, J. (2013). Femtosecond-laser ablation dynamics of dielectrics: basics and applications for thin films. *Reports on Progress in Physics, 76*(3), 39. doi:10.1088/0034-4885/76/3/036502

Barsoum, M. W. (2000). The MN+ 1AXN phases: A new class of solids: Thermodynamically stable nanolaminates. *Progress in solid state chemistry, 28*(1-4), 201-281.

Becker, P. M., Olsson, A. A., & Simpson, J. R. (1999). *Erbium-doped fiber amplifiers: fundamentals and technology*: Elsevier.

Bonaccorso, F., & Sun, Z. P. (2014). Solution processing of graphene, topological insulators and other 2d crystals for ultrafast photonics. *Optical Materials Express, 4*(1), 63-78. doi:10.1364/ome.4.0063

Chen, B., Zhang, X., Guo, C., Wu, K., Chen, J., & Wang, J. (2016). Tungsten diselenide Q-switched erbium-doped fiber laser. *Optical Engineering, 55*(8), 081306.

Chen, B., Zhang, X., Wu, K., Wang, H., Wang, J., & Chen, J. (2015). Q-switched fiber laser based on transition metal dichalcogenides MoS 2, MoSe 2, WS 2, and WSe 2. *Optics express, 23*(20), 26723-26737.

Chen, H., Chen, S.-P., Jiang, Z.-F., & Hou, J. (2015). Versatile long cavity widely tunable pulsed Yb-doped fiber laser with up to 27655th harmonic mode locking order. *Optics express, 23*(2), 1308-1318.

Chen, Y., Jiang, G., Chen, S., Guo, Z., Yu, X., Zhao, C., . . . Tang, D. (2015). Mechanically exfoliated black phosphorus as a new saturable absorber for both Q-switching and mode-locking laser operation. *Optics express, 23*(10), 12823-12833.

Chen, Y., Jiang, G., Chen, S., Guo, Z., Yu, X., Zhao, C., . . . Fan, D. (2015). Mechanically exfoliated black phosphorus as a new saturable absorber for both Q-switching and Mode-locking laser operation. *Optics Express, 23*(10), 12823-12833. doi:10.1364/OE.23.012823

Cheng, K.-N., Lin, Y.-H., & Lin, G.-R. (2013). Single-and double-walled carbon nanotube based saturable absorbers for passive mode-locking of an erbium-doped fiber laser. *Laser Physics, 23*(4), 045105.

Desurvire, E., Giles, C. R., Simpson, J. R., & Zyskind, J. L. (1991). Erbium-doped fiber amplifier: Google Patents.

Dong, L., & Samson, B. (2016). *Fiber lasers: basics, technology, and applications*: CRC press.

Dong, Y., Chertopalov, S., Maleski, K., Anasori, B., Hu, L., Bhattacharya, S., . . . Podila, R. (2018). Saturable absorption in 2D Ti3C2 MXene thin films for passive photonic diodes. *Advanced Materials, 30*(10), 1705714.

Dong, Z., Li, H., Xia, H., Liu, Y., Wang, Z., & Chen, Y. (2012). *Passively Q-switched erbium-doped fiber laser using a graphene saturable absorber.* Paper presented at the Asia Communications and Photonics Conference.

Dubey, A. K., & Yadava, V. (2008). Laser beam machining - A review. *International Journal of Machine Tools & Manufacture, 48*(6), 609-628. doi:10.1016/j.ijmachtools.2007.10.017

Enyashin, A. N., & Ivanovskii, A. L. (2013). Structural and electronic properties and stability of MX enes Ti2C and Ti3C2 functionalized by methoxy groups. *The Journal of Physical Chemistry C, 117*(26), 13637-13643.

Gao, J., Ning, T., Liu, Y., Shang, X., Han, X., Guo, Q., . . . Zhang, H. (2019). Generation of high-energy rectangular pulses in a nonlinear polarization rotation mode-locked ring fiber laser. *Applied optics, 58*(28), 7897-7903.

Ghidiu, M., Lukatskaya, M. R., Zhao, M.-Q., Gogotsi, Y., & Barsoum, M. W. (2014). Conductive two-dimensional titanium carbide 'clay'with high volumetric capacitance. *nature, 516*(7529), 78-81.

Giles, C. R., Burrus, C. A., DiGiovanni, D. J., Dutta, N. K., & Raybon, G. (1991). Characterization of erbium-doped fibers and application to modeling 980-nm and 1480-nm pumped amplifiers. *Ieee Photonics Technology Letters, 3*(4), 363-365. doi:10.1109/68.82113

Giles, C. R., & Desurvire, E. (1991). Modeling erbium-doped fiber amplifiers. *Journal of Lightwave Technology, 9*(2), 271-283.

Gonzalez-Julian, J. (2021). Processing of MAX phases: From synthesis to applications. *Journal of the American Ceramic Society, 104*(2), 659-690.

Halim, J., Cook, K. M., Naguib, M., Eklund, P., Gogotsi, Y., Rosen, J., & Barsoum, M. W. (2016). X-ray photoelectron spectroscopy of select multi-layered transition metal carbides (MXenes). *Applied surface science, 362*, 406-417.

Halim, J., Lukatskaya, M. R., Cook, K. M., Lu, J., Smith, C. R., N slund, L.-Å., . . . Eklund, P. (2014). Transparent conductive two-dimensional titanium carbide epitaxial thin films. *Chemistry of Materials, 26*(7), 2374-2381.

Hasan, T., Sun, Z., Wang, F., Bonaccorso, F., Tan, P. H., Rozhin, A. G., & Ferrari, A. C. (2009). Nanotube–polymer composites for ultrafast photonics. *Advanced Materials, 21*(38-39), 3874-3899.

Haynes, R., Bland-Hawthorn, J., Large, M. C., Klein, K.-F., & Nelson, G. W. (2004). *New age fibers: the children of the photonic revolution.* Paper presented at the Optical Fabrication, Metrology, and Material Advancements for Telescopes.

Hofer, M., Ober, M., Haberl, F., & Fermann, M. (1992). Characterization of ultrashort pulse formation in passively mode-locked fiber lasers. *IEEE Journal of Quantum Electronics, 28*(3), 720-728.

Hoffman, E., Vinson, D., Sindelar, R., Tallman, D., Kohse, G., & Barsoum, M. (2012). MAX phase carbides and nitrides: Properties for future nuclear power plant in-core applications and neutron transmutation analysis. *Nuclear Engineering and Design, 244*, 17-24.

Ilday, F., Wise, F., & Sosnowski, T. (2002). High-energy femtosecond stretched-pulse fiber laser with a nonlinear optical loop mirror. *Optics letters, 27*(17), 1531-1533.

Ilina, I. V., Khramova, Y. V., Ivanova, A. D., Filatov, M. A., & Sitnikov, D. S. (2021). *Novel techniques for embryo microsurgery based on femtosecond lasers for applications in assisted reproductive technologies.* Paper presented at the European Conference on Biomedical Optics.

Ippen, E., Shank, C., & Dienes, A. (1972). Passive mode locking of the cw dye laser. *Applied Physics Letters, 21*(8), 348-350.

Ivanovskii, A. L., & Enyashin, A. N. (2013). Graphene-like transition-metal nanocarbides and nanonitrides. *Russian Chemical Reviews, 82*(8), 735.

Jafry, A. A. A., Kasim, N., Nizamani, B., Muhammad, A. R., Harun, S. W., & Yupapin, P. (2020). MAX phase Ti3AlC2 embedded in PVA and deposited onto D-shaped fiber as a passive Q-switcher for erbium-doped fiber laser. *Optik, 224*, 165682.

Jhon, Y. I., Koo, J., Anasori, B., Seo, M., Lee, J. H., Gogotsi, Y., & Jhon, Y. M. (2017). Metallic MXene saturable absorber for femtosecond mode-locked lasers. *Advanced Materials, 29*(40), 1702496.

Jhon, Y. I., Lee, J., Jhon, Y. M., & Lee, J. H. (2021). Ultrafast mode-locking in highly stacked Ti3C2Tx MXenes for 1.9-μm infrared femtosecond pulsed lasers. *Nanophotonics, 10*(6), 1741-1751.

Jiang, L., Wang, A. D., Li, B., Cui, T. H., & Lu, Y. F. (2018). Electrons dynamics control by shaping femtosecond laser pulses in micro/nanofabrication: modeling, method, measurement and application. *Light-Science & Applications, 7*, 27. doi:10.1038/lsa.2017.134

Jiang, X., Liu, S., Liang, W., Luo, S., He, Z., Ge, Y., . . . Wen, Q. (2018). Broadband nonlinear photonics in few-layer MXene Ti3C2Tx (T= F, O, or OH). *Laser & Photonics Reviews, 12*(2), 1700229.

Jin, S., Su, T., Hu, Q., & Zhou, A. (2020). Thermal conductivity and electrical transport properties of double-A-layer MAX phase Mo2Ga2C. *Materials Research Letters, 8*(4), 158-164.

Keiser, G. (2003). Optical fiber communications. Wiley Encyclopedia of Telecommunications.

Keller, U. (2003a). Recent developments in compact ultrafast lasers. *Nature, 424*, 831. doi:10.1038/nature01938

Keller, U. (2003b). Recent developments in compact ultrafast lasers. *nature, 424*(6950), 831-838.

Keller, U. (2003c). Recent developments in compact ultrafast lasers. *nature, 424*(6950), 831.

Keller, U., Weingarten, K. J., Kartner, F. X., Kopf, D., Braun, B., Jung, I. D., . . . derAu, J. A. (1996). Semiconductor saturable absorber mirrors (SESAM's) for femtosecond to nanosecond pulse generation in solid-state lasers. *Ieee Journal of Selected Topics in Quantum Electronics, 2*(3), 435-453. doi:10.1109/2944.571743

Koester, C. J., & Snitzer, E. (1964). Amplification in a fiber laser. *Applied optics, 3*(10), 1182-1186.

Kwon, S., Lee, J., & Lee, J. H. (2021). A Q-switched fiber laser using a Ti2AlN-based saturable absorber. *Laser physics, 31*(2), 025103.

Lee, J., Kwon, S., & Lee, J. H. (2019). Ti 2 AlC-based saturable absorber for passive Q-switching of a fiber laser. *Optical Materials Express, 9*(5), 2057-2066.

Lee, J., Lee, J., Koo, J., Chung, H., & Lee, J. H. (2016). Linearly polarized, Q-switched, erbium-doped fiber laser incorporating a bulk-structured bismuth telluride/polyvinyl alcohol saturable absorber. *Optical Engineering, 55*(7), 076109.

Lee, J., Lee, J., Koo, J., & Lee, J. H. (2016). Graphite saturable absorber based on the pencil-sketching method for Q-switching of an erbium fiber laser. *Applied optics, 55*(2), 303-309.

Li, P., Chen, Y., Yang, T., Wang, Z., Lin, H., Xu, Y., . . . Zhang, Y. (2017). Two-dimensional CH3NH3PbI3 perovskite nanosheets for ultrafast pulsed fiber lasers. *ACS applied materials & interfaces, 9*(14), 12759-12765.

Li, X., Wang, Y., Wang, Y., Zhao, W., Yu, X., Sun, Z., . . . Wang, Q. J. (2014). Nonlinear absorption of SWNT film and its effects to the operation state of pulsed fiber laser. *Optics Express, 22*(14), 17227-17235.

Liu, H. H., Chow, K. K., Yamashita, S., & Set, S. Y. (2013). Carbon-nanotube-based passively Q-switched fiber laser for high energy pulse generation. *Optics & Laser Technology, 45*, 713-716. doi:https://doi.org/10.1016/j.optlastec.2012.05.005

Liu, W., Liu, M., OuYang, Y., Hou, H., Lei, M., & Wei, Z. (2018). CVD-grown MoSe2 with high modulation depth for ultrafast mode-locked erbium-doped fiber laser. *Nanotechnology, 29*(39), 394002.

Lumholt, O., Rasmussen, T., & Bjarklev, A. (1993). Modelling of extremely high concentration erbium-doped silica waveguides. *Electronics Letters, 29*(5), 495-496.

M'Sallem, Y. B., Le, Q. T., Bramerie, L., Nguyen, Q.-T., Borgne, E., Besnard, P., . . . Rusch, L. A. (2011). Quantum-dash mode-locked laser as a source for 56-Gb/s DQPSK modulation in WDM multicast applications. *IEEE Photonics Technology Letters, 23*(7), 453-455.

Malmström, M., Margulis, W., Tarasenko, O., Pasiskevicius, V., & Laurell, F. (2012). Soliton generation from an actively mode-locked fiber laser incorporating an electro-optic fiber modulator. *Optics express, 20*(3), 2905-2910.

Manzeli, S., Ovchinnikov, D., Pasquier, D., Yazyev, O. V., & Kis, A. (2017). 2D transition metal dichalcogenides. *Nature Reviews Materials, 2*(8), 17033.

Mao, D., Jiang, B., Gan, X., Ma, C., Chen, Y., Zhao, C., . . . Zhao, J. (2015). Soliton fiber laser mode locked with two types of film-based Bi 2 Te 3 saturable absorbers. *Photonics Research, 3*(2), A43-A46.

Mao, D., Zhang, S., Wang, Y., Gan, X., Zhang, W., Mei, T., . . . Zhao, J. (2015). WS 2 saturable absorber for dissipative soliton mode locking at 1.06 and 1.55 μm. *Optics Express, 23*(21), 27509-27519.

Martinez, A., & Sun, Z. (2013). Nanotube and graphene saturable absorbers for fibre lasers. *Nature Photonics, 7*(11), 842-845.

Mary, R., Choudhury, D., & Kar, A. K. (2014). Applications of fiber lasers for the development of compact photonic devices. *IEEE Journal of Selected Topics in Quantum Electronics, 20*(5), 72-84.

Ming, N., Tao, S., Yang, W., Chen, Q., Sun, R., Wang, C., . . . Zhang, H. J. O. e. (2018). Mode-locked Er-doped fiber laser based on PbS/CdS core/shell quantum dots as saturable absorber. *26*(7), 9017-9026.

Miranda, R., Lopes, G., Quintino, L., Rodrigues, J., & Williams, S. (2008). Rapid prototyping with high power fiber lasers. *Materials & Design, 29*(10), 2072-2075.

Moneron, G., Medda, R., Hein, B., Giske, A., Westphal, V., & Hell, S. W. (2010). Fast STED microscopy with continuous wave fiber lasers. *Optics express, 18*(2), 1302-1309.

Naguib, M., Kurtoglu, M., Presser, V., Lu, J., Niu, J., Heon, M., . . . Barsoum, M. W. (2011). Two-dimensional nanocrystals produced by exfoliation of Ti3AlC2. *Advanced Materials, 23*(37), 4248-4253.

Nelson, L. E., Jones, D., Tamura, K., Haus, H. A., & Ippen, E. (1997). Ultrashort-pulse fiber ring lasers. *Applied Physics B: Lasers & Optics, 65*(2).

Nikodem, M. P., Sergeant, H., Kaczmarek, P., & Abramski, K. M. (2008). *Actively mode-locked fiber laser using acousto-optic modulator*. Paper presented at the 16th Polish-Slovak-Czech Optical Conference on Wave and Quantum Aspects of Contemporary Optics.

Nishizawa, N. (2014). Ultrashort pulse fiber lasers and their applications. *Japanese journal of applied physics, 53*(9), 090101.

Niu, K., Sun, R., Chen, Q., Man, B., & Zhang, H. (2018a). Passively mode-locked Er-doped fiber laser based on SnS 2 nanosheets as a saturable absorber. *Photonics Research, 6*(2), 72-76.

Niu, K., Sun, R., Chen, Q., Man, B., & Zhang, H. J. P. R. (2018b). Passively mode-locked Er-doped fiber laser based on SnS 2 nanosheets as a saturable absorber. *6*(2), 72-76.

Nizamani, B., Salam, S., Jafry, A., Zahir, N., Jurami, N., Khudus, M. A., . . . Harun, S. (2020). Indium tin oxide coated D-shape fiber as a saturable absorber for generating a dark pulse mode-locked laser. *Chinese Physics Letters, 37*(5), 054202.

Okhotnikov, O., Grudinin, A., & Pessa, M. (2004). Ultra-fast fibre laser systems based on SESAM technology: new horizons and applications. *New journal of physics, 6*(1), 177.

Okhotnikov, O., & Pessa, M. (2004). Dilute nitride saturable absorber mirrors for optical pulse generation. *Journal of Physics: Condensed Matter, 16*(31), S3107.

Optimizing the pumping configuration for the power scaling of in-band pumped erbium doped fiber amplifiers. (2012). *Optics Express, 20*(13), 13886-13895. doi:10.1364/OE.20.013886

Paschotta, R. (2008). *Field guide to laser pulse generation* (Vol. 14): SPIE press Bellingham.

Pedersen, B., Thompson, B. A., Zemon, S., Miniscalco, W. J., & Wei, T. (1992). Power requirements for erbium-doped fiber amplifiers pumped in the 800, 980, and 1480 nm bands. *Ieee Photonics Technology Letters, 4*(1), 46-49. doi:10.1109/68.124872

Perevislov, S., Sokolova, T., & Stolyarova, V. (2021). The Ti3SiC2 max phases as promising materials for high temperature applications: Formation under various synthesis conditions. *Materials Chemistry and Physics, 267*, 124625.

Pierce, M. C., Jackson, S. D., Golding, P. S., Dickinson, B., Dickinson, M. R., King, T. A., & Sloan, P. (2001). *Development and application of fiber lasers for medical applications.* Paper presented at the Optical Fibers and Sensors for Medical Applications.

Popa, D., Sun, Z., Hasan, T., Torrisi, F., Wang, F., & Ferrari, A. C. (2011). Graphene Q-switched, tunable fiber laser. *Applied Physics Letters, 98*(7), 073106.

Quimby, R. S., Miniscalco, W. J., & Thompson, B. (1994). Clustering in erbium-doped silica glass fibers analyzed using 980 nm excited-state absorption. *Journal of Applied Physics, 76*(8), 4472-4478. doi:10.1063/1.357278

Radovic, M., & Barsoum, M. W. (2013). MAX phases: bridging the gap between metals and ceramics. *American Ceramics Society Bulletin, 92*(3), 20-27.

Saglamyurek, E., Jin, J., Verma, V. B., Shaw, M. D., Marsili, F., Nam, S. W., . . . Tittel, W. (2015). Quantum storage of entangled telecom-wavelength photons in an erbium-doped optical fibre. *Nature Photonics, 9*(2), 83-87. doi:10.1038/nphoton.2014.311

Salam, S., Wong, W. R., Al-Masoodi, A., & Harun, S. W. (2019a). High-energy Q-switched ytterbium-doped all-fiber laser with tris-(8-hydroxyquinoline) aluminum as saturable absorber. *Optical Materials Express, 9*(8), 3215-3225.

Salam, S., Wong, W. R., Al-Masoodi, A. H. H., & Harun, S. W. (2019b). High-energy Q-switched ytterbium-doped all-fiber laser with tris-(8-hydroxyquinoline) aluminum as saturable absorber. *Optical Materials Express, 9*(8), 3215-3225. doi:10.1364/OME.9.003215

Set, S. Y., Yaguchi, H., Tanaka, Y., & Jablonski, M. (2004). Ultrafast fiber pulsed lasers incorporating carbon nanotubes. *IEEE Journal of Selected Topics in Quantum Electronics, 10*(1), 137-146.

Shang, X.-X., Guo, L.-G., Zhang, H.-N., Li, D.-W., & Yue, Q.-Y. (2020). Titanium Disulfide Based Saturable Absorber for Generating Passively Mode-Locked and Q-Switched Ultra-Fast Fiber Lasers. *Nanomaterials, 10*(10), 1922.

Shang, X., Guo, L., Zhang, H., Li, D., & Yue, Q. J. N. (2020). Titanium Disulfide Based Saturable Absorber for Generating Passively Mode-Locked and Q-Switched Ultra-Fast Fiber Lasers. *10*(10), 1922.

Sharma, U., Kim, C.-S., & Kang, J. U. (2004). Highly stable tunable dual-wavelength Q-switched fiber laser for DIAL applications. *IEEE Photonics Technology Letters, 16*(5), 1277-1279.

Shi, W., Fang, Q., Zhu, X., Norwood, R. A., & Peyghambarian, N. (2014). Fiber lasers and their applications. *Applied optics, 53*(28), 6554-6568.

Shi, W., Schulzgen, A., Amezcua, R., Zhu, X., & Alam, S.-U. (2017). Fiber lasers and their applications: introduction. *JOSA B, 34*(3), FLA1-FLA1.

Silvestroni, L., Melandri, C., & Gonzalez-Julian, J. (2021). Exploring processing, reactivity and performance of novel MAX phase/ultra-high temperature ceramic composites: The case study of Ti3SiC2. *Journal of the European Ceramic Society, 41*(12), 6064-6069.

Snitzer, E., Hoffman, F., & Crevier, R. (1963). *Neodymium-glass-fiber laser*. Paper presented at the JOURNAL OF THE OPTICAL SOCIETY OF AMERICA.

Sobon, G., Sotor, J., Jagiello, J., Kozinski, R., Librant, K., Zdrojek, M., . . . Abramski, K. M. (2012). Linearly polarized, Q-switched Er-doped fiber laser based on reduced graphene oxide saturable absorber. *Applied Physics Letters, 101*(24), 4. doi:10.1063/1.4770373

Soffer, B., & Hoskins, R. (1964). Generation of Giant Pulses from a Neo-dymium Laser by a Reversibly Bleachable Absorber. *nature, 204*(4955), 276-276.

Sokol, M., Natu, V., Kota, S., & Barsoum, M. W. (2019). On the chemical diversity of the MAX phases. *Trends in Chemistry, 1*(2), 210-223.

Song, Y., Liang, Z., Jiang, X., Chen, Y., Li, Z., Lu, L., . . . Lu, S. (2017). Few-layer antimonene decorated microfiber: ultra-short pulse generation and all-optical thresholding with enhanced long term stability. *2D Materials, 4*(4), 045010.

Sotor, J., Sobon, G., Macherzynski, W., Paletko, P., & Abramski, K. M. (2015). Black phosphorus saturable absorber for ultrashort pulse generation. *Applied Physics Letters, 107*(5), 051108.

Spühler, G. J., Paschotta, R., Fluck, R., Braun, B., Moser, M., Zhang, G., . . . Keller, U. (1999). Experimentally confirmed design guidelines for passively Q-switched microchip lasers using semiconductor saturable absorbers. *Journal of the Optical Society of America B, 16*(3), 376-388. doi:10.1364/JOSAB.16.000376

Sugioka, K., & Cheng, Y. (2014a). Ultrafast lasers—reliable tools for advanced materials processing. *Light: Science & Applications, 3*(4), e149-e149.

Sugioka, K., & Cheng, Y. (2014b). Ultrafast lasers—reliable tools for advanced materials processing. *Light: Science & Applications, 3*(4), e149.

Sun, S., Yang, F., Sui, Z., Zhu, M., Chen, S., Wang, Y., . . . Chen, X. (2022). Demonstration of passively Q-switched and mode-locked operations through dispersion control in Er-doped fiber lasers with a cylindrite-based saturable absorber. *Journal of luminescence, 250*, 119064.

Sun, Z. (2011). Progress in research and development on MAX phases: a family of layered ternary compounds. *International Materials Reviews, 56*(3), 143-166.

Sun, Z. M. (2011). Progress in research and development on MAX phases: a family of layered ternary compounds. *International Materials Reviews, 56*(3), 143-166.

Tiu, Z., Ooi, S., Guo, J., Zhang, H., & Ahmad, H. (2019). application of transition metal dichalcogenide in pulsed fiber laser system. *Materials Research Express, 6*(8), 082004.

Wagener, J., Wysocki, P., Digonnet, M., Shaw, H., & DiGiovanni, D. (1993). Effects of concentration and clusters in erbium-doped fiber lasers. *Optics Letters, 18*(23), 2014-2016.

Wagner, W. G., & Lengyel, B. A. (1963). Evolution of the giant pulse in a laser. *Journal of applied physics, 34*(7), 2040-2046.

Wang, G. (2017). Wavelength-switchable passively mode-locked fiber laser with mechanically exfoliated molybdenum ditelluride on side-polished fiber. *Optics & Laser Technology, 96*, 307-312.

Wang, J., Cai, Z., Xu, P., Du, G., Wang, F., Ruan, S., . . . Hasan, T. (2015). Pulse dynamics in carbon nanotube mode-locked fiber lasers near zero cavity dispersion. *Optics Express, 23*(8), 9947-9958.

Wang, L., Li, X., Wang, C., Luo, W., Feng, T., Zhang, Y., & Zhang, H. (2019). Few-Layer Mxene Ti3C2Tx (T=F, O, Or OH) for Robust Pulse Generation in a Compact Er-Doped Fiber Laser. *ChemNanoMat, 5*(9), 1233-1238. doi:10.1002/cnma.201900309

Wang, M., Chen, C., Huang, C., & Chen, H. (2014). Passively Q-switched Er-doped fiber laser using a semiconductor saturable absorber mirror. *Optik, 125*(9), 2154-2156.

Wang, Y., Huang, W., Wang, C., Guo, J., Zhang, F., Song, Y., . . . Li, J. (2019). An all-optical, actively Q-switched fiber laser by an antimonene-based optical modulator. *Laser & Photonics Reviews, 13*(4), 1800313.

Wang, Z., Chen, Y., Zhao, C., Zhang, H., & Wen, S. (2012). Switchable dual-wavelength synchronously Q-switched erbium-doped fiber laser based on graphene saturable absorber. *IEEE Photonics Journal, 4*(3), 869-876.

Wang, Z., Li, H., Luo, M., Chen, T., Xia, X., Chen, H., . . . Song, Y. (2020). MXene photonic devices for near-infrared to mid-infrared ultrashort pulse generation. *ACS Applied Nano Materials, 3*(4), 3513-3522.

Wang, Z., Xu, Y., Dhanabalan, S. C., Sophia, J., Zhao, C., Xu, C., . . . Zhang, H. (2016). Black phosphorus quantum dots as an efficient saturable absorber for bound

soliton operation in an erbium doped fiber laser. *IEEE Photonics Journal, 8*(5), 1-10.

Woodward, R., Howe, R., Runcorn, T., Hu, G., Torrisi, F., Kelleher, E., & Hasan, T. (2015). Wideband saturable absorption in few-layer molybdenum diselenide (MoSe 2) for Q-switching Yb-, Er-and Tm-doped fiber lasers. *Optics express, 23*(15), 20051-20061.

Wu, K., Chen, B., Zhang, X., Zhang, S., Guo, C., Li, C., . . . Zou, W. (2018). High-performance mode-locked and Q-switched fiber lasers based on novel 2D materials of topological insulators, transition metal dichalcogenides and black phosphorus: review and perspective. *Optics Communications, 406*, 214-229.

Wu, K., Zhang, X., Wang, J., Li, X., & Chen, J. (2015). WS 2 as a saturable absorber for ultrafast photonic applications of mode-locked and Q-switched lasers. *Optics express, 23*(9), 11453-11461.

Xie, G., Ma, J., Lv, P., Gao, W., Yuan, P., Qian, L., . . . Tang, D. (2012). Graphene saturable absorber for Q-switching and mode locking at 2 μm wavelength. *Optical Materials Express, 2*(6), 878-883.

Xu, N., Ma, P., Fu, S., Shang, X., Jiang, S., Wang, S., . . . Zhang, H. J. N. (2020). Tellurene-based saturable absorber to demonstrate large-energy dissipative soliton and noise-like pulse generations. *9*(9), 2783-2795.

Xu, N., Ming, N., Han, X., Man, B., & Zhang, H. (2019). Large-energy passively Q-switched Er-doped fiber laser based on CVD-Bi 2 Se 3 as saturable absorber. *Optical Materials Express, 9*(2), 373-383.

Xu, N., Wang, H., Zhang, H., Guo, L., Shang, X., Jiang, S., & Li, D. J. N. (2020). Palladium diselenide as a direct absorption saturable absorber for ultrafast mode-locked operations: from all anomalous dispersion to all normal dispersion. *9*(14), 4295-4306.

Xue, M., Zhang, X., Tang, H., & Li, C. (2014). Synthesis of high purity Cr_2AlC nanolamellas with improved tribological properties for oil-based additives. *RSC advances, 4*(74), 39280-39286. doi:10.1039/C4RA06719C

Yan, P., Lin, R., Ruan, S., Liu, A., Chen, H., Zheng, Y., . . . Hu, J. (2015). A practical topological insulator saturable absorber for mode-locked fiber laser. *Scientific reports, 5*, 8690.

Yang, Y., Loeblein, M., Tsang, S., Chow, K., & Teo, E. (2014). Three-dimensional graphene based passively mode-locked fiber laser. *Optics express, 22*(25), 31458-31465.

Yang, Y., Yang, S., Li, C., & Lin, X. (2019). Passively Q-switched and mode-locked Tm-Ho co-doped fiber laser using a WS2 saturable absorber fabricated by chemical vapor deposition. *Optics & Laser Technology, 111*, 571-574.

Yue, W., Wang, Y., Xiong, C.-D., Wang, Z.-Y., & Qiu, Q. (2013). Intensity noise of erbium-doped fiber laser based on full quantum theory. *Journal of the Optical Society of America B, 30*(2), 275-281. doi:10.1364/JOSAB.30.000275

Yusoff, R. A. M., Jafry, A. A. A., Kasim, N., Zulkipli, N. F., Samsamnun, F. S. M., Yasin, M., & Harun, S. W. (2020). Q-switched and mode-locked erbium-doped fiber laser using gadolinium oxide as saturable absorber. *Optical Fiber Technology, 57*. doi:10.1016/j.yofte.2020.102209

Zervas, M. N., & Codemard, C. A. (2014). High power fiber lasers: a review. *IEEE Journal of Selected Topics in Quantum Electronics, 20*(5), 219-241.

Zhang, H., Tang, D., Knize, R. J., Zhao, L., Bao, Q., & Loh, K. P. (2010). Graphene mode locked, wavelength-tunable, dissipative soliton fiber laser. *Applied Physics Letters, 96*(11), 111112.

Zhang, Y., Qi, Y., Huo, X., Chen, B., Bai, Z., Yang, X., . . . Lu, Z. (2021). Study of the influence of SESAM parameters on the evolution of mode-locked pulses at different repetition rates. *Applied Physics B, 127*(8), 1-10.

Zhao, X., Hu, G., Zhao, B., Li, C., Pan, Y., Liu, Y., . . . Zheng, Z. (2016). Picometer-resolution dual-comb spectroscopy with a free-running fiber laser. *Optics express, 24*(19), 21833-21845.

Zuikafly, S. N. F., Khalifa, A., Ahmad, F., Shafie, S., & Harun, S. (2018). Conductive graphene as passive saturable absorber with high instantaneous peak power and pulse energy in Q-switched regime. *Results in Physics, 9*, 371-375.

Zulkipli, N. F., Batumalay, M., Samsamnun, F. S. M., Mahyuddin, M. B. H., Izam, T., Khudus, M., & Harun, S. W. (2020). Q-switching pulses generation with samarium oxide film saturable absorber. *Microwave and Optical Technology Letters, 62*(3), 1049-1055. doi:10.1002/mop.32118

Zulkipli, N. F., Jafry, A. A. A., Apsari, R., Samsamnun, F. S. M., Batumalay, M., Khudus, M., . . . Harun, S. W. (2020). Generation of Q-switched and mode-locked pulses with Eu2O3 saturable absorber. *Optics and Laser Technology, 127*. doi:10.1016/j.optlastec.2020.106163